

REPORT NO: CG-D-62-80

LEVEL

12

THEORETICAL ESTIMATES OF THE VARIOUS MECHANISMS INVOLVED IN ICEBERG DETERIORATION IN THE OPEN OCEAN ENVIRONMENT

F. M. White
M. L. Spaulding
L. Gominho

Departments of Ocean and Mechanical Engineering
University of Rhode Island
Kingston, Rhode Island 02881

AD A091557

U. S. Coast Guard Research and Development Center
Avery Point Groton, Connecticut 06340



MAY 1980

FINAL REPORT

DTIC
NOV 5 1980

DDC FILE COPY

Document is available to the U. S. Public through the National Technical Information Service
Springfield, Virginia 22161

8011 03 039

PREPARED FOR

U. S. DEPARTMENT OF TRANSPORTATION
UNITED STATES COAST GUARD

OFFICE OF RESEARCH AND DEVELOPMENT
WASHINGTON D. C. 20593

NOTICE

This document is disseminated under the sponsorship of the Department of Transportation in the interest of information exchange. The United States Government assumes no liability for its contents or use thereof.

The United States Government does not endorse products or manufacturers. Trade or manufacturers' names appear herein solely because they are considered essential to the object of this report.

The contents of this report reflect the views of the Coast Guard Research and Development Center, which is responsible for the facts and accuracy of data presented. This report does not constitute a standard, specification, or regulation.

Donald L. Birkimer, For

DONALD L. BIRKIMER, Ph.D., P.E.
Technical Director

U.S. Coast Guard Research and Development Center
Avery Point, Groton, Connecticut 06340

9 Final rept.

Technical Report Documentation Page

1. Report No. CG-D-62-80, 7/80	2. Government Accession No. AD A091557	3. Recipient's Catalog No.	
4. Title and Subtitle 6 THEORETICAL ESTIMATES OF THE VARIOUS MECHANISMS INVOLVED IN ICEBERG DETERIORATION IN THE OPEN OCEAN ENVIRONMENT.		5. Report Date 11 MAY 1980	6. Performing Organization Code
7. Author(s) 10 F. M. White M. L. Spaulding L. Gominho	8. Performing Organization Report No. 18 USCG-D, CGR/DC		9. Work Unit No. (TRAIS)
9. Performing Organization Name and Address Departments of Ocean and Mechanical Engineering University of Rhode Island Kingston, Rhode Island 02881		11. Contract or Grant No. 15 DOT-CG-81-79-1978 NEW	12. Type of Report and Period Covered
12. Sponsoring Agency Name and Address Department of Transportation United States Coast Guard Office of Research and Development Washington, D.C. 20593		14. Sponsoring Agency Code	
15. Supplementary Notes The contract under which this report was submitted was under the technical supervision of the Coast Guard Research and Development Center, Groton, Connecticut 06340. R&D Center Report Number CG R&D 7/80 has been assigned.			
16. Abstract Theoretical estimates are developed for a variety of mechanisms for the deterioration of icebergs in the open ocean environment. Although all the estimates are of an elementary nature, primarily algebraic correlations, the estimates seem to be in good agreement with the limited experimental data available. Formulas are given for computing the static stability of an iceberg from observations of the exposed shape. Simple theoretical estimates are made for the response of an iceberg to a sudden change in wind or water current and the speed at which a berg is driven by the wind. These dynamic estimates are supplemented by wind tunnel measurements of the drag of the submerged portion of model tabular and non-tabular bergs. Solar insolation and buoyant meltwater convection are shown to be minor contributions to deterioration, with melt rates of 2-20 cm/day at best. Forced underbody convection due to wind-driven effects is more important, with melt rates estimated at 5-20 cm/day/°C of water/ice temperature difference. The most important mechanism is wave erosion, with waterline melt rates estimated as high as 150 cm/day/°C. Digital computer finite difference results for the fracture of an overhanging ice slab plus wave erosion theory lead to a theoretical estimate for the calving time of an iceberg subjected to a wave environment.			
17. Key Words Iceberg Deterioration, Melting, Calving, Wave Erosion, Drag, Wind Response, Forced Convection, Buoyant Convection, Stability		18. Distribution Statement Document is available to the U.S. public through the National Technical Information Service, Springfield, Virginia 22161	
19. Security Classif. (of this report) UNCLASSIFIED	20. Security Classif. (of this page) UNCLASSIFIED	21. No. of Pages	22. Price

305500 Jhu

CONTENTS

	PAGE
ABSTRACT	i
NOMENCLATURE	ii
1. INTRODUCTION	1
Literature on Deterioration Processes	2
2. SURVEY OF ENVIRONMENTAL PARAMETERS	7
The Properties of Seawater	7
Simplified Formulation of the Stefan Problem	12
Weather Conditions in the Labrador Sea	14
3. ICEBERG STABILITY ESTIMATES	20
Introduction	20
Static Stability Theory	22
Tabular and Non-tabular Composite Shapes	32
4. ELEMENTARY ICEBERG DYNAMICS	38
Introduction	38
Simplified Equation of Motion	38
Response to a Sudden Change in Water Velocity	40
Effect of the Basset History Term	41
Response of an Iceberg to Sudden Wind Velocity	44
Steady Wind-Driven Iceberg Motion	44
Measurements of Submerged Body Iceberg Drag	49
5. SURFACE MELTING DUE TO INSOLATION	55
6. MELTING DUE TO VERTICAL BUOYANT CONVECTION	59
Introduction	59
Four Theoretical Estimates	61
7. MELTING DUE TO FORCED CONVECTION	69
Introduction	69
Approximate Solution for Two Iceberg Shapes	70
Melting at the Root of an Ice Flaw	73
8. WAVE EROSION OF AN ICEBERG	77
Introduction	77
The Wave Friction Factor Diagram	78
The Reynolds Analogy	82
Calculations of Iceberg Erosion by Waves	85
Laboratory Wave Erosion Experiments	91

Session For FIS CRAM TIC FOR Unpublished Application	Attribution/ Responsibility/Date Name of User Control <div style="text-align: center; font-size: 2em; font-weight: bold;">A</div>
--	---

CONTENTS...	PAGE
9. CALVING OF OVERHANGING ICE SLABS	98
Introduction	98
Thin Plate Theory	100
Thick Plate Theory	101
Finite Element Solution	101
Application to Calving by Wave Erosion	110
10. CONCLUSIONS	115
REFERENCES	118

ABSTRACT

Theoretical estimates are developed for a variety of mechanisms for the deterioration of icebergs in the open ocean environment. Although all the estimates are of an elementary nature, primarily algebraic correlations, the estimates seem to be in good agreement with the limited experimental data available. Formulas are given for computing the static stability of an iceberg from observations of the exposed shape. Simple theoretical estimates are made for the response of an iceberg to a sudden change in wind or water current and the speed at which a berg is driven by the wind. These dynamic estimates are supplemented by wind tunnel measurements of the drag of the submerged portion of model tabular and non-tabular bergs. Solar insolation and buoyant meltwater convection are shown to be minor contributions to deterioration, with melt rates of 2-20 cm/day at best. Forced underbody convection due to wind-driven effects is more important, with melt rates estimated at 5-20 cm/day/ $^{\circ}$ C of water/ice temperature difference. The most important mechanism is wave erosion, with waterline melt rates estimated as high as 150 cm/day/ $^{\circ}$ C. Digital computer finite difference results for the fracture of an overhanging ice slab plus wave erosion theory lead to a theoretical estimate for the calving time of an iceberg subjected to a wave environment.

NOMENCLATURE

A_a	frontal area of exposed iceberg surface
A_w	frontal area of submerged iceberg surface
B	dimensionless drag parameter, Eq.(40)
$C_{1,2,3}$	stress analysis constants, Eqs. (83) and (86)
C_D	drag coefficient, $\text{Drag}/(\frac{1}{2}\rho V^2 A)$
C_F	local friction coefficient, $\tau_w/(\frac{1}{2}\rho V^2)$
C_{fw}	wave friction factor, Eq.(66)
C_H	Basset history parameter, Eq.(37)
C_M	hydrodynamic mass ratio, m_h/m , Eq.(31)
C_O	empirical stability constant = 0.93, Eqs.(28,29)
c_p	specific heat at constant pressure
g	acceleration of gravity
Gr_x	local Grashof number, Eqs. (44,47)
H	wave height (also iceberg height in Figure 10)
I	area moment of inertia, Eq.(12)
k	wave number, $2\pi/\lambda$
K	dynamic parameter defined by Eqs.(32,35)
L	iceberg characteristic length = v/A
Le	Lewis number = κ/κ_S
L_O	waterline length, Eq.(63)
m	iceberg mass
\overline{MG}	metacentric height, Figure 9
n	empirical exponent, Eq.(43)
Nu_x	local Nusselt number, Eq.(43)
Pr	Prandtl number = ν/κ
R	ice slab fillet radius, Figure 36b.
q_w	wall heat transfer rate per unit area

NOMENCLATURE...

Re_a	wave orbit Reynolds number, Eq.(67)
Re_H	wave height Reynolds number = H^2/Tv_w
Re_L	iceberg length Reynolds number = VL/v_w
S	salinity
Sc	Schmidt number = $PrLe$
St_x	local Stanton number, Eq.(60)
t	time (Chap. 4); ice slab thickness (Chap. 9)
T	wave period
T_f	ice freezing temperature, Eqs.(2,3)
T_i	ice surface temperature
T_m	temperature at maximum water density, Eq.(1)
T_w	ambient water temperature
V	characteristic velocity
V_a	air velocity
V_f	steady wind-driven iceberg velocity, Eq.(39)
V_m	ice melting rate
V_w	water velocity
u_m	horizontal wave orbit velocity, Eq.(70)
w_m	vertical wave orbit velocity, Eq.(70)
W	two-dimensional waterline width
W_{wl}	three-dimensional waterline width

GREEK SYMBOLS:

α	linearized salinity-density effect, Eq.(56)
β	slab overhang ratio = B/A, Figure 36
γ	specific weight (also density ratio in Eq. 18)
Γ	latent heat of melting = 334 J/g for ice
δ_u	velocity boundary layer thickness
δ_T	thermal boundary layer thickness
δ_S	salinity boundary layer thickness
ϵ	ice surface roughness height
ζ	Poisson's ratio, = 0.34 for ice
κ	thermal diffusivity
κ_S	salinity diffusivity
λ	wave length = $2 / k$
μ	absolute viscosity
ν	kinematic viscosity
π	3.14159...
ρ_a	air density
ρ_i	ice density
ρ_w	water density
σ_{max}	fracture stress
τ_w	wall shear stress
U_a	above-water iceberg volume, Figure 9
U_b	below-water iceberg volume, Figure 9
\dot{U}	strip-volume wave erosion melting rate, Eq.(78)
ℓ	ice slab overhang distance, Figure 36
ℓ_r	overhang length which causes calving fracture

Chapter 1

INTRODUCTION

As the title of this report states, its purpose is to establish a theoretical basis, using practical engineering estimates, of the relative importance of various mechanisms involved in iceberg deterioration in the open ocean environment. Emphasis is placed primarily on the moderate-sized irregular icebergs typical of the Labrador Sea and Newfoundland Bank, although many of the results will also be applicable to the large tabular bergs of the Antarctic Sea. The ultimate goal is to produce engineering predictions sufficiently quantitative that they can be used in the field. That is, accurate formulas could be stored on a shipboard computer and, when an iceberg is sighted, some simple measurements such as exposed iceberg size, sea state, water temperature, and wind velocity could be used as input to the computer. The formulas would then predict the estimated loss of mass of the berg during, say, a one-day period. This estimate could be updated by daily sightings or by statistical weather predictions by the U.S. Navy Fleet Numerical Weather Central.

The present report discusses and develops engineering formulas for a variety of iceberg deterioration mechanisms. It is believed that these formulas are an improvement over existing literature on the subject. Yet it cannot be said that the results constitute a definitive tool for use by persons working in an iceberg environment, primarily because

of the lack of adequate field data for comparison. This is especially true with regard to estimates of wave erosion and calving of icebergs. This report derives new and interesting formulas for wave calving effects, but further experimentation is strongly recommended.

Literature on Deterioration Processes

Although it has been long thought that the melting of icebergs contributes significantly to the physical and possibly biological oceanography of the polar seas, the literature on such melting is relatively sparse. Interest in iceberg deterioration has intensified in this decade due to problems such as oil exploration in the Arctic, protection of shipping lanes and fisheries in the North Atlantic, plans for aquaculture in the Antarctic, and the use of icebergs as a fresh water source. An eloquent description of icebergs and their environment, including melting processes, is given in Chapter 3 of the text by Groen (1969). An alternate description, from the viewpoint of a glaciologist, is given in the text by Paterson (1975). An important introduction to iceberg deterioration mechanisms was given by Kollmeyer (1965), and the present report follows up many of his ideals. Detailed quantitative estimates of melting rates were made by Weeks and Campbell (1973), which served as the stimulus in 1977 for the First International Conference on Iceberg Utilization (Husseiny 1977). The 54 papers from that conference proceedings have been a valuable input to the present report. A second iceberg utilization conference was held 1-4 April 1980 in Cambridge, England. Of particular interest in the first

such conference was a keynote paper outlining the problems involved in iceberg technology (Weeks and Mellor 1977).

Deterioration processes are also important from the point of view of the dangers icebergs present to shipping, fisheries, and oil drilling in arctic waters. Such problems were discussed in the recent First International Iceberg Dynamics Symposium, held June 4-5, 1979 in St. John's Newfoundland. The proceedings of that conference are to be published imminently as Vol. 1, Nos. 3 and 4 of the new journal Cold Regions Science and Technology, Elsevier Publishing Company, Amsterdam. At that conference Kollmeyer (1979) gave an interesting keynote paper on the major sources of Arctic icebergs.

As mentioned, field data on iceberg melting is sparse. Morgan and Budd (1977) used statistical data on the drifting rates and size distribution of antarctic icebergs to estimate their melt rates. The Morgan and Budd data was recently re-evaluated by Neshyba and Josberger (1979) to give a more quantitative estimate. There are also periodic reports of the melting of an individual iceberg. Groen (1969) on pages 117 and 118 discusses a nontabular Greenland iceberg whose exposed height was 75 meters on April 11, 1921 and was only 18 meters high 31 days later. Similarly a tabular followed by the International Ice Patrol during April-May 1976 diminished in area from 19 to 11 hectares in only 25 days, even though the water surface temperature was only 2° to 4°C. Such rapid melting cannot be completely accounted for by the most obvious mechanism, buoyant free convection. Other less

obvious effects, such as winds, waves, and calving, must contribute greatly to the demise of an iceberg.

Probably the most detailed estimates of iceberg deterioration rates in the literature are given in the recent paper by Job (1978). Job outlines the following as the most important mechanisms of deterioration:

1. Melting of the exposed surface by:
 - a) solar radiation; b) warm air convection.
2. Forced convection melting of the submerged bottom and undersides due to differential velocity between the iceberg and the seawater. This convection can be enhanced by surface waviness and roughness and by ambient water turbulence.
3. Buoyancy-induced natural convection along the submerged sides and, to a lesser extent, along the bottom. This effect can be enhanced by bubble release from the ice.
4. Convection induced by wallowing or overturning due to a calving event or after melting to an unstable shape.
5. Waterline wave erosion and undercutting, followed by calving of the resultant ice overhang.
6. Differential melting along cracks, faults, or inhomogeneous inclusions in the iceberg, leading to further calving.
7. Subsurface calving due to upthrust on underwater shelves formed by other melting mechanisms.
8. Fracture of the ice due to thermal stresses induced by

wallowing or overturning in warm waters.

We will investigate most of these mechanisms in the remainder of this report. Items #7 and #8 are practically impossible to quantify due to lack of available theory or shape effects, while #4 is thought to be insignificant due to the very short time spent by an iceberg in the wallowing or overturning states.

As pointed out by Job (1978) there are two further uncertainties in making iceberg melting estimates: 1) the markedly lower density in the upper portion of Antarctic bergs;[†] 2) strongly variable salinity profile in the water close to the ice surface. Again these two effects are nearly impossible to quantify except statistically.

A composite idealized picture of these deterioration mechanisms is shown in Figure 1. We will attempt to make numerical estimates of most of these effects. The figure indicates the possibility of wave-induced bending as a fracture mechanism, but it is found that the stresses induced by wave passage can only approach fracture level for the very largest of (Antarctic) tabular bergs (Holdsworth and Glynn 1978, Holdsworth 1977).

We should also note that at least two relatively simple theoretical models of ice growth and melting have recently been published: the dynamic sea-ice model of Hibler (1979) and the ice-shelf melting model of Gade (1979), the latter of which can be applied to large (Antarctic) tabular bergs.

[†]Arctic icebergs, being formed from glaciers, are of relatively uniform density.

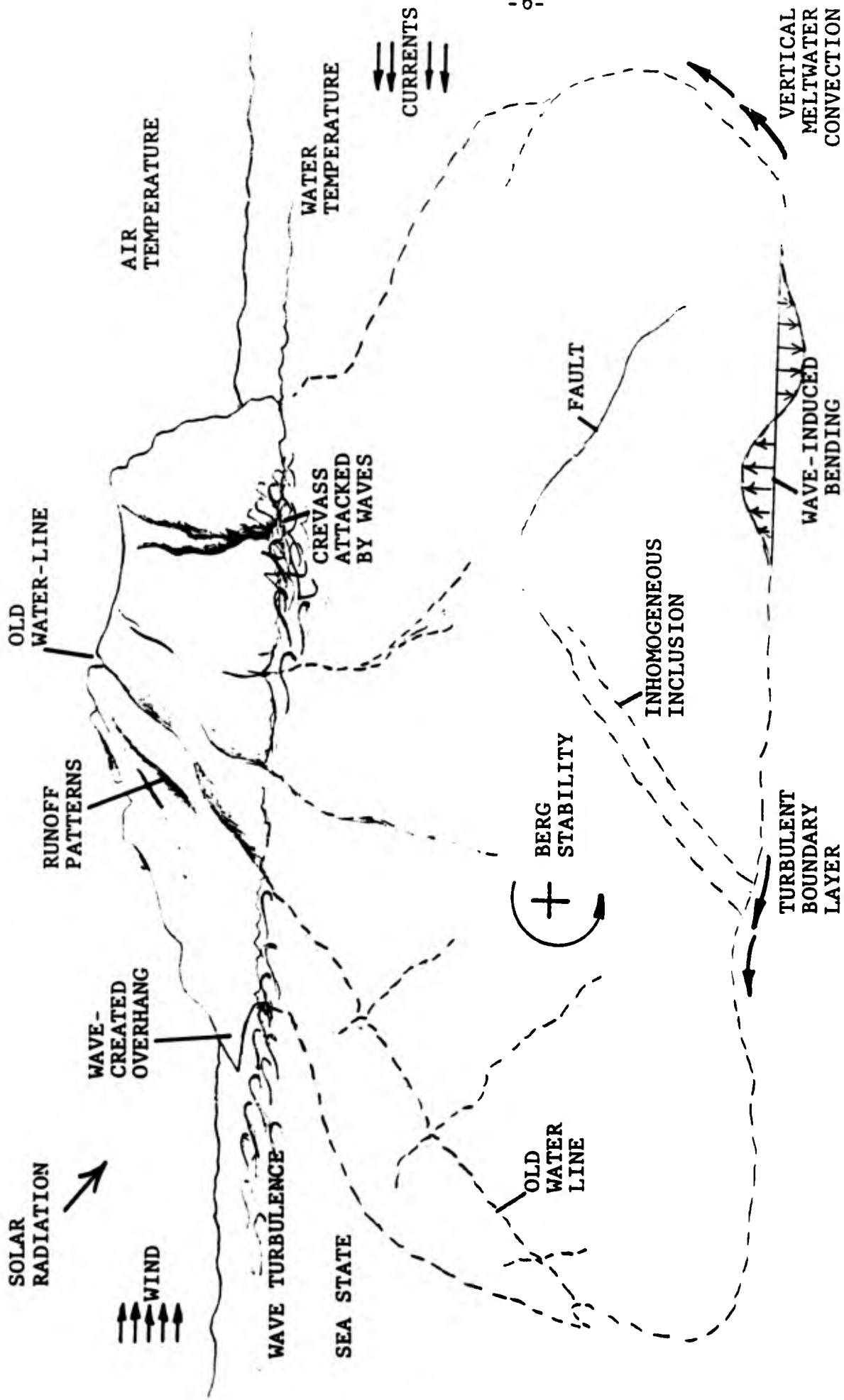


Figure 1. ILLUSTRATION OF IMPORTANT ICEBERG DETERIORATION PARAMETERS.

Chapter 2

SURVEY OF ENVIRONMENTAL PARAMETERS

Before embarking upon detailed engineering calculations of heat transfer and stress analysis, let us review the physical oceanographic and environmental parameters which affect these estimates.

The Properties of Seawater

The ambient fluid for these studies is of course seawater, with temperatures ranging typically from -1° to $+10^{\circ}\text{C}$ and salinities from 30 to $35^{\circ}/\text{oo}$. For such cold waters the variation of density with temperature is non-linear. The ice surfaces, being of glacial origin, are nearly pure (zero salinity) water and usually bubbly. Thus the melt water near an iceberg varies in salinity from zero to ambient and has temperature varying from the freezing point to ambient.

Figure 2 shows the equation of state of seawater at these low temperatures, as computed from the empirical algebraic relation of Gebhart and Mollendorf (1977), which is the most accurate curve-fit yet devised for the data. The locus of points of maximum density are given by the relation

$$T_m(^{\circ}\text{C}) = 4.03 - 0.21216 S^{\circ}/\text{oo} \quad (1)$$

This is shown as a dash-dot line on Figure 2. The freezing point of water is given for high salinity by the relation of Fujino et al. (1974):

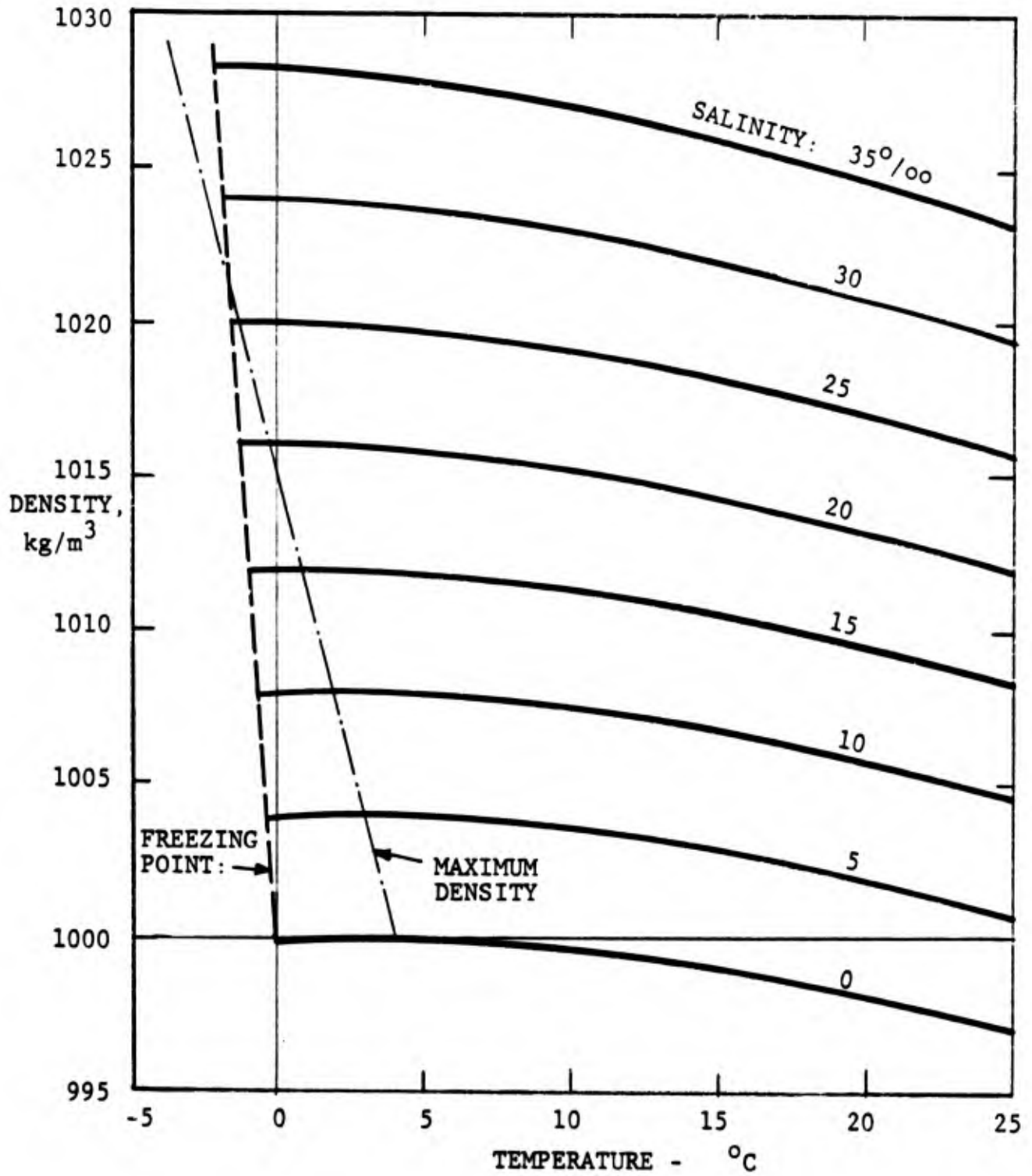


Figure 2. THE DENSITY OF SEAWATER AT ONE ATMOSPHERE PRESSURE.
(AFTER GEBHART AND MOLLENDORF 1977)

$$T_f(^{\circ}\text{C}) = -0.036 - 0.0499 S - 0.000112 S^2$$

for $17.7 < S < 35^{\circ}/00$ (2)

The freezing point for low salinity is given by Kaufman (1960):

$$T_f(^{\circ}\text{C}) = -0.05392 S, \quad \text{for } S < 17.7^{\circ}/00 \quad (3)$$

The freezing point is shown on Figure 2 as a dashed line. As pointed out by Josberger (1979a), if the ambient seawater state lies in the triangle between the freezing point and the maximum density point in Figure 2, the buoyancy-induced flow near the ice surface is upward due to both the cooling and dilution effects. But environmental ambient conditions are rarely in this triangle, which is more likely encountered in laboratory experiments. For ambient states to the right of this triangle in Figure 2, the dilution buoyancy is upward and the cooling buoyancy downward and there may be a bi-directional boundary layer flow, especially if the ambient is near the maximum-density line. Also, at higher ambient temperatures, greater than about 14°C , Josberger (1979a) shows that the cooling buoyancy begins to dominate, so that the net buoyant flux is downward. However, an iceberg will not generally encounter such warm waters until it is near the Gulf Stream. Thus the net buoyancy flow on an iceberg surface is usually upward due to dominant dilution effects.

For either forced-convection or natural-convection flows, the relative thicknesses of the velocity, temperature, and salinity boundary layers are related to the relative sizes

of the molecular diffusivities of momentum, heat, and salt. The ratio of momentum diffusivity or kinematic viscosity ν to the thermal diffusivity κ is called the Prandtl number:

$$\text{Pr} = \nu/\kappa \quad (4)$$

If the Prandtl number is greater than unity, the temperature boundary layer will be thinner than the velocity layer, thus enhancing the heat transfer. This is the case with seawater. As shown in Figure 3a, the Prandtl number of cold Arctic waters varies from about 9 to 14, and for turbulent flows the boundary layer thickness ratio will be approximately

$$\delta_T/\delta_U \approx \text{Pr}^{-1/3} = 0.42 \text{ to } 0.48 \quad (5)$$

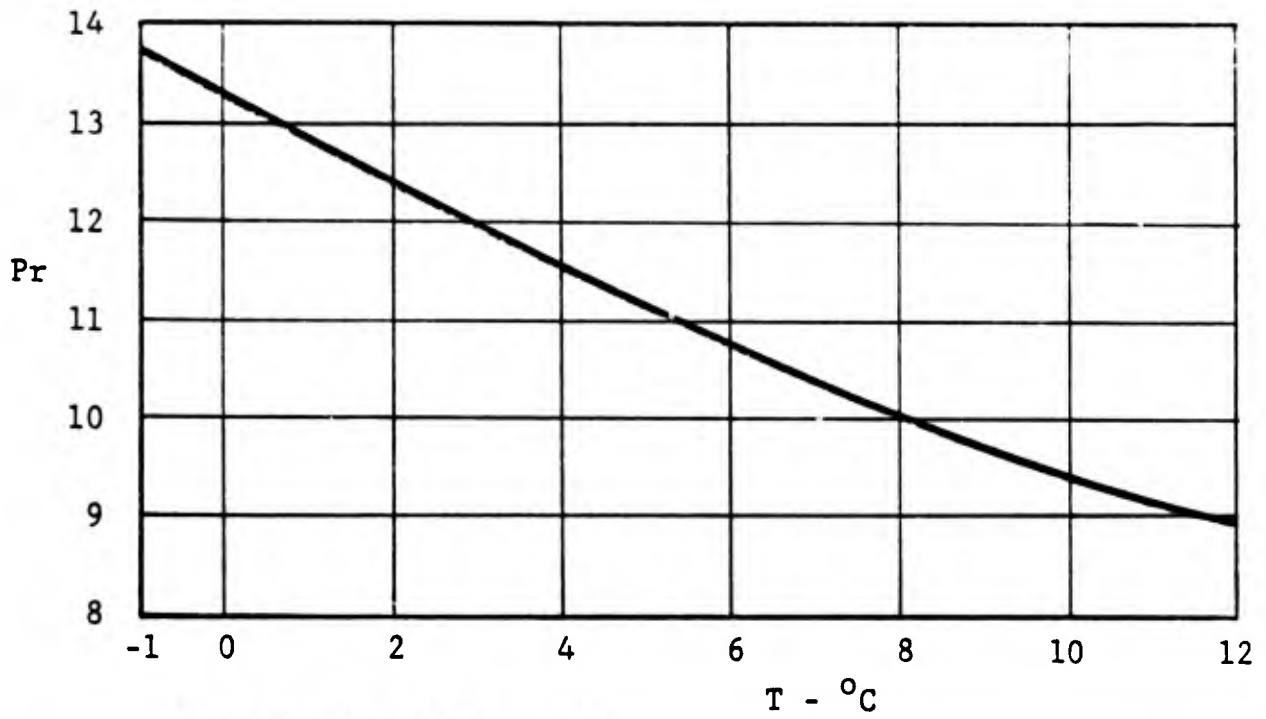
Similarly, the ratio of thermal to saline diffusivity is called the Lewis number:

$$\text{Le} = \kappa/\kappa_S \quad (6)$$

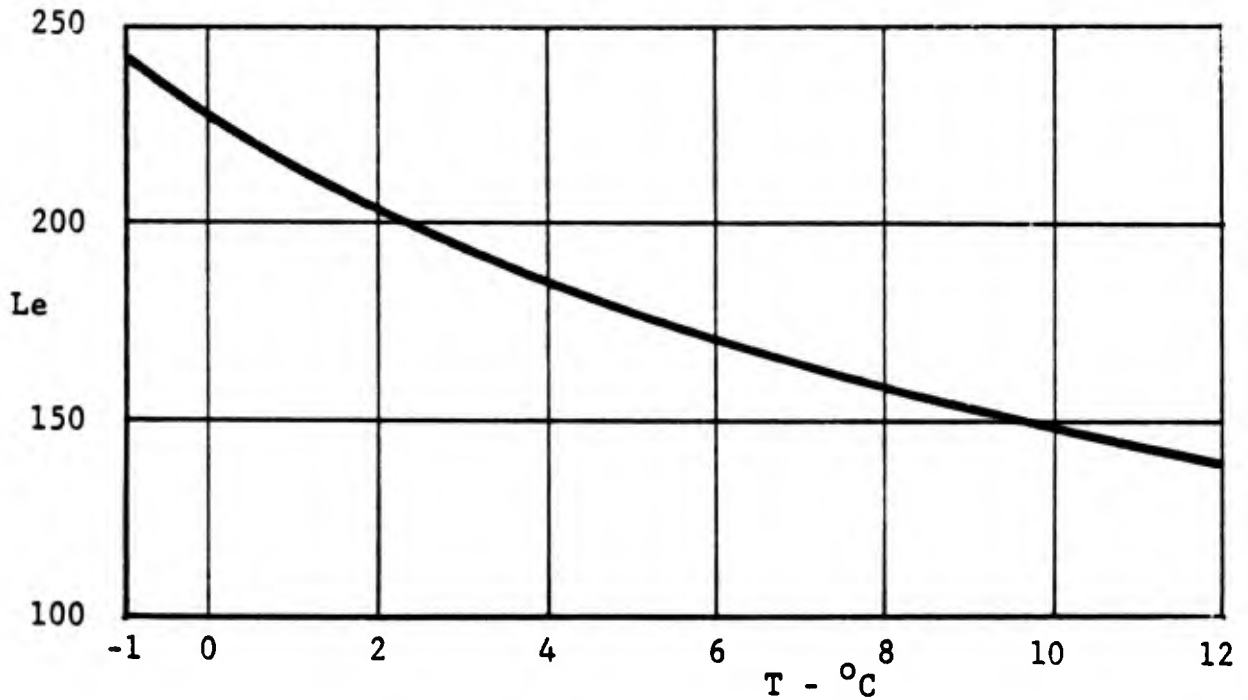
Values of the Lewis number of seawater are given in Figure 3b and vary from about 140 to 240. Thus we expect the salt and temperature layer thicknesses to vary approximately as

$$\delta_S/\delta_T \approx \text{Le}^{-1/3} = 0.16 \text{ to } 0.19 \quad (7)$$

These estimates are verified in numerical computations by Josberger (1979a) for buoyant convection near a vertical ice wall.



(a) PRANDTL NUMBER: ν/κ



(b) LEWIS NUMBER: κ/κ_S

Figure 3. MOLECULAR DIFFUSION PROPERTIES OF SEAWATER:

a) PRANDTL NUMBER (AFTER KREITH 1973);

b) LEWIS NUMBER (AFTER CALDWELL 1974).

Simplified Formulation of the Stefan Problem

When attempting engineering calculations of iceberg deterioration and melting, one must avoid the temptation to become enmeshed in the detailed mechanics of heat conduction in a melting or ablating surface. This is the so-called "Stefan" problem, which has spawned a voluminous literature in the field of applied mechanics. The Stefan problem treats conduction with moving boundaries, using coordinate transformation in various geometries. Whole textbooks have been written about the mathematical theory of the Stefan problem, such as Ockendon and Hodgkins (1975). Numerical finite-difference and finite-element methods have been devised for transient heat conduction in a melting body, in both a general formulation (Lazaridis 1970) and for specific body shapes (Budhia & Kreith 1972, Stewartson and Waechter 1976).

Figure 4 shows the latent heat of ice as a function of temperature and pressure, after Hobbs (1974). Since an iceberg surface experiences a maximum pressure of the order of 20 bars, its latent heat is approximately constant, equal to 334 kJ/kg.

In analyzing iceberg melting, it may seem superficially necessary to treat the process as a coupled Stefan problem, because the interior of the ice is usually much colder than the surface (Weeks and Mellor 1977). However, the rate of melting of ice is so slow (a few centimeters per hour) that transient conduction in the ice is essentially a quasisteady

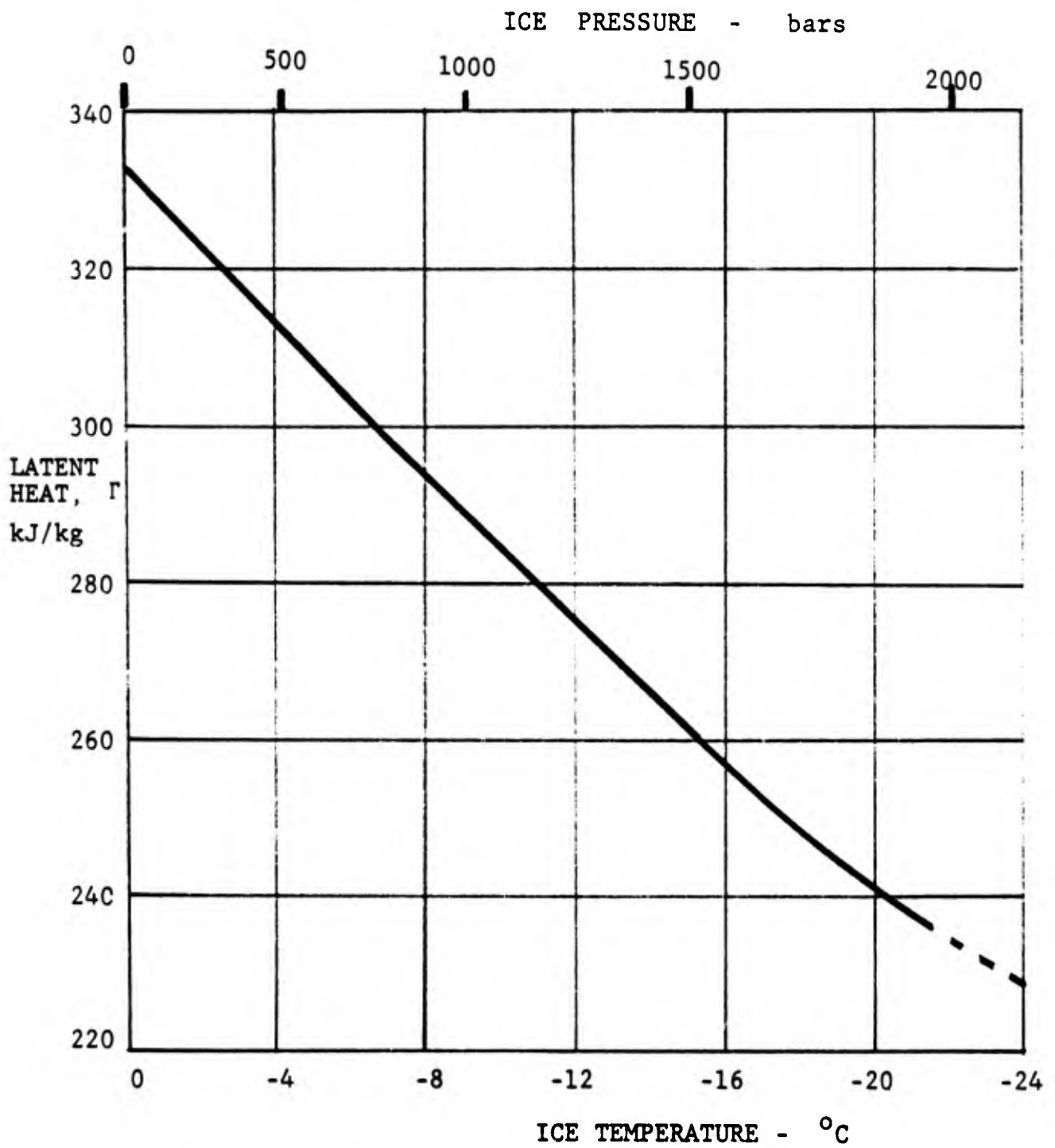


Figure 4. THE LATENT HEAT OF MELTING OF ICE, AFTER HOBBS (1974).

process. Further, in the real environment, there always exist sufficient ambient turbulence, wave action, relative water currents, and buoyancy to effectively remove melt water from the ice surface as soon as it is formed. Therefore we choose not to be concerned with the details of the moving-boundary melting conduction problem. Melting rates computed in this report simply assume that all heat delivered to the ice surface from the environment is expended in melting the ice. If q_w is the heat transfer rate per unit area at the surface, the rate of melting or recession velocity V_m of the ice wall will simply be calculated by the relation

$$V_m = q_w / (\rho_i \Gamma) \quad (8)$$

where ρ_i is the ice density (approximately 0.9 g/cm^3) and Γ is the latent heat of melting of ice. From Figure 4 at 0°C , $\Gamma = 334 \text{ kJ/kg} = 144 \text{ Btu/lbm}$ and is the value which will be consistently used in this report.

Weather Conditions in the Labrador Sea

Since the heat transfer computations in this report primarily relate to the effects of wind, waves, and ambient temperatures, it is well to review the probability of occurrence of these parameters in an iceberg environment. For purposes of illustration we confine the discussion to the Labrador Sea, for which weather data are available from several sources: the U. S. Naval Oceanographic Office (1967), the Mariner's Weather Log (NOAA bimonthly), and the Summaries

of Synoptic Weather Observations (U. S. Navy annually). A good illustration is the data from Ocean Weather Station "Bravo", which occupied a central position in the Labrador Sea ($56^{\circ}30'N$, $51^{\circ}00'W$) until removed in 1973.

Figure 5 shows long-term monthly averages of air temperature and sea-surface water temperature from this ocean station. The air temperature on the average varies between -4° and $+8^{\circ}C$ throughout the year, and sea-surface temperature varies from $+2$ to $+8^{\circ}C$. Excursions from maximum to minimum air and sea temperatures are relatively small, typically $\pm 3^{\circ}C$.

Figure 6 shows the monthly measured frequency of occurrence of wind speeds at station "Bravo". It is seen that the winds in the Labrador Sea are rarely calm and rarely greater than 47 knots (24 m/s). Most probable wind speeds in the winter are from 11 to 47 knots and somewhat lesser in the summer, perhaps 4 to 33 knots. As we shall see, wind can be a large contribution to iceberg melting due to its effect on differential water velocities.

Finally, Figures 7 and 8 show the probability of occurrence of wave heights and periods, respectively, at station Bravo. Winter wave heights range from 2 to 6 meters or even greater, and summer heights are from 1 to 3 meters. The distribution of wave periods is more uniform throughout the year, ranging from 3 seconds to about 11 seconds. Median wave period is 6.5 sec in the winter and 6.0 sec in the summer. These four figures support a general picture of the Labrador Sea as a windy, wavy, cold environment.

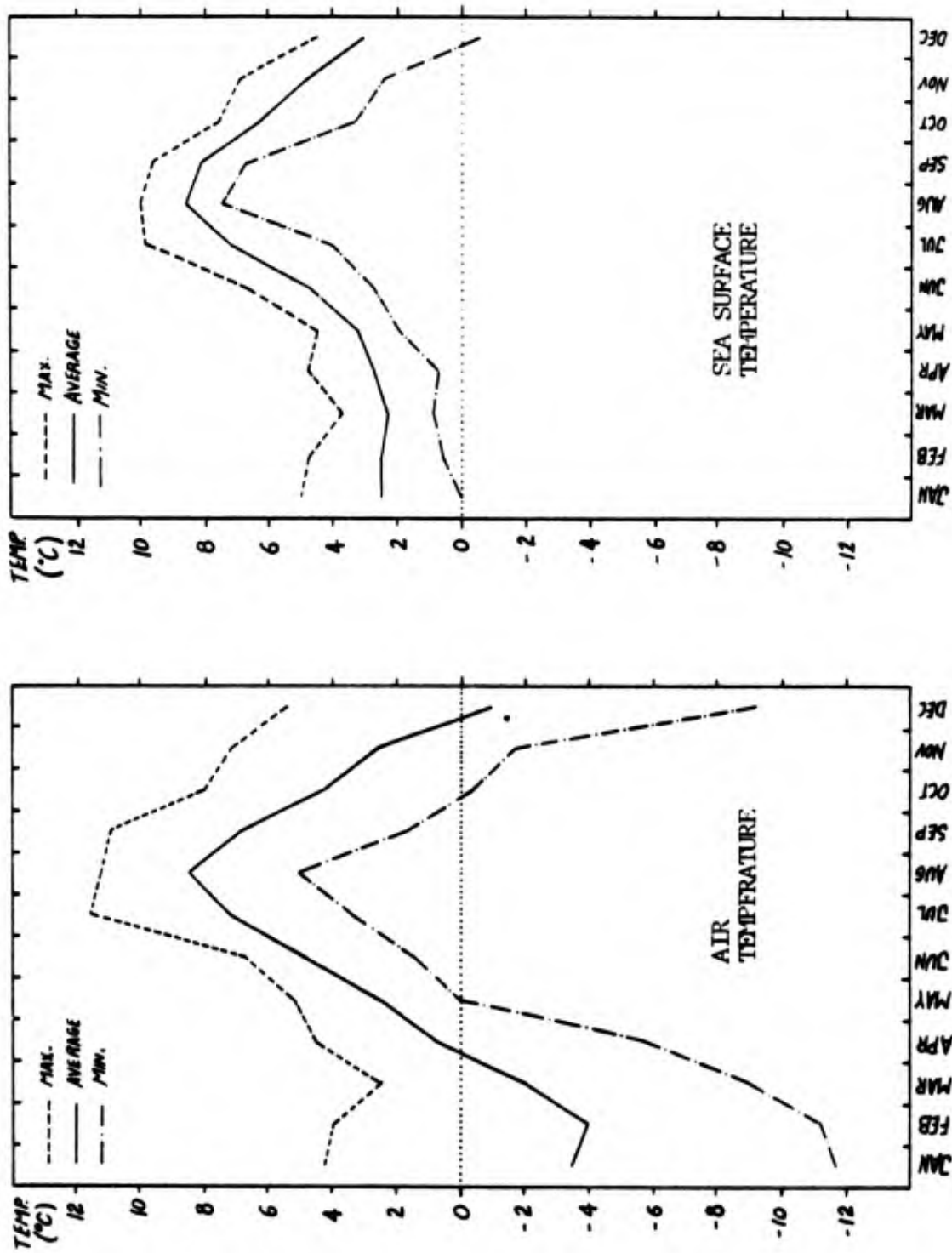


Figure 5. MEASURED MONTHLY AIR AND SEA-SURFACE TEMPERATURES FROM OCEAN STATION "BRAVO" IN THE LABRADOR SEA (56°30'N, 51°00'W).

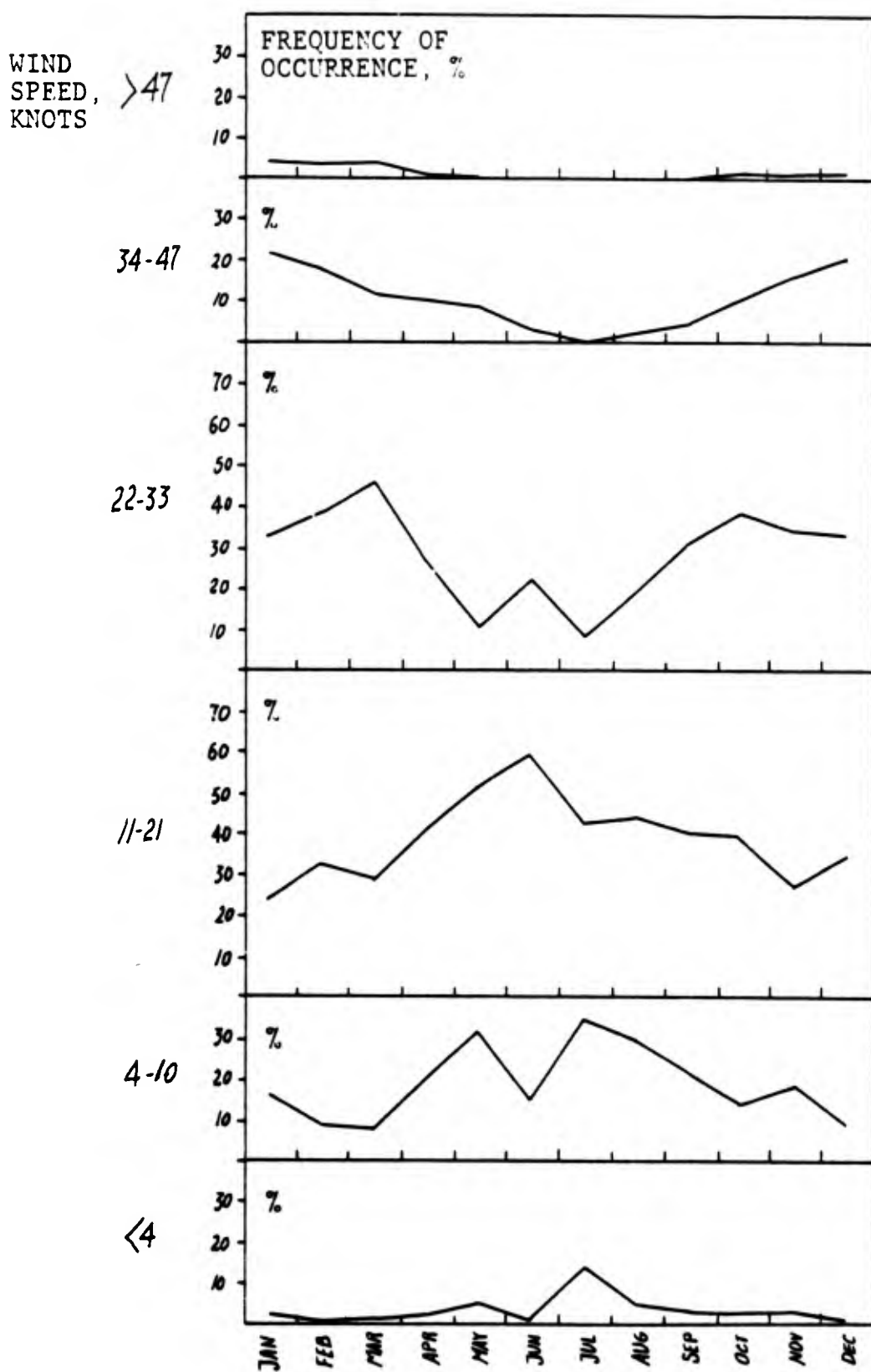


Figure 6. MEASURED MONTHLY FREQUENCY OF OCCURRENCE OF WIND SPEEDS FROM OCEAN STATION "BRAVO" IN THE LABRADOR SEA (56°30'N, 51°00'W).

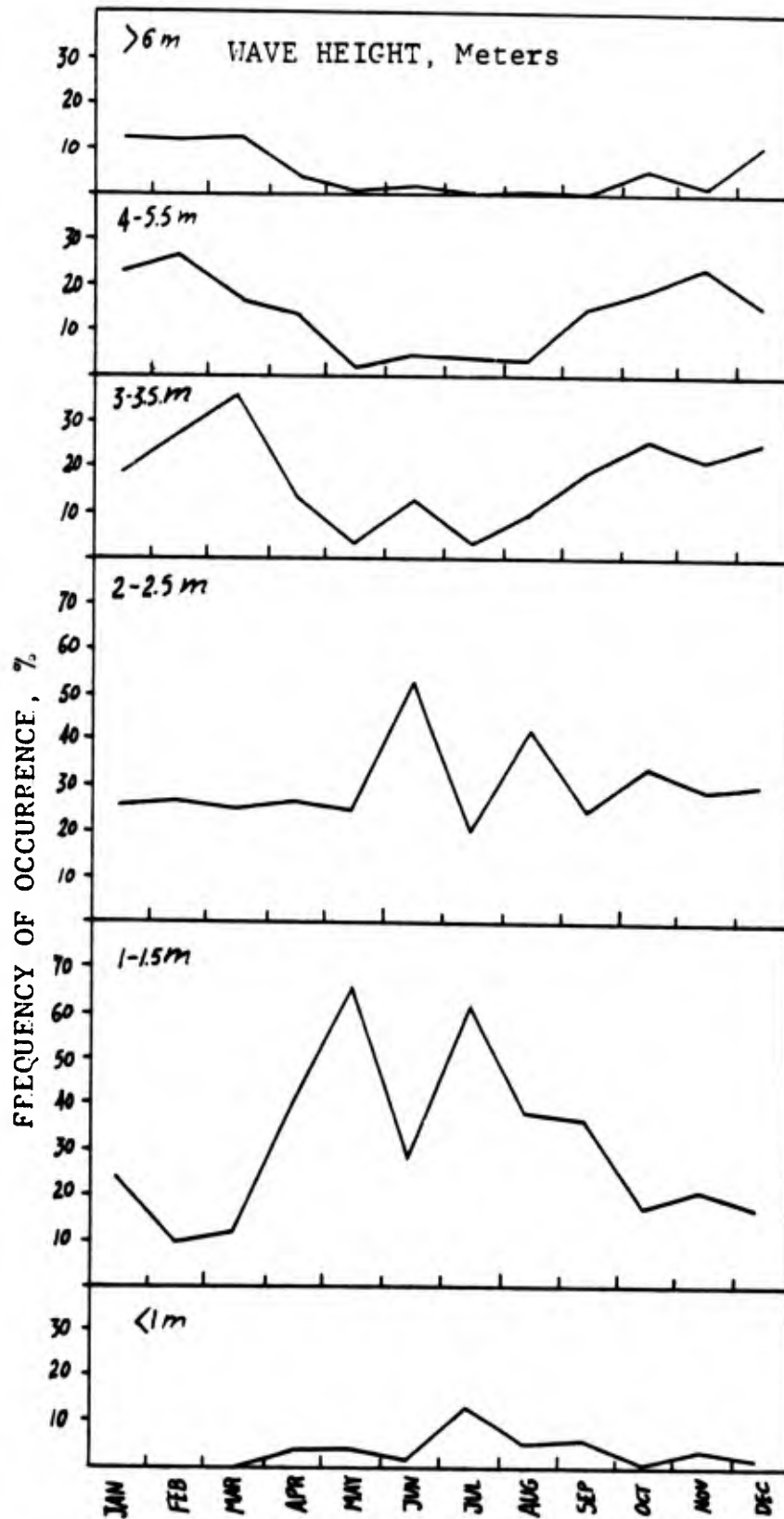


Figure 7. MEASURED MONTHLY FREQUENCY OF OCCURRENCE OF WAVE HEIGHTS FROM OCEAN STATION "BRAVO" IN THE LABRADOR SEA ($56^{\circ}30'N$, $51^{\circ}00'W$).

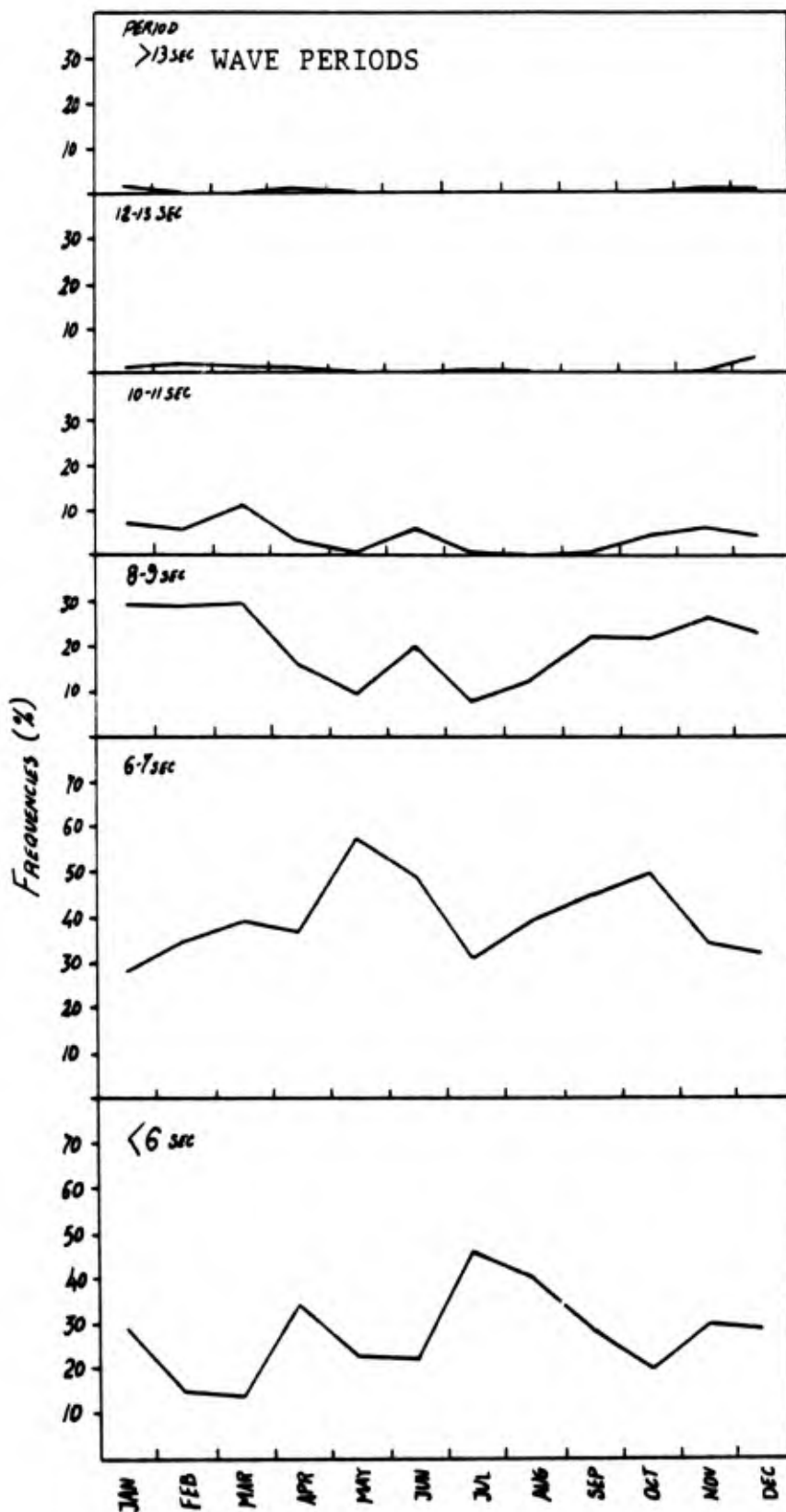


Figure 8. MEASURED MONTHLY FREQUENCY OF OCCURRENCE OF WAVE PERIODS FROM OCEAN STATION "BRAVO" IN THE LABRADOR SEA (56°30'N, 51°00'W).

Chapter 3

ICEBERG STABILITY ESTIMATES

Introduction

In developing a model to estimate deterioration it is important to consider the stability of the iceberg, since as ice is lost either through melting or instantaneously due to calving the iceberg may roll, thus exposing new surfaces to melting and changing the drag characteristics of the bergs. While the theoretical basis exists for making these stability computations, progress in this effort has been hampered by a lack of adequate data.

At the present time the most common measurement of icebergs, other than detailed descriptions and photographs of the above water shapes [used by the Ice Patrol as a classification scheme - Figure 1 of Murray (1969)] are a number of draft measurements. This data is normally presented in terms of the ratio of draft to above-water height, and attempts are made to correlate these observations with the shape classification. A review of the available observations, plus some additional measurements, has been made by Robe (1976).

A comprehensive review of the literature shows that numerous investigators have discussed the problem but few have made any real attempts to provide a simple tool to estimate iceberg stability, with one exception. Using simple static stability theory and sixteen assumed shapes chosen to approximate the above-water classification scheme given by the Ice Patrol, Allaire (1972) predicted minimum stable ratios

Table 1 - ABOVE-WATER ICEBERG SHAPE CLASSIFICATIONS
(Murray 1969)

a. BLOCKY	Steep precipitous sides with horizontal or flat top. Very solid berg. Length: height ratio 2.5:1.
b. DRYDOCK	Eroded so that a large U-shaped slot is formed with twin columns or pinnacles. Slot extends into the water line or close to it.
c. DOME	Large smooth rounded top. Solid type of berg.
d. PINNACLED	Large central spire or pyramid of one or more spires dominating the space. Less massive than dome-shaped berg of similar dimensions.
e. TABULAR	Horizontal or flat-topped berg with length: height ratio of 5:1.
f. GROWLER	A mass of glacial ice that has calved from a berg or is the remains of a berg.

of waterline width to above-water height. He was able to show that these ratios were distinct for each of the four iceberg shape classifications, being approximately 6:1 for blocky or tabular shapes, 4:1 for drydock shapes, 3.8:1 for dome shapes and 1.8:1 for pinnacled shapes. This work was an important step forward but unfortunately required a definitive shape classification before stability estimates could be made, and since most icebergs do not fall into exactly one category the procedure was not particularly simple to use in practice. In addition, even the shapes Allaire selected to be in the same classification showed significant (± 1) variations in the minimum stable width to above-water height ratios.

It is the object of the present chapter to develop a simple computational procedure to estimate stability of any shape iceberg using, as much as possible, information that is available through observation of the above-water portion of the iceberg.

Static Stability Theory

Static stability theory for an iceberg is well known and is determined by the relative positions of G, the center of gravity of the body, and M, the metacenter. As the berg rotates through a small angle, the center of gravity shifts so that the body appears to rotate about the metacenter. Therefore if M lies above G the body is stable while if M lies below G the body is unstable. If M and G are coincident the body is neutrally stable. The most commonly used measure of stability is therefore the distance \overline{MG} , called the metacentric height:

$$\begin{aligned}\overline{MG} > 0 & \quad \text{stable} \\ \overline{MG} = 0 & \quad \text{neutral stability} \\ \overline{MG} < 0 & \quad \text{unstable}\end{aligned}\tag{9}$$

The metacentric height \overline{MG} can also be rewritten, with reference to the definition sketch in Figure 9, as

$$\overline{MG} = \overline{MB} - \overline{BG}\tag{10}$$

where B denotes the center of buoyancy which is located at the centroid of the below-surface berg volume v_b . Also note that the total iceberg volume v is given by

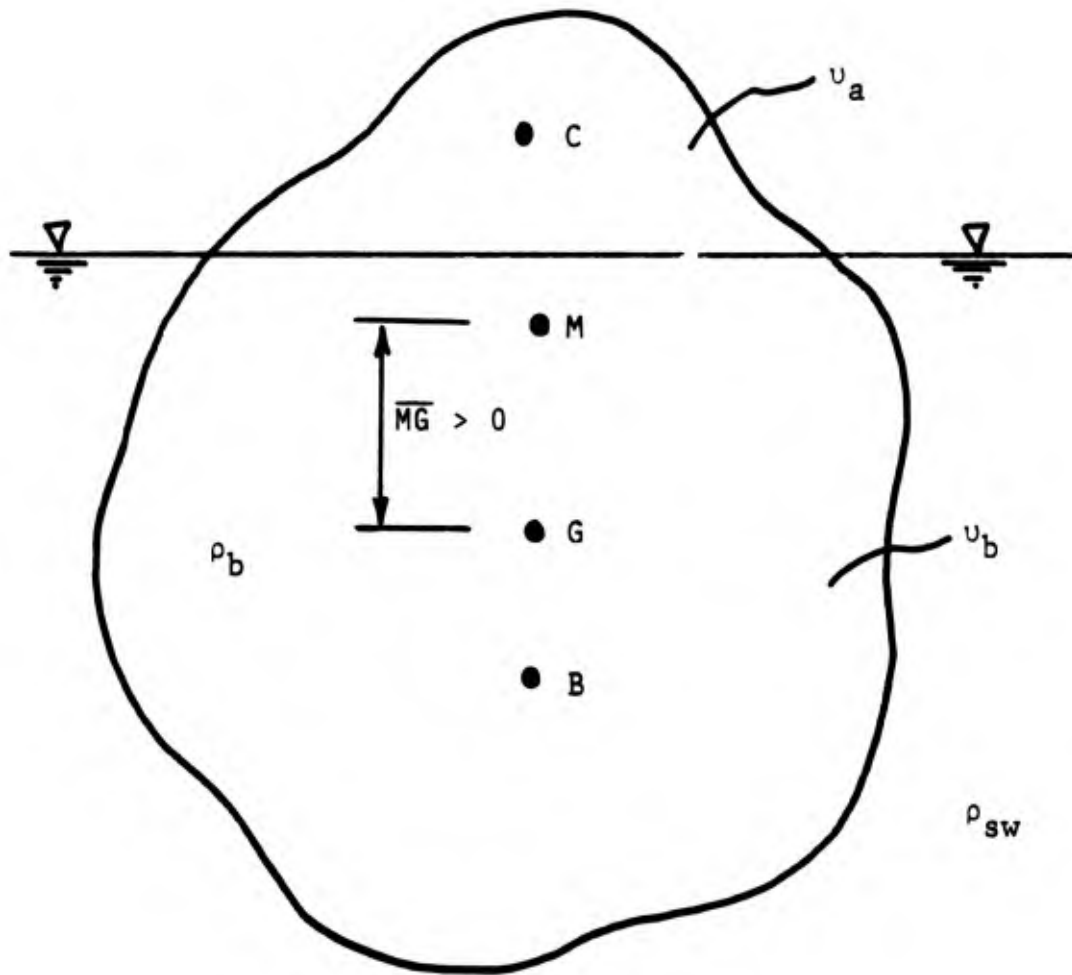


Figure 9. Definition Sketch for Iceberg Stability.

$$v = v_b + v_a \quad (11)$$

where v_a is the above-water berg volume in Figure 9.

Assuming a uniform density body it can be shown that \overline{MB} is given by

$$\overline{MB} = I/v_b \quad (12)$$

where I is the area moment of inertia of the centerline area. Equation (10) can then be written as

$$\overline{MG} = \frac{I}{v_b} - \overline{BG} \quad (13)$$

Taking moments about G it can further be shown that

$$\overline{GB} = \overline{CG} \frac{v_a}{v_b} \quad (14)$$

where C is the center of gravity of the above-water portion of the iceberg. Hence, \overline{MG} is given by

$$\overline{MG} = \frac{I}{v_b} [I - \overline{CG} v_a] \quad (15)$$

Knowing the average density for icebergs, (0.90gm/cm² Smith 1931, Matuso 1966) and sea water, ($\rho_{sw} = 1.027\text{gm/cm}^3$) can relate the total iceberg volume to the below-surface portion by

$$v_b = \frac{\rho_b}{\rho_{sw}} v \approx 0.88 v \quad (16)$$

or to the above-surface portion using Figure 9:

$$v_a = (1 - \frac{\rho_b}{\rho_{sw}}) v \approx 0.12 v \quad (17)$$

Letting

$$\gamma = \rho_b / \rho_{sw} \quad (18)$$

Equations (16) and (17) can be rewritten as

$$v_b = \gamma v \quad (19)$$

$$v_a = (1 - \gamma) v \quad (20)$$

Substituting Equations (19) and (20) into Equation (15) gives

$$\overline{MG} = \frac{1-\gamma}{\gamma v_a} [I - \overline{CG} v_a] \quad (21)$$

Taking the rectangular berg as a simple illustration, it can be shown that

$$\overline{CG} = \frac{1}{2} \gamma H \quad (22)$$

where H is the overall iceberg height. The area moment of inertia about the waterline is

$$I = \frac{1}{12} W_{wl}^3 L \quad (23)$$

where W_{wl} is the waterline width and L is the other horizontal dimension. Also, the above-water volume can be related to the overall height by

$$H = \frac{v_a}{(1 - \gamma) LW} \quad (24)$$

where W is the average berg width and for a rectangular berg $W_{wl} = W$. Substituting Equations (22), (23) and (24) into Equation (21) gives

$$\overline{MG} = \frac{1-\gamma}{\gamma U_a} \left[\frac{W_w l^3 L}{12} - \frac{1}{2} \frac{\gamma U_a}{(1-\gamma) LW} \right] \quad (25)$$

If one further assumes a two dimensional body, $L = 1$ and Equation (25) becomes

$$\overline{MG} = \frac{1-\gamma}{\gamma U_a} \left[\frac{W_w l^3}{12} - \frac{1}{2} \frac{\gamma U_a}{(1-\gamma) W} \right] \quad (26)$$

A cursory analysis shows that iceberg stability depends on the area moment of inertia of the water line area, the position of the center of gravity of the total berg, and the above-water iceberg volume. Although most information necessary to solve Equation (25) can be obtained from observing the above-water portion of the berg, it is clear that information about below-water shape is necessary to determine iceberg stability with high accuracy.

A review of the available literature (Robe et al. 1976; Smith 1931; Murray 1969) shows that iceberg shapes are extremely complex, with randomness often being used to describe their above-water shape. The information on below-water shapes is almost non-existent other than measurements of draft (Robe et al. 1976).

Faced with lack of data but realizing the need to provide a simple estimate of berg stability based on observable (above-water) parameters, it seems that the concept of an equivalent rectangular berg can be a useful tool. For instance, the total berg volume could be estimated using Equation (20) and the empirical relationship outlined by Robe and Farmer (1976):

$$v_a = 0.41 L_c W_c H_c \quad (27)$$

where L_c , W_c , and H_c are the longest side, shortest side, and highest height, respectively. Given this information and a relationship between the waterline width and the average berg width such as

$$W = C_o W_{wl} \quad (28)$$

where C_o is an empirically determined constant, one could use Equation (26) to determine berg stability.

The final recommended engineering estimate for iceberg stability is the following approximation:

$$\overline{MG} = \frac{(1-\gamma) W_{wl}^3}{12 \gamma v_a} - \frac{1}{2 C_o W_{wl}} \quad (29)$$

where v_a should be interpreted as the above-water volume per unit length normal to the plan view, that is, the above-water elevation area. Through this relation all information necessary to estimate iceberg stability can be obtained from simple above-water iceberg dimension measurements, except for the width parameter C_o . Also, the need to type-classify bergs in order to estimate stability (Allaire 1972) is eliminated.

Equation (29) could be employed in several plan views to evaluate pitch and roll stabilities, with values of W and v_a being estimated.

The key to success of this methodology depends on the ability to accurately estimate the dimensions of the above-water portion of the berg and to determine a value for the width parameter C_o . Since the first problem has been

addressed in detail by Robe et al. (1976), it remains only to address the second.

Restricting the analysis to two-dimensional bodies, a computer program was developed to predict the stability of arbitrarily shaped icebergs using the theory outlined above. Body dimensions were varied by changing the above-water height-to-waterline width ratio to determine the neutral stability condition ($M^* = 0$). Equation (29) then allowed a calculation of the width parameter C_0 to best represent each shape. The goal of this effort was to determine if a generally applicable value of C_0 could be found.

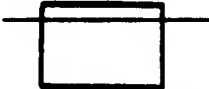
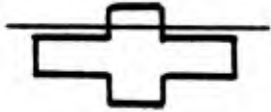
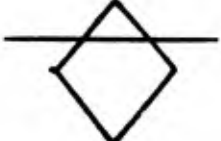
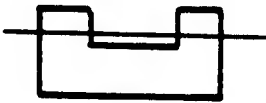
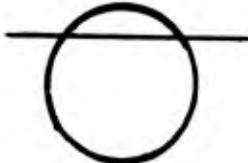
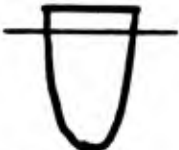
The results of this analysis are shown in Table 2 for a variety of different shapes. The first seven shapes in the table are those used by Allaire (1972), while the last two represent composites derived from all available data on underwater berg shape. A review of the table shows wide variations in C_0 , particularly for the pyramid, cross, and diamond. Fortunately, shapes such as these are not likely to be common. The remaining shapes then display only a $\pm 20\%$ variation from a constant-width approximation. Hence it appears possible to provide at least a first-order estimate of C_0 which might be generally applicable. Arbitrarily selecting the rectangular dry dock, half ellipsoid, nontabular, and tabular shapes as representative gives $C_0 = 0.93$ by a simple arithmetic average.

It is interesting to note that given the $\pm 10.5\%$ error estimated in measuring the iceberg volume when photographs

are analyzed in detail (Robe and Farmer 1976) results in a $\pm 20\%$ error in calculating the second term in Equation (25). This suggests that the error introduced by uncertainties in C_0 are probably no worse than those involved in iceberg volume measurements.

A simple test was established to gain additional insight into the problem of estimating stability, given one's ability to estimate the above-water volume and assuming a fixed value of C_0 . Five arbitrarily shaped icebergs were constructed and the computer program located the approximate waterline and calculated \overline{MG} for each. The test subject was then given a sketch of the above-water portion of the body with the waterline width and maximum above-water heights given and asked to compute \overline{MG} using Equation (29) with $C_0 = 0.93$. All persons thus tested correctly predicted the sign of \overline{GM} with the absolute error depending on one's ability to calculate the above-water volume (area, in this case). Errors inherent in finding the above-water volumes were in general larger than those which could be attributed to uncertainty in C_0 . The shapes tested are shown in Figure 10. The reader is invited to take the same test.

TABLE 2

		WIDTH PARAMETER
SHAPE		C_0
1. PYRAMID		1.39
2. RECTANGLE		1.00
3. CROSS		1.89
4. DIAMOND		1.31
5. DRY DOCK		0.98
6. CIRCULAR		1.15
7. HALF ELLIPSOID		0.92
8. NON TABULAR		0.81
9. TABULAR		0.93

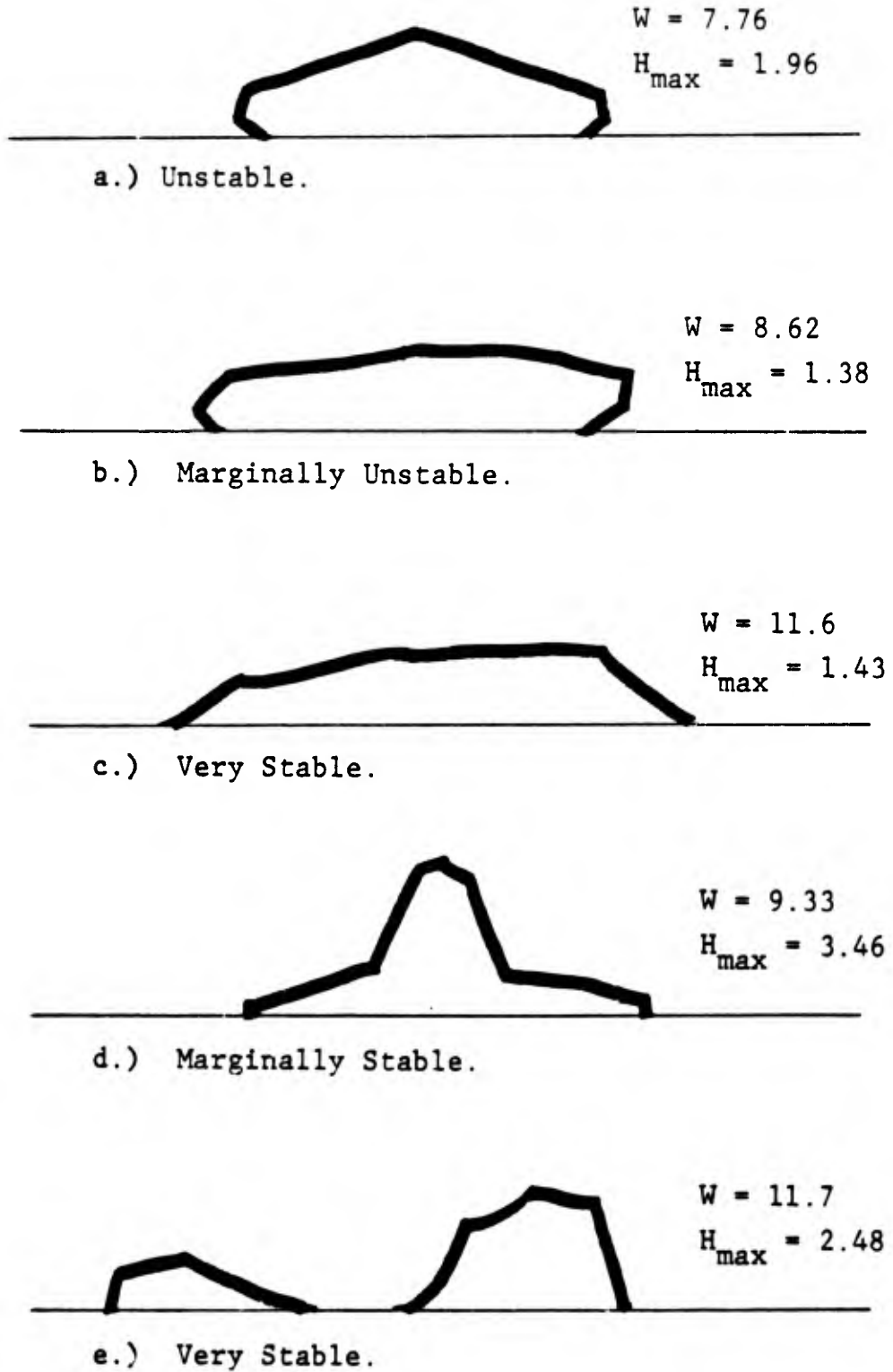


Figure 10. ESTIMATION OF ICEBERG STABILITY FROM OBSERVED ABOVE-WATER SHAPE, USING Eq. (29).

Tabular and Nontabular Composite Shapes

At present there are no definitive below-water shape classifications similar to Table 1 for the above-water geometries. Apparently only a portion of the existing measurements of underwater shape are available in the open literature. Both shape and draft have been measured, by both sonar and radar techniques, and there are at least four published works on below-water shapes: Robe (1976), Robe and Farmer (1976), Sukov (1977), and Rossiter and Gustajtis (1978). In addition, certain below-water size classifications have been suggested by Mountain (1979).

The heat transfer and dynamic response computations in the present report suggest that some attention should be paid to below-water shape. Therefore, based upon the data sources listed above, we have proposed two generic shapes - tabular and nontabular - which represent to some reasonable approximation the variety of iceberg shapes occurring in the field.

Figure 11 shows our model shape selected to represent a large, symmetric, "tabular" iceberg below-water shape. The theoretical static stability of this shape is given by the computer-graphic display in Figure 12. The bar chart showing "arms" denotes the horizontal distance between the center of gravity G and the center of bouyancy B. For static equilibrium, the arm should be zero, and we see in Figure 12 that this occurs at reference angles of 0° , 87° , and 180° .

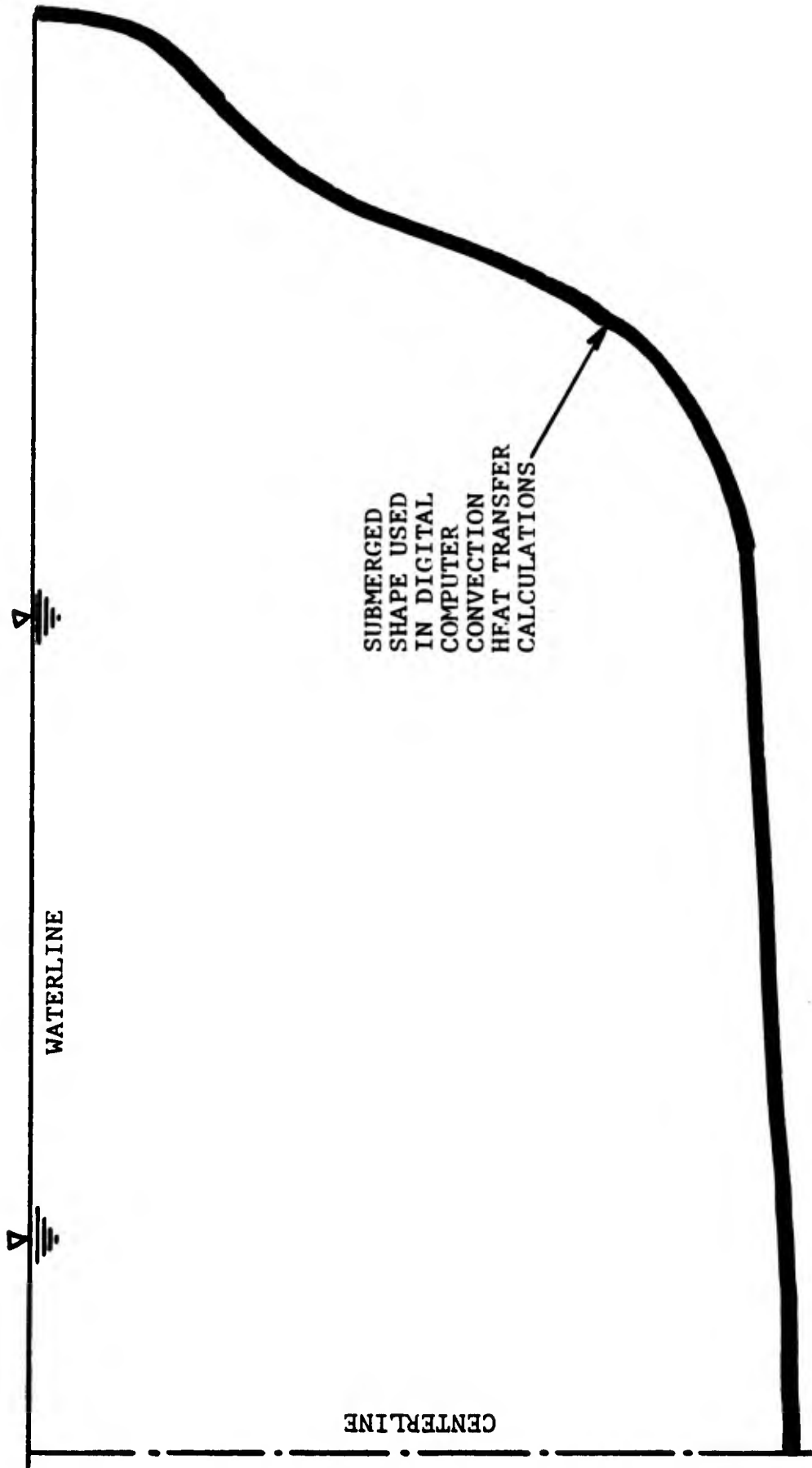


Figure 11. COMPOSITE MODEL OF A LARGE 'TABULAR' ICEBERG

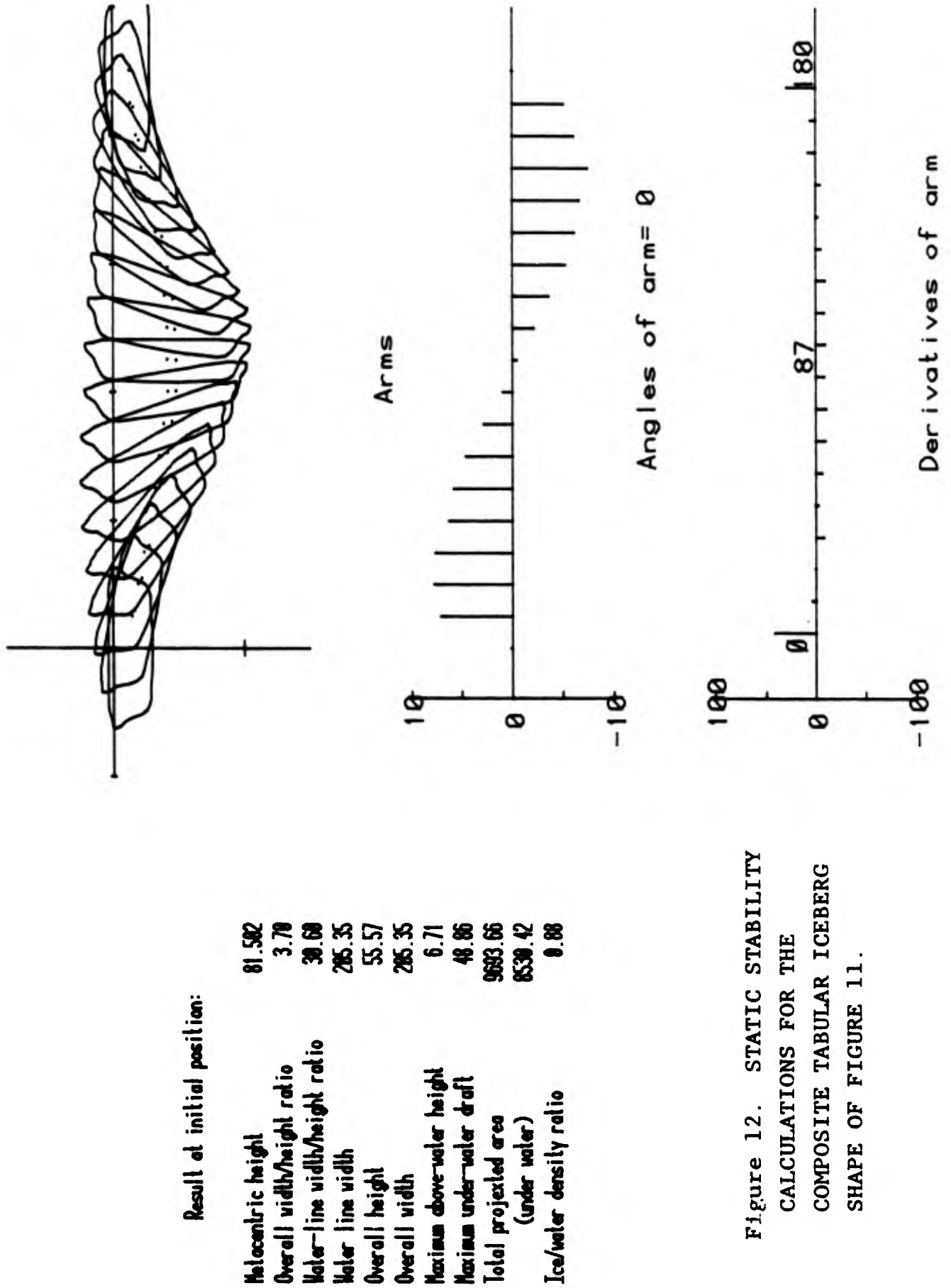


Figure 12. STATIC STABILITY
CALCULATIONS FOR THE
COMPOSITE TABULAR ICEBERG
SHAPE OF FIGURE 11.

static stability, the "derivative of the arm", which represents the metacentric height, must be positive. We see that this occurs only at 0° and 180° , not at 87° . Thus our proposed "tabular" berg is stable floating lengthwise, either side up, and we assume that an angle of 0° is its normal position.

Figure 13 shows our proposed below-water shape of a small, symmetric, "nontabular" berg. The stability display for this shape is given in Figure 14, showing static equilibrium (zero arm) at 0° , 62° , 127° , and 180° . The metacentric height is positive only at 0° and 127° . It is possible that this smaller, more compact iceberg could be overturned by a storm or large waves or a small amount of melting changes. Again we assume that its normal position is at 0° angle.

Drag measurements for these two composite iceberg shapes will be given in Chapter 4, and convective heat transfer computations are given in Chapter 6.

In closing this section on static stability considerations, we direct the reader's attention to the very interesting paper by Benedict (1979), who models the below-water shapes by three different methods: ellipsoids, collections of small cubes, and a power-series of spherical harmonic shape functions.

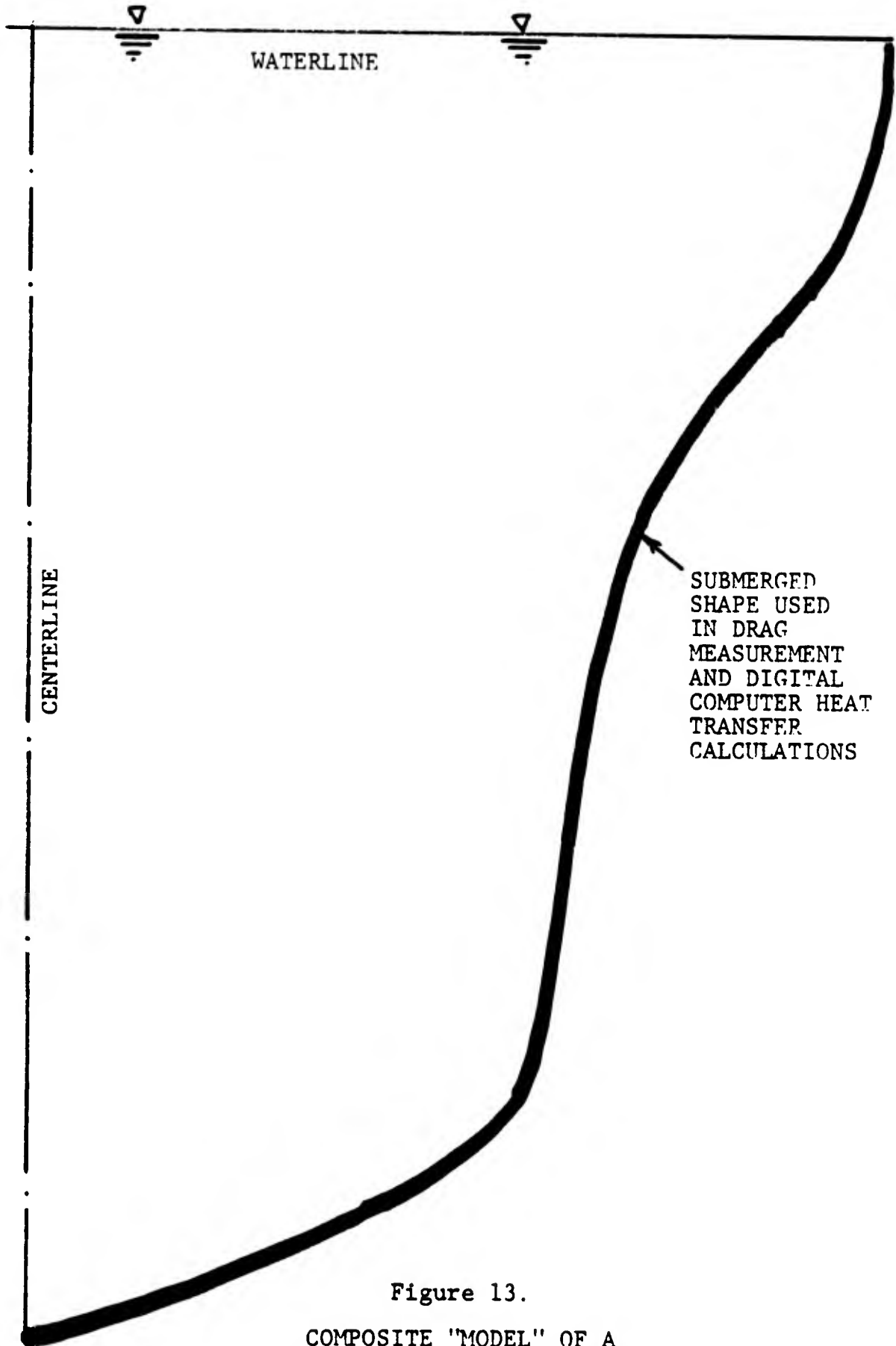


Figure 13.
COMPOSITE "MODEL" OF A
NON-TABULAR ICEBERG

Result at initial position:

Melocentric height	21.883
Overall width/height ratio	1.33
Water-line width/height ratio	11.28
Water line width	149.71
Overall height	113.12
Overall width	150.88
Maximum above-water height	13.37
Maximum under-water draft	99.75
Total projected area	11622.81
(under water)	18227.37
Ice/water density ratio	0.88

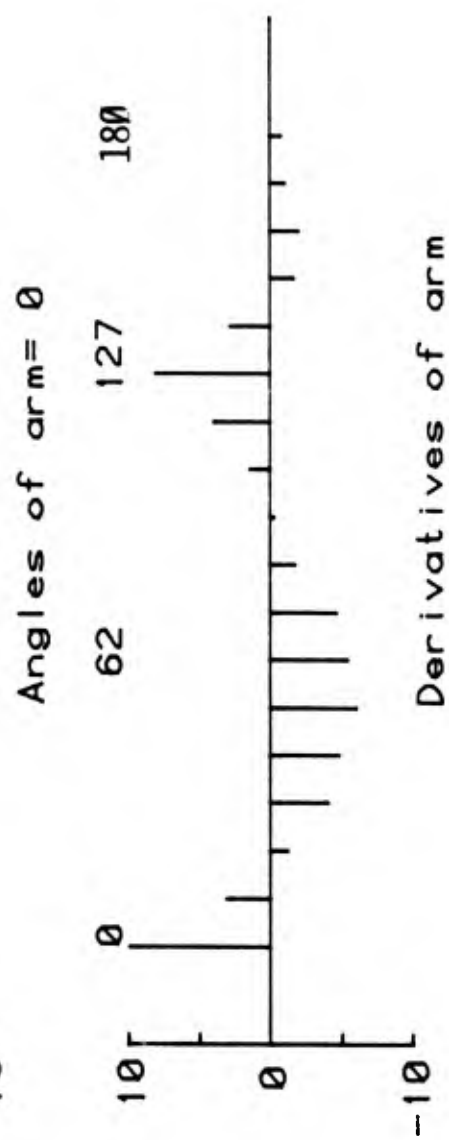
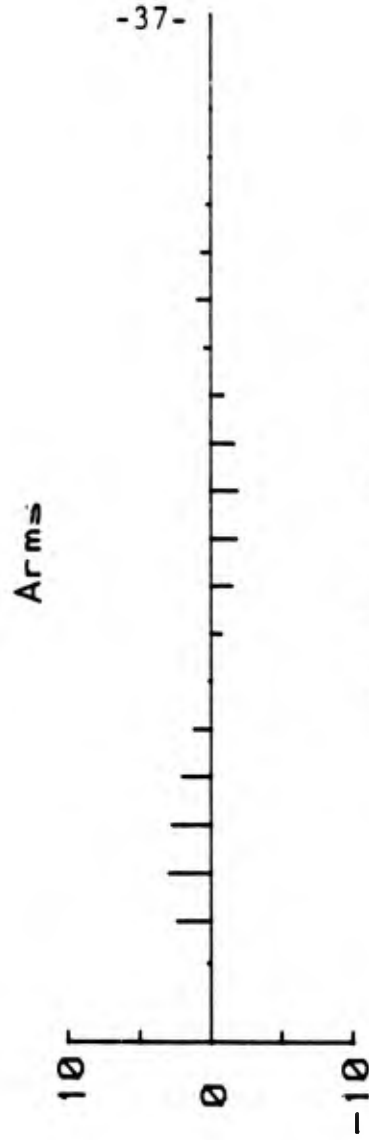
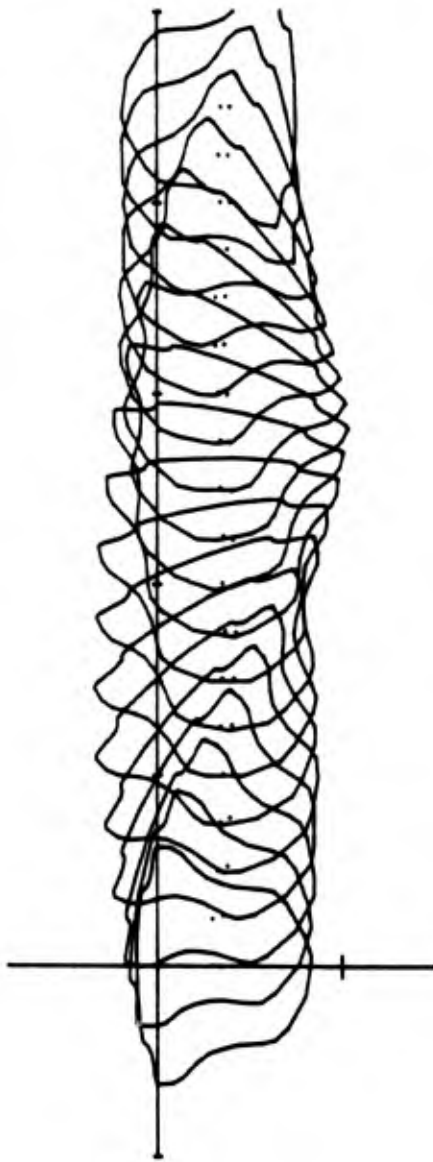


Figure 14. STATIC STABILITY
CALCULATIONS FOR THE
COMPOSITE NON-TABULAR
BERG SHAPE OF FIGURE 13.

Chapter 4

ELEMENTARY ICEBERG DYNAMICS

Introduction

Chapter 3 treated iceberg statics; here we develop some elementary results for iceberg dynamics. It is clear that forced convection due to relative motion between the seawater and the berg can be a major contribution to the melting process. In particular, the wind, causing drag on the exposed surface, can drive an iceberg at a quite different velocity from the local water currents. The wind will also drive the surface waters and set up a depth-variable water current profile. Finally, we need to estimate the transient motion of an iceberg subjected to variable winds or currents.

Simplified Equation of Motion

For tracking a drifting iceberg, one needs to account for the transient three-dimensional wind and current fields and to solve for berg position in the two horizontal coordinates, including Coriolis and geostrophic effects. A detailed iceberg-drift model of this type has been developed by Mountain (1979) and used by the U. S. Coast Guard to predict the positions of individual icebergs with reasonable accuracy. A similar but less complex model was given by Murray (1969). Data on drifting icebergs have been taken by Robe and Maier (1979), Robe, Maier and Russell (1979), and by Riggs et al. (1979). This type of theory and experiment was a key topic at the Iceberg Dynamics Symposium in 1979.

For short-term iceberg melting computations, it is not necessary to know the exact track of the berg. Rather, one needs to estimate the relative wind and water velocities near the berg over, say, a one-day period. Coupled with data for average local water and air temperature, these relative velocities should be sufficient to predict the average mass loss due to convection for that day. We therefore assume that the iceberg relative velocity can be predicted by a one-dimensional force balance:

$$\begin{aligned} \text{Iceberg relative acceleration} &= \\ &= \text{Net wind drag} + \text{Net water drag} \end{aligned} \quad (30)$$

Let subscripts "a" and "w" denote the air and water, respectively. Then Eq. (30) may be rewritten in terms of the drag coefficients and relative velocities:

$$m(1 + C_M) \frac{d}{dt}(V - V_w) = \frac{1}{2} C_{Dw} \rho_w A_w (V_w - V) |V_w - V| + \frac{1}{2} C_{Da} \rho_a A_a (V_a - V) |V_a - V| \quad (31)$$

where V is the iceberg velocity and C_M is its hydrodynamic mass coefficient (White 1975). Even though $\rho_a \ll \rho_w$, the two drag terms may be comparable since $V_a \gg V_w$. Equation (31) may be solved for iceberg velocity $V(t)$ given various scenarios for wind and water motion $V_a(t)$ and $V_w(t)$. In the present analysis we have neglected Coriolis effects.

Response to a Sudden Change in Water Velocity

As an initial example, suppose that air drag is negligible and that an iceberg at rest suddenly encounters a water current velocity of speed V_0 . Then Eq. (31) reduces to

$$(V_0 - V)^{-2} d(V_0 - V) = K dt, \quad K = \frac{C_{Dw} \rho_w A_w}{2m(1+C_M)} \quad (32)$$

The variables are separated and may be integrated from $t = 0$, $V = 0$, to any velocity $V(t)$. The result is

$$V/V_0 = KV_0 t / (1 + KV_0 t) \quad (33)$$

Thus, if V_0 is constant, the iceberg accelerates and eventually approaches the water velocity $V = V_0$. The iceberg reaches 95% of its final velocity V_0 at a time

$$t_{95\%} = 19 / (KV_0) \quad (34)$$

The parameter K from Eq. (32) has dimensions of inverse length. If we define an iceberg length scale L as the ratio of total iceberg volume to its total frontal area A , then

$$K = \frac{C_{Dw}}{2(1+C_M)} \frac{\rho_w}{\rho_i} \frac{A_w}{A} L^{-1} \quad (35)$$

Further, for a rectangular or blocky (tabular) berg, the term $(\rho_w A_w / \rho_i A)$ is equal to unity. For this case, Eq. (35) reduces to

$$t_{95\%} = \frac{L}{\bar{V}_0} \frac{38(1+C_M)}{C_{Dw}} \quad (\text{Sudden current } V_0) \quad (36)$$

If we assume, for example, that $C_{Dw} \doteq 0.8$ and $C_M \doteq 0.5$, Eq. (36) predicts that $t_{95\%} \doteq 71 L/V_0$, or the time to approach final berg velocity equals the time it takes the water current to move 71 iceberg lengths. This time is of the order of several hours, e.g. if $L = 300$ m and $V_0 = 50$ cm/s, we compute $t_{95\%} \doteq 43000$ s = 12 hours. During this time, there will be substantial differences between the iceberg and water velocity and hence forced convection melting may be important.

Effect of the Basset History Term

Equation (30) is a balance between drag and inertia terms for the iceberg. It has long been known that a body accelerating in a viscous fluid also encounters a so-called "history" term, first derived by Basset (1888) for very small (creeping flow) Reynolds numbers. Experiments have shown that the Basset history term can be important for bodies accelerating at Reynolds numbers as high as 10^5 (Clift et al. 1978). The question arose at the June 1979 Iceberg Dynamics Conference as to whether the history effect might even be important for an iceberg. No answer was forthcoming at that time, so here we make an illustrative computation to illustrate its effect.

The Basset history term arises because a body accelerating in a viscous fluid begins to wallow, so to speak, in its own previously created vorticity, thus altering its instantaneous force balance. In the notation of Odar (1969), the history

term is an effective "force" to be added to the right hand side of Eq. (31):

$$F_{\text{history}} = C_H A_w \left(\frac{1}{\pi} \rho_w \mu_w \right)^{\frac{1}{2}} \int_0^t \frac{dV}{dt'} (t-t')^{-\frac{1}{2}} dt' \quad (37)$$

where C_H is a dimensionless "history coefficient". We are neglecting the history effect of the air on the exposed iceberg because of the small density and viscosity of air. Odar (1969) recommends a value $C_H = 6.0$ for a spherical body at low acceleration rates, which we take as a reasonable approximation for an iceberg.

Adding Eq. (37) to the right hand side of Eq. (31), one can repeat the computation of $V(t)$ for an iceberg accelerated from rest by a sudden water velocity, neglecting winds. This time, because of the complexity of Eq. (37), a digital computer solution is necessary. The results are shown in Figure 15. The history effect reduces the acceleration and increases the time to reach terminal velocity. However, Figure 15 shows that the effect is very small for iceberg Reynolds numbers ($10^6 - 10^8$) and can be ten percent or more for Re less than 10^5 . In iceberg dynamics, then, we conclude that the Basset history effect can be safely neglected.

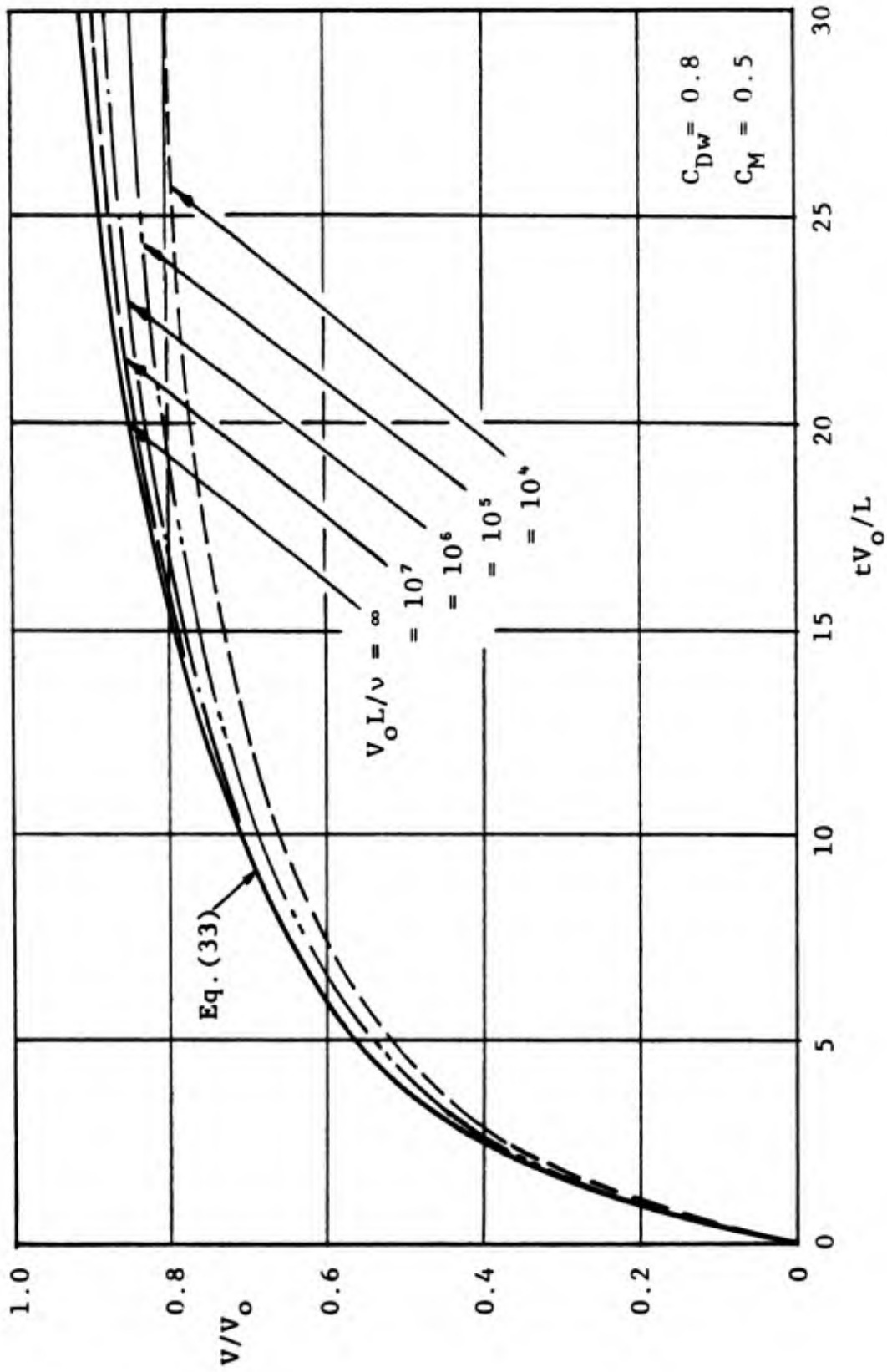


Figure 15. RESPONSE OF A FLOATING ICEBERG TO A CURRENT WHICH SUDDENLY CHANGES FROM ZERO TO SPEED V_0 . THE DYNAMIC MODEL INCLUDES THE BASSETT HISTORY TERM, WHICH VARIES WITH REYNOLDS NUMBER.

Response of an Iceberg to Sudden Wind Velocity

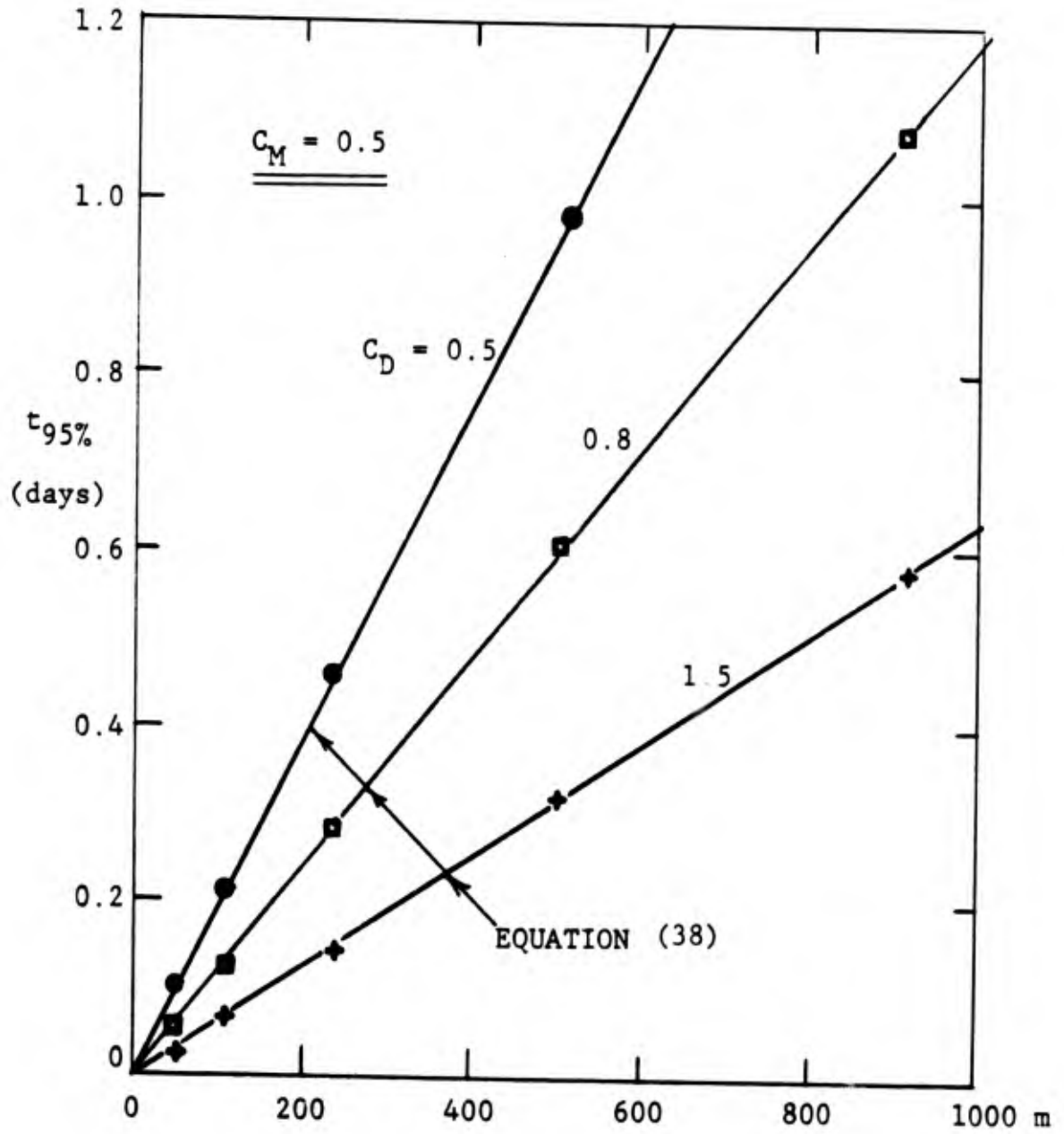
Now consider the case where the iceberg is at rest with negligible water velocity and is suddenly subjected to a wind velocity of speed V_a . Equation (31) applies, but the water-drag term cannot be neglected, because the wind drives the berg until it develops a significant relative velocity with the water. Since the exact solution for this coupled wind-water case is not known to the writers, Eq. (31) was solved on a digital computer for $V(t)$, assuming for simplicity that $C_{Da} = C_{Dw}$ for assumed winds of various speeds. Figure 16 is for ten-knot winds (5.14 m/s) and shows the time $t_{95\%}$ for the iceberg to reach 95% of its final steady wind-driven motion. The computed times have the same form predicted by Eq. (36) but with a different coefficient:

$$t_{95\%} = \frac{L}{\bar{V}_a} \frac{280(1+C_M)}{C_D} \quad (\text{Sudden Wind } V_a) \quad (38)$$

These times are comparable to Eq. (36) and of the order of hours. For example, if $L = 300$ m, $V_a = 10$ m/s, $C_D = 0.8$, and $C_M = 0.5$, Eq. (38) predicts $T_{95\%} = 15750$ s = 4.4 hours.

Steady Wind-Driven Iceberg Motion

If the winds are steady, after a start-up time given by Eq. (38), the iceberg will be driven at a steady velocity which balances the wind and water drag. From Eq. (31) with zero relative acceleration, the final iceberg velocity V_f must be such that, if Coriolis effects are neglected,



CHARACTERISTIC LENGTH: $L = \frac{\text{ICEBERG VOLUME}}{\text{FRONTAL AREA}}$

Figure 16. RESPONSE OF AN ICEBERG TO SUDDENLY APPLIED TEN-KNOT WINDS: TIME TO REACH 95% OF THE FINAL WIND-DRIVEN VELOCITY. PLOTTED POINTS ARE DIGITAL COMPUTER SOLUTIONS.

$$C_{Da} \rho_a A_a (V_a - V_f)^2 = C_{Dw} \rho_w A_w (V_f - V_w)^2 \quad (39)$$

This may be solved for either V_f or, more appropriately, the relative velocity $V_f - V_w$:

$$V_f = \frac{V_a + B V_w}{1 + B} \quad (40)$$

$$V_f - V_w = \frac{V_a - V_w}{1 + B}$$

where $B = (C_{Dw} \rho_w A_w) / (C_{Da} \rho_a A_a)$ is a dimensionless shape factor of order fifty. Since typical wind speeds, especially in the Labrador Sea area (Figure 6) are two orders of magnitude greater than water currents, the relative velocity is given to excellent accuracy by

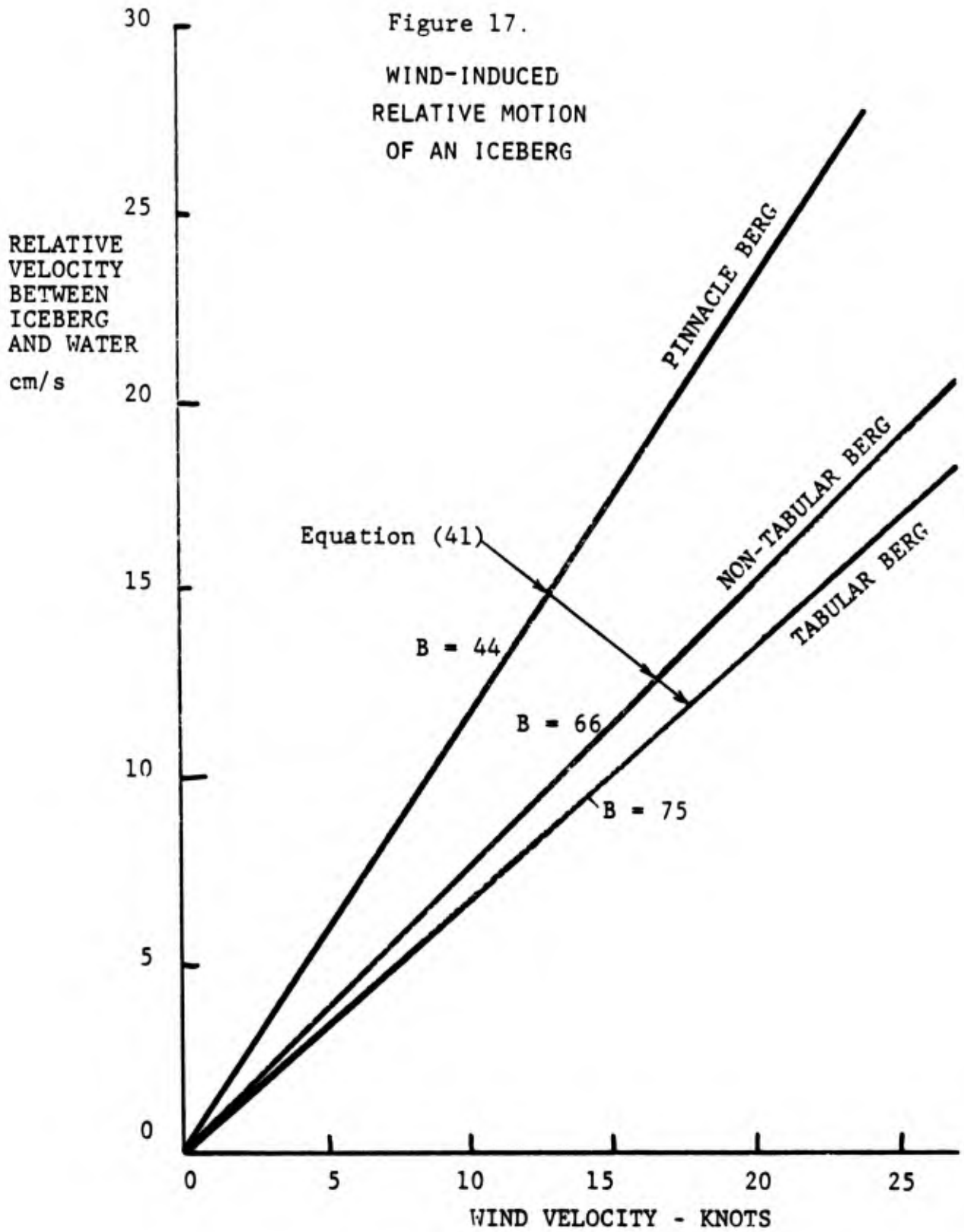
$$V_f - V_w \doteq V_a / (1+B) \quad (41)$$

The shape factor B may be estimated from drag data for various geometries simulating the exposed and submerged portions of an iceberg (Pao 1961, White 1979), plus data for actual iceberg shapes given in the present chapter (Figures 19 and 20). The results vary with the iceberg shape and may be estimated as follows:

Pinnacle berg:	$B \doteq$	44 ± 5	
Non-tabular berg:	$B \doteq$	66 ± 8	(42)
Tabular berg:	$B \doteq$	75 ± 9	

Figure 17 plots the relative velocity from Eq. (41) for these three iceberg shapes. Since prevailing wind speeds in the Labrador Sea are from 10 to 30 knots, icebergs subjected to steady winds would be driven at relative velocities from 5 to 30 cm/s, which can result in significant forced convection melting rates on the submerged surface. We will return to Figure 17 later after having developed a suitable forced convection melting rate formula for tabular and non-tabular icebergs.

As mentioned, a steady wind will not only drive the iceberg at some relative velocity but will also set up a wind-driven current profile in the water. Available data and theory on wind-driven current profiles are summarized in a comprehensive review paper by Huang (1979). The profiles take several hours to set up and extend downwards from 5 to 50 meters, depending upon wind duration and the surface water stratification. Recent theories for wind-driven surface layers are given by Madsen (1977) and by Reed (1980). When fully set-up, the maximum surface velocity is approximately 2%-3% of the wind speed. As seen in Eq. (40), such a surface velocity would have a negligible effect on the magnitude of the wind-driven relative velocity $V_f - V_w$. However, the existence of a variable wind-driven current profile could result in significant differences (10-20 cm/s) in relative current speeds from the waterline to the bottom of an iceberg. Thus, even in the initial stages of wind effects, forced convection will be an important melting mechanism.



Measurements of Submerged Body Iceberg Drag

The writers could find no published data on the drag of actual iceberg shapes. Mountain (1979) uses a value $C_D = 1.5$ in his dynamic model but cites no source for this assumption. Since some of the dynamic results given here are strongly dependent on C_D , such as Figure 16, it was decided to perform some simple experiments on iceberg submerged shapes.

The University of Rhode Island has a 35-meter-long tow tank and it would be possible to measure iceberg drag by towing model icebergs in this tank. However, the force on a small towed model is dominated by wave drag, whereas icebergs are so large that their wave drag is negligible. It was therefore decided to eliminate wave drag entirely by testing the submerged shape of an iceberg in a wind tunnel. Two submerged shapes were tested: the "tabular" shape defined by Figure 11, and the "non-tabular" shape of Figure 13.

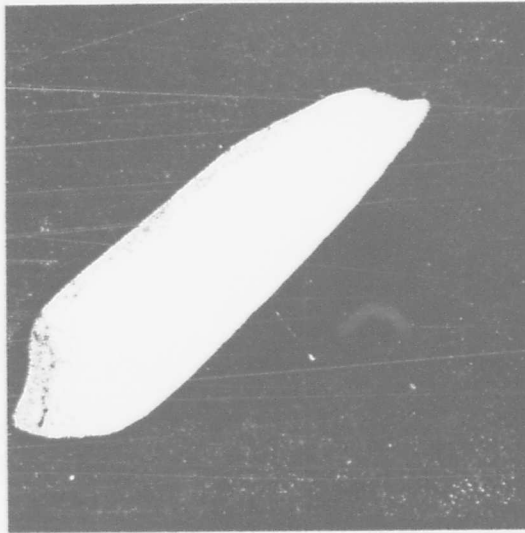
The iceberg models were constructed and tested by Peter G. McFadden, a senior mechanical engineering student at the University. The models were made by covering a Styrofoam base with plaster molded to fit the shapes of Figures 11 and 13. After drying, the plaster was sanded to an average roughness of less than one millimeter. The models had an average length of 50 cm and a frontal area of approximately 600 cm^2 . The wind tunnel at the University of Rhode Island has a test section area of 8500 cm^2 , thus model blockage was about 7%. Maximum tunnel air velocity is 31 m/s, giving a maximum model Reynolds number of 10^6 . This is much less

than a typical iceberg Reynolds number of 10^7 , but the drag coefficient of blunt bodies is relatively insensitive to high Reynolds numbers (White 1979).

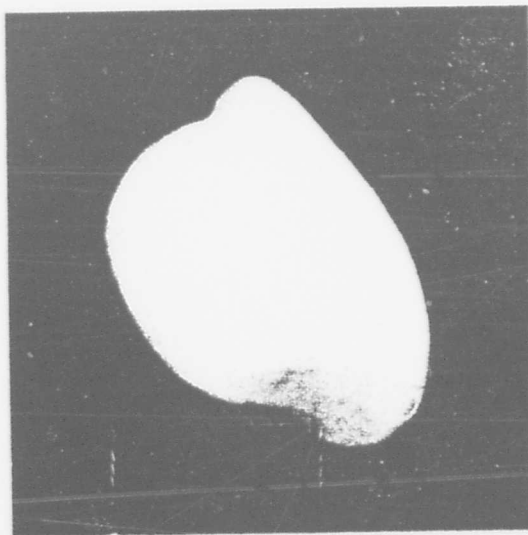
Figure 18 shows the non-tabular berg model which was tested. Both models were mounted upside down (compared to an actual submerged iceberg) near the floor of the tunnel test section, and the drag was measured for speeds between 3 and 31 m/s. Corrections were made for model blockage and the clearance between the model and the floor.

Figure 19 shows the measured drag coefficient of the non-tabular berg model (similar to Figure 13). Transition of the laminar boundary layer, with a corresponding drop in the drag coefficient, seems to occur at about $Re_L = 2 \times 10^5$. A turbulent boundary layer on the model seemed fully established at about $Re_L = 5 \times 10^5$, as determined by inspection of tiny threads attached to the model for flow visualization. At the highest Reynolds number tested, 8×10^5 , the non-tabular berg drag coefficient is $C_D \approx 0.77$, which is thought to be a reasonable estimate for C_D of a real iceberg of this general shape.

Figure 20 shows the measured drag coefficient of the tabular berg model (similar to Figure 11). The body is relatively slender, closer to a "wing" than a blunt obstruction, and the laminar boundary layer undergoes transition without a large change in C_D . Turbulence seemed fully established at about $Re_L = 8 \times 10^5$. At the highest Reynolds



a) Tabular model.



b) Non-tabular model.

Figure 18. Wind tunnel models for measuring the submerged-body drag of an iceberg.

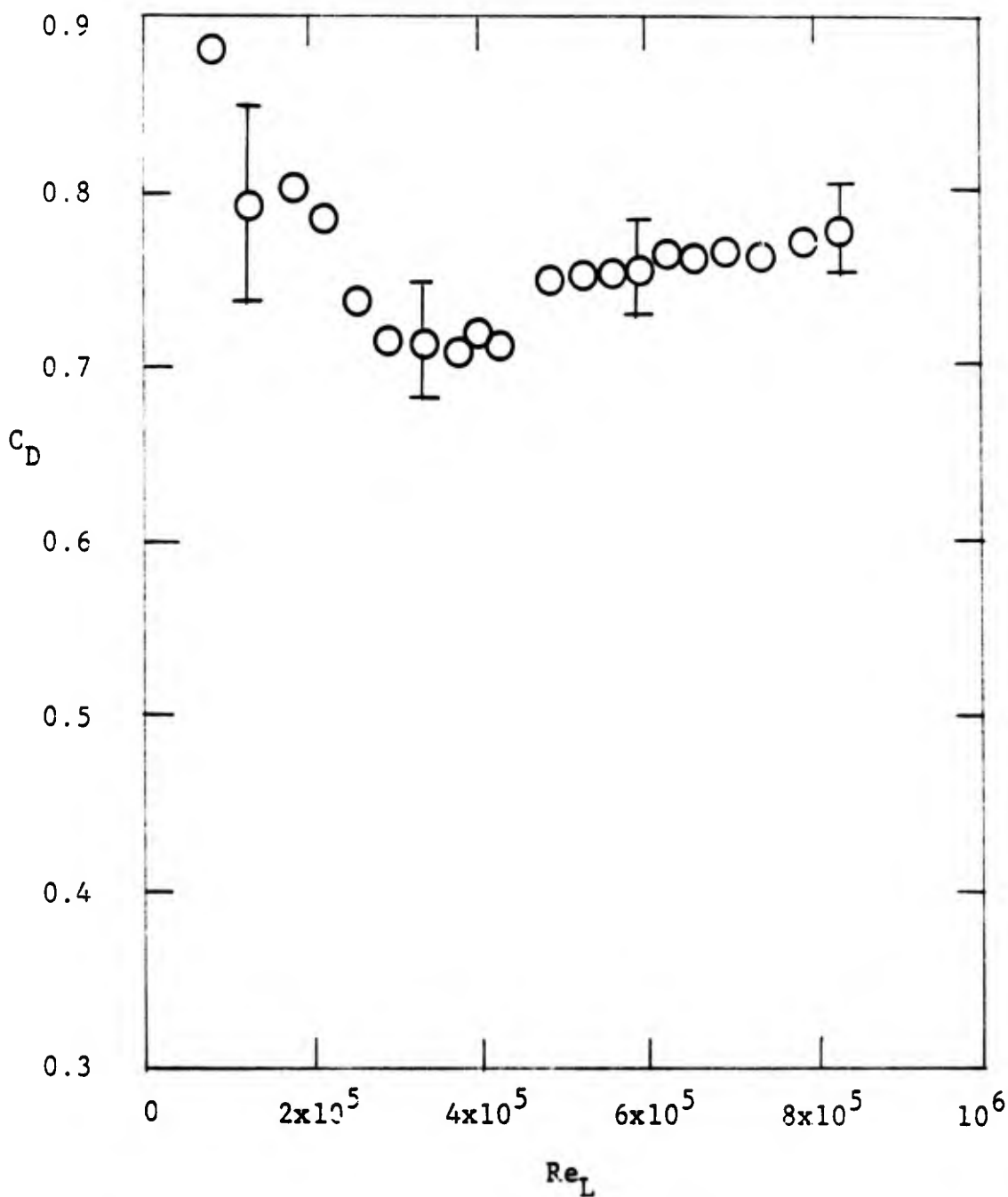


Figure 19. DRAG COEFFICIENT (BASED ON FRONTAL AREA)
OF THE SUBMERGED PORTION OF A MODEL NON-TABULAR BERG.
(SEE FIGURE 13)

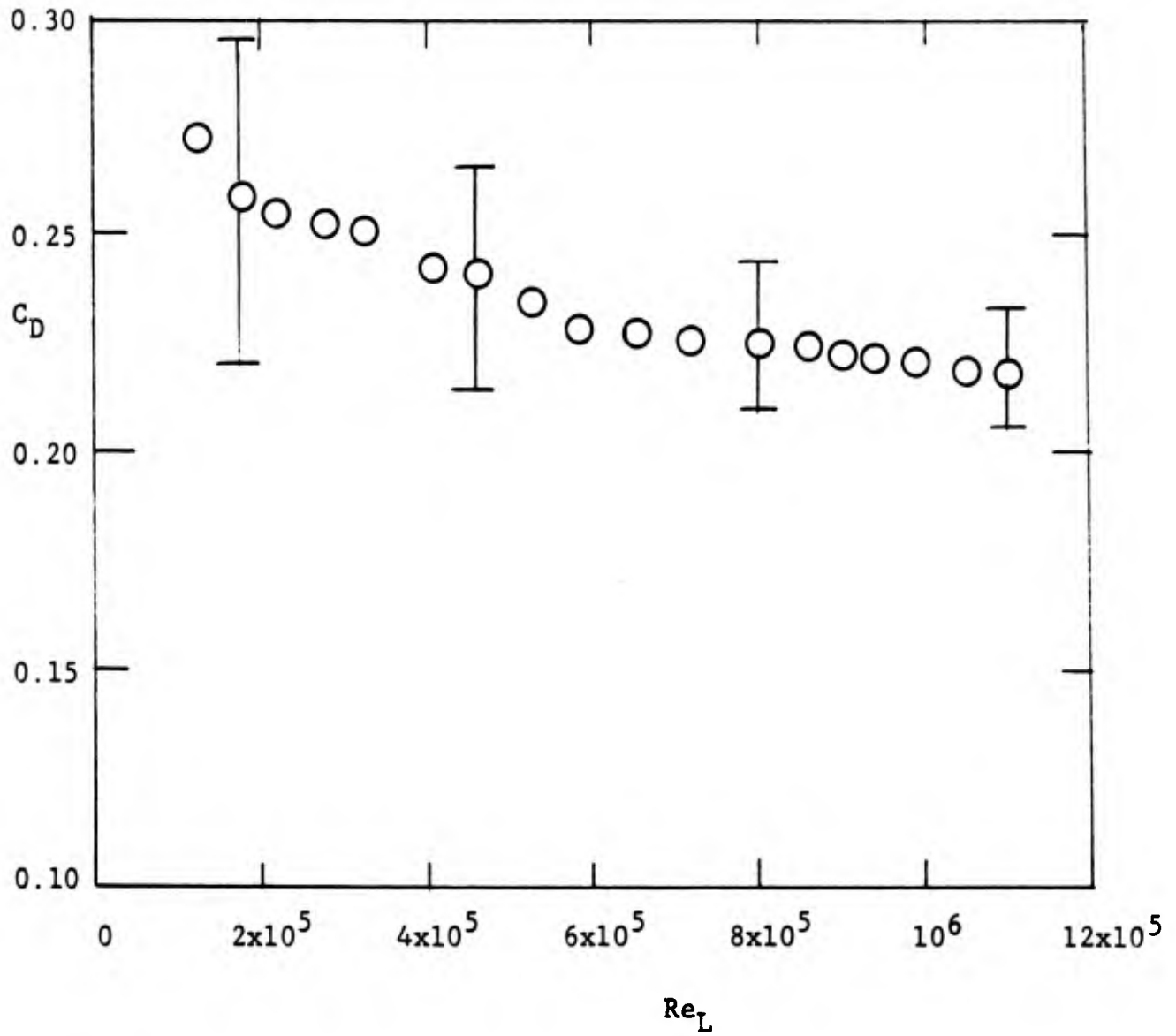


Figure 20. DRAG COEFFICIENT (BASED ON FRONTAL AREA)
OF THE SUBMERGED PORTION OF A MODEL
TABULAR ICEBERG (SEE FIGURE 11).

number tested, 1.1×10^6 , $C_D \approx 0.22$, which is also thought to be a reasonable estimate for a real iceberg of this shape.

This drag data, although limited to only two simulated shapes, indicates that the drag coefficient of the submerged portion of an iceberg is strongly dependent on berg shape. When based on frontal area, a relatively flat berg has a surprisingly small drag coefficient. A non-tabular berg, with a relatively high draft-to-width ratio, has a drag coefficient of approximately 0.8. It appears that a drag coefficient of 1.5 is probably not realistic except possibly for extremely rough surfaces or irregular shapes such as a drydock-type iceberg.

Chapter 5

SURFACE MELTING DUE TO INSOLATION

Because of the high density and thermal conductivity of seawater, it is clear that most of the melting of an iceberg takes place on its submerged surfaces. At the same time, a minor but steady source of melting is the effect of solar radiation absorbed by the exposed iceberg surface.

Although the Labrador Sea is at high latitude (52° - 68° N), its solar insolation is significant, especially in the summer months. A very comprehensive discussion of solar radiation effects is given in the text by Duffie and Beckman (1974). Monthly values of measured and interpolated solar insolation for the entire earth are given in the monograph by de Jong (1973). Figure 21 shows Jong's values of measured insolation for the center of the Labrador Sea (60° N) and for the waters east of Newfoundland (50° N). Both regions have comparable insolation, the more northerly point being less foggy than Newfoundland, and the ratio of insolation received to maximum incident radiation is about 50%.

The albedo of ice is strongly sensitive to the condition of its surface: its roughness, incidence angle with the sun, amount of bubble content, and snow or frost cover. Measured values of ice albedo in the literature vary from less than 10% (clear, flat ice surface) to 60% (bubbly, frosted ice). Hobbs (1974) suggests 60% as representative of Arctic ice, but de Jong (1973) and Budyko (1972) suggest 30-40% as a mean value for sea ice.

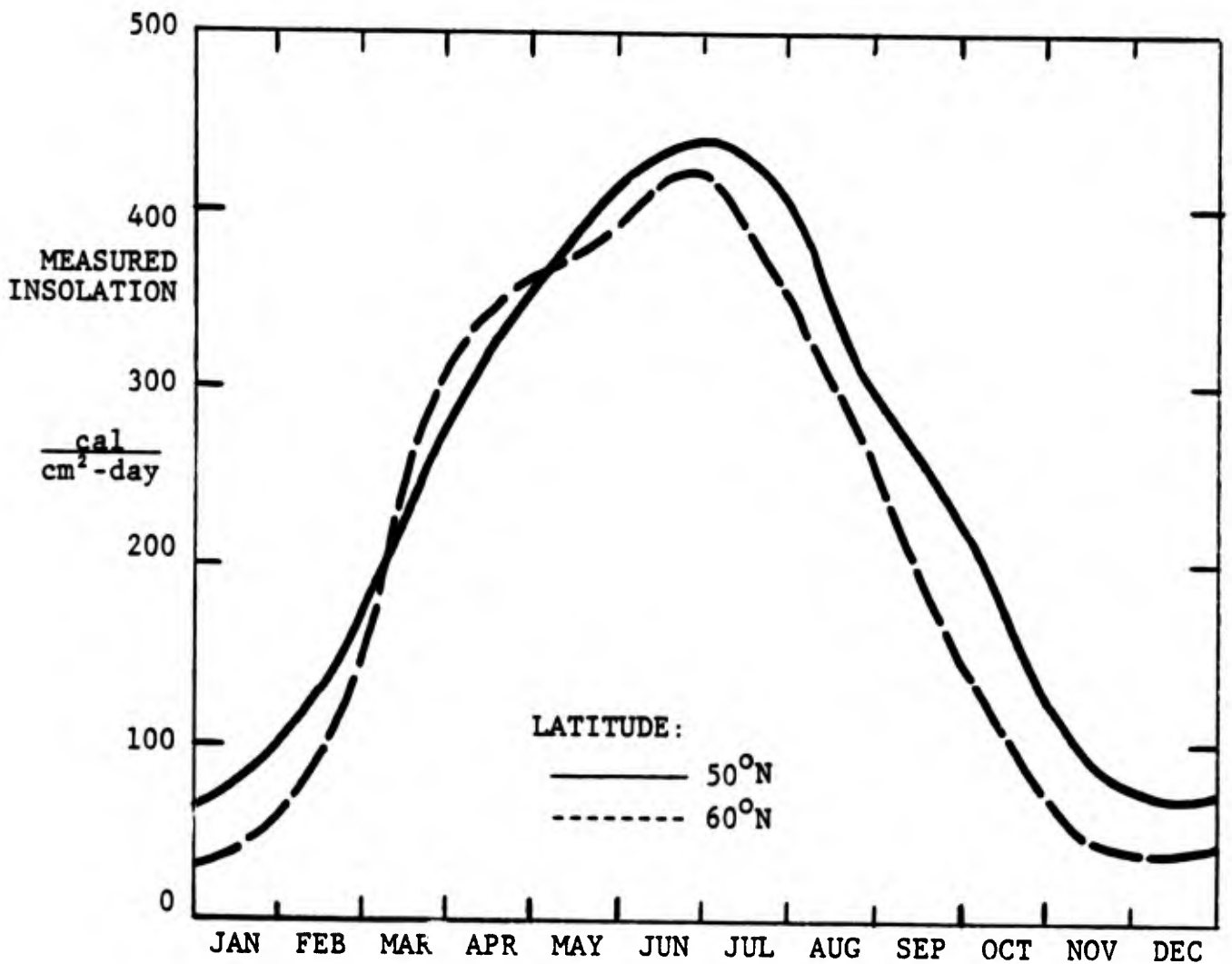
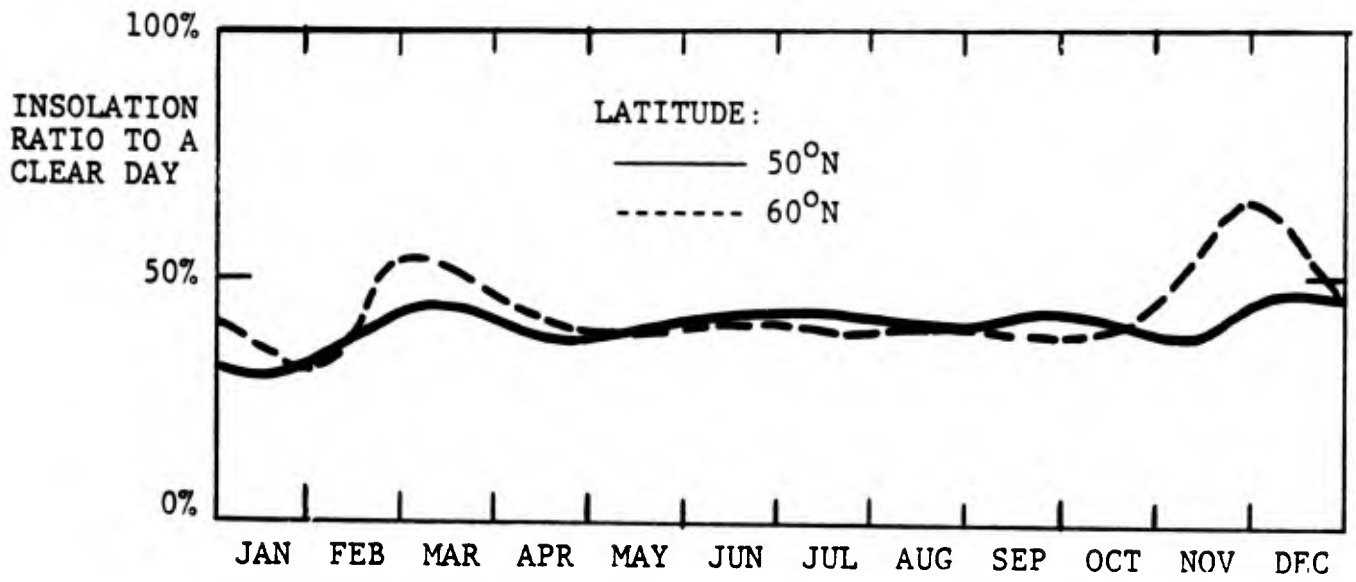


Figure 21. AVERAGE MEASURED MONTHLY SOLAR INSOLATION IN THE LABRADOR SEA, AFTER DE JONG (1973).

To obtain a reasonable estimate of surface melting for purposes of this report, we assume a mean albedo of 35% and make the simple Stefan approximation that each 334 J of solar energy absorbed by the exposed iceberg surface melts away one gram of ice. The results of this calculation are shown in Figure 22 for an average day and a clear day. Summer melting rates on the exposed surface can be as high as 7 cm/day, which is comparable to the submerged buoyant melting rate at a seawater temperature of about 4°C. Average solar melting rates vary from 0.5 cm/day in the winter to 3.8 cm/day in July. It is proposed that Figure 22 can serve as an engineering estimate for predicting this particular mechanism for deterioration of an iceberg.

An analysis of surface run-off from ice due to solar insolation is given by Colbeck (1977), while Gilpin (1977) develops a theory of radiative heating in an ice surface exposed to the sun.

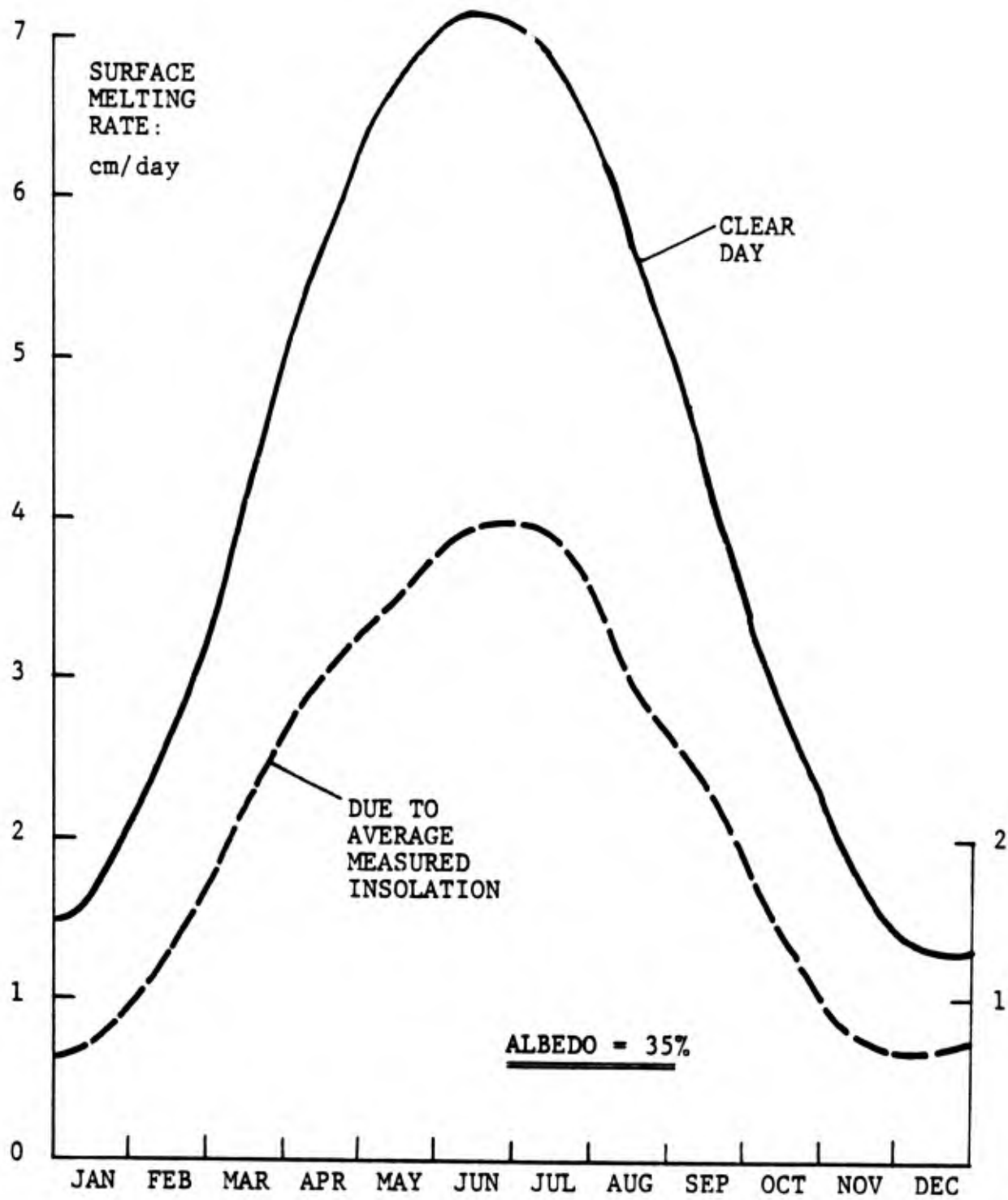


Figure 22. ICEBERG SURFACE MELTING RATE DUE TO INSOLATION AT 50°N LATITUDE.

Chapter 6

MELTING DUE TO VERTICAL BUOYANT CONVECTION

Introduction

Turning now to melting mechanisms on the submerged part of an iceberg, we begin with the most obvious process: natural convection of the buoyant melt water moving up the berg sides. This buoyant convection mechanism has probably been emphasized too much in previous studies. Certainly it can be a dominant process for Antarctic icebergs, which have deep drafts and nearly vertical sides. Wind effects are not so significant for a tabular Antarctic berg, which has such a large mass and a relatively small drag coefficient. For example, if $L = 2000$ m and $C_D = 0.2$ (Figure 20), Eq. (38) predicts that a ten-knot wind will take 227 hrs or 9.5 days to accelerate the berg to 95% of its terminal speed. For Arctic icebergs, the present study would rank wave erosion as the most important deterioration mechanism, followed by wind-driven convection, with buoyant natural convection third in importance.

If, as usually happens, the ambient seawater conditions are outside the small triangle between freezing and maximum density in Figure 2, the thermal and saline buoyancy effects will oppose each other. Thermal buoyancy will be downward and saline buoyancy upward, and the saline effect will dominate above the lowest meter or so of the vertical ice wall. A sketch of the flow field near the bottom of an ice wall in seawater is shown in Figure 23, after Josberger (1979a).

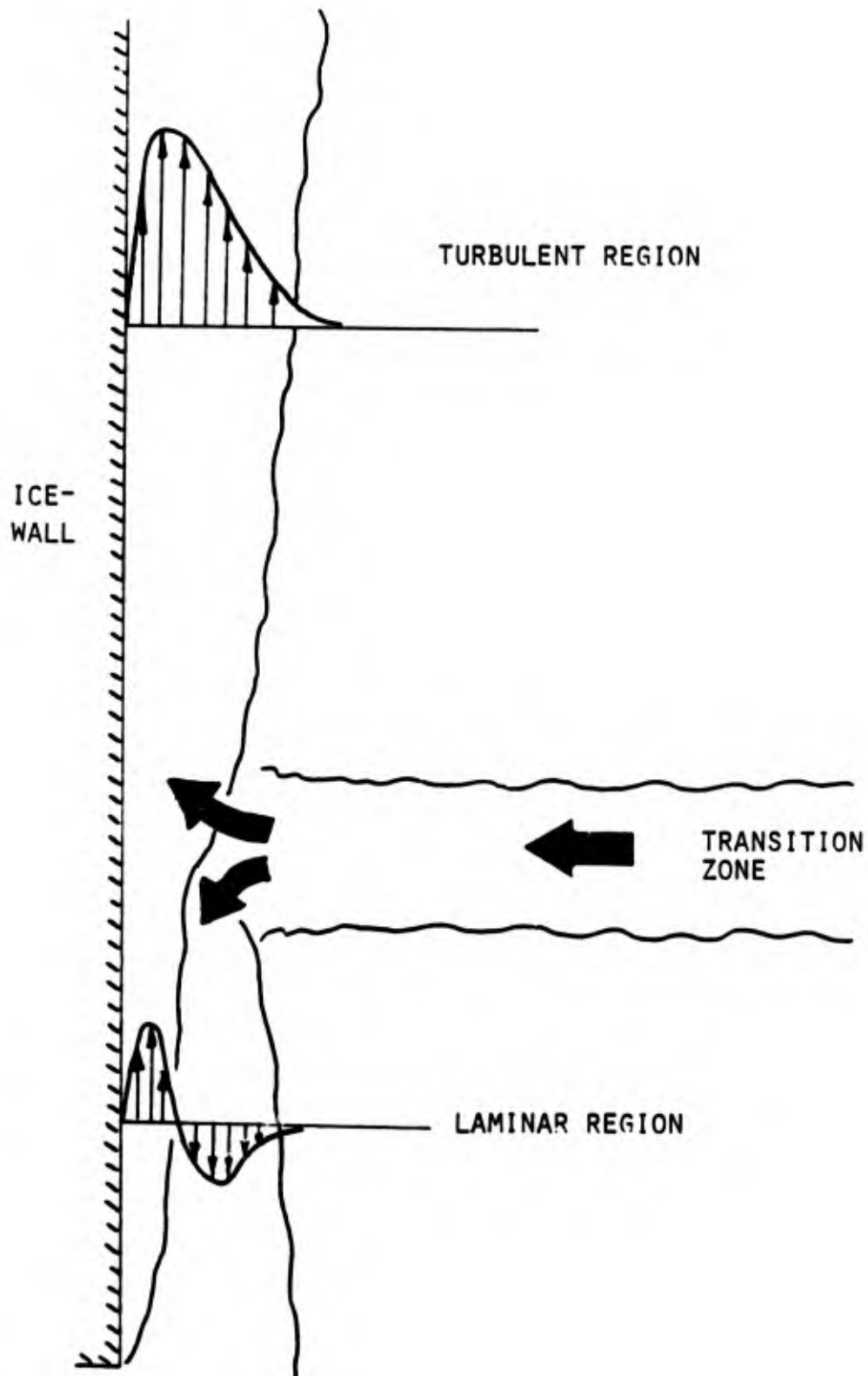


Figure 23. SKETCH OF THE OBSERVED BI-DIRECTIONAL BUOYANT BOUNDARY LAYER NEAR THE BOTTOM OF A MELTING VERTICAL ICE WALL (JOSBERGER 1979a).

The laminar boundary layer, which is typically bidirectional, occurs only on the lowest meter of the berg, followed by a transition zone and an upward turbulent buoyant layer. If the water is extremely warm, greater than about 15°C, the turbulent layer also may be bidirectional and even have a net downward flow (Josberger 1979a), but this is rare for an iceberg environment.

Four Theoretical Estimates

The problem of turbulent natural convection on a vertical wall, with thermal buoyancy effects only, has been the subject of dozens of experimental and theoretical studies. A comprehensive review of this work is given by Gebhart (1979). All of these studies lead essentially to a local Nusselt number equal to a function of the Prandtl number times a power of the Grashof number:

$$Nu_x = \frac{q_w x}{k \Delta T} = fcn(Pr) Gr_x^n \quad (43)$$

where q_w is the local heat transfer rate per unit area and ΔT is the driving temperature difference, $T_{fluid} - T_{wall}$. For thermal buoyancy, the Grashof number is defined as

$$Gr_x = \frac{g x^3}{\nu^2} \beta \Delta T \quad (44)$$

where β is the coefficient of thermal expansion. For laminar flow (Kreith 1973), the exact analytical solution gives $n = 0.25$.

For turbulent flow, an exact value of n is not known, but the various studies indicate that it is somewhere between

0.3 and 0.4. Some results in the literature are as follows:

$$\begin{aligned} n_{\text{turbulent}} &= 0.29 \quad \text{Waibler (1957)} \\ &= 1/3 \quad \text{George \& Capp (1979),} \\ &\quad \text{Larson \& Schoenhals (1964),} \\ &\quad \text{Mason \& Seban (1974),} \\ &\quad \text{Noto \& Matsumoto (1975),} \\ &\quad \text{Saunders (1939),} \\ &\quad \text{Touloukian et al. (1948)} \\ &= 0.36 \quad \text{Kato et al. (1968)} \\ &= 0.38 \quad \text{Cebeci \& Khattab (1975)} \\ &= 0.39 \quad \text{Tuan (1959)} \\ &= 0.40 \quad \text{Eckert \& Jackson (1951)} \end{aligned} \tag{45}$$

For what it is worth, the weighted average of these values is 0.347, and all of them are considerably above the laminar result $n = 0.25$.

With n known, Eq. (43) predicts that the wall heat transfer rate varies with distance x along the wall as

$$q_w \sim x^{3n-1} \tag{46}$$

For laminar flow, $n = 0.25$, we see that q_w decreases as $x^{-1/4}$. For turbulent flow, except for Waibler's results for rather small Grashof numbers, all the results in Eq. (45) indicate that q_w is either independent of x ($n = 1/3$) or increases with x . A large iceberg would be expected to have a higher buoyant melting rate than a small laboratory ice-wall model. However, this prediction would probably not hold in the neighborhood of the transition zone in Fig. 23, where local melting could be more intense.

The writers have found only two analytical studies in

the literature which study buoyant convection near the fluid freezing point, using the exact equation of state of seawater plotted in Figure 2. One is a laminar flow study by Gebhart and Mollendorf (1978), while the second assumes turbulent flow with a similarity assumption for the eddy diffusivities (Josberger 1979a). In both analyses the algebra is quite complex because of the nonlinearity of the equation of state, but some numerical estimates can be obtained relative to buoyant ice melting.

With both thermal and saline buoyancy, the Grashof number should be redefined as

$$Gr_x = \frac{gx^3}{\nu^2} \left(\frac{\Delta\rho}{\rho}\right)_{av} \quad (47)$$

where $\Delta\rho/\rho$ represents the net buoyancy averaged across the boundary layer:

$$\left(\frac{\Delta\rho}{\rho}\right)_{av} = \frac{1}{\delta} \int_0^{\delta} \left(\frac{\Delta\rho}{\rho}\right) dy \quad (48)$$

and y is the coordinate normal to the ice-wall. Calculations for laminar flow are made by Gebhart and Mollendorf (1978), who give the following recommendation for an effective net density difference:

$$\left(\frac{\Delta\rho}{\rho}\right)_{av} = 1.7 \times 10^{-6} (0.72T_w - T_m)^{0.85} (T_w - T_i) \quad (49)$$

where T_w is the ambient seawater temperature, T_i the ice-wall temperature, and T_m the temperature at the point of maximum density (Figure 2), all in $^{\circ}\text{C}$. Let us assume as an engineering estimate that Eq. (49) is also valid for turbulent flow. Then

the local heat transfer rate can be estimated by substituting Eqs. (47) and (49) into, say, the most popular vertical buoyancy correlation in the literature (Saunders 1939, Kreith 1973) for water flow:

$$\text{Nu}_x \doteq 0.17 \text{Gr}_x^{1/3} \quad (50)$$

The melting rate $V_m = q_w / \rho_i \Gamma$ from Eq. (8) can then be computed and plotted in Figure 24 versus the driving temperature difference $\Delta T = T_w - T_i$. The rates, shown as a solid line, vary from 8 m/yr at 2°C to 120 m/yr at 12°C.

A second theoretical estimate was given by Josberger (1979a), who used a similarity theory to scale his low-Grashof-number turbulent melting rates up to iceberg sizes. Josberger's theory assumes that the eddy diffusivities are functions only of the traditional laminar similarity variable $\eta = cy/x^{3/4}$ (Kreith 1973), which effectively "laminarizes" the theory and leads to the prediction that turbulent heat transfer should also vary as $x^{-3/4}$, which seems to be at variance with the data of Eq. (45). In any case, Josberger did not compare the actual theory with experiment but rather used the scaling law $q_w \sim x^{-3/4}$ to extrapolate his turbulent melting data (over a 70-cm length of ice sheet) up to a 200-meter ice-wall simulating an Antarctic iceberg. After fitting a power-law to the data, the resulting scaled melting rate expression is

$$V_m \text{ (m/yr)} \doteq 5.66 (T_w - T_i)^{1.63} D^{-3/4} \quad (51)$$

with temperatures in °C and the draft D in meters. Figure 24

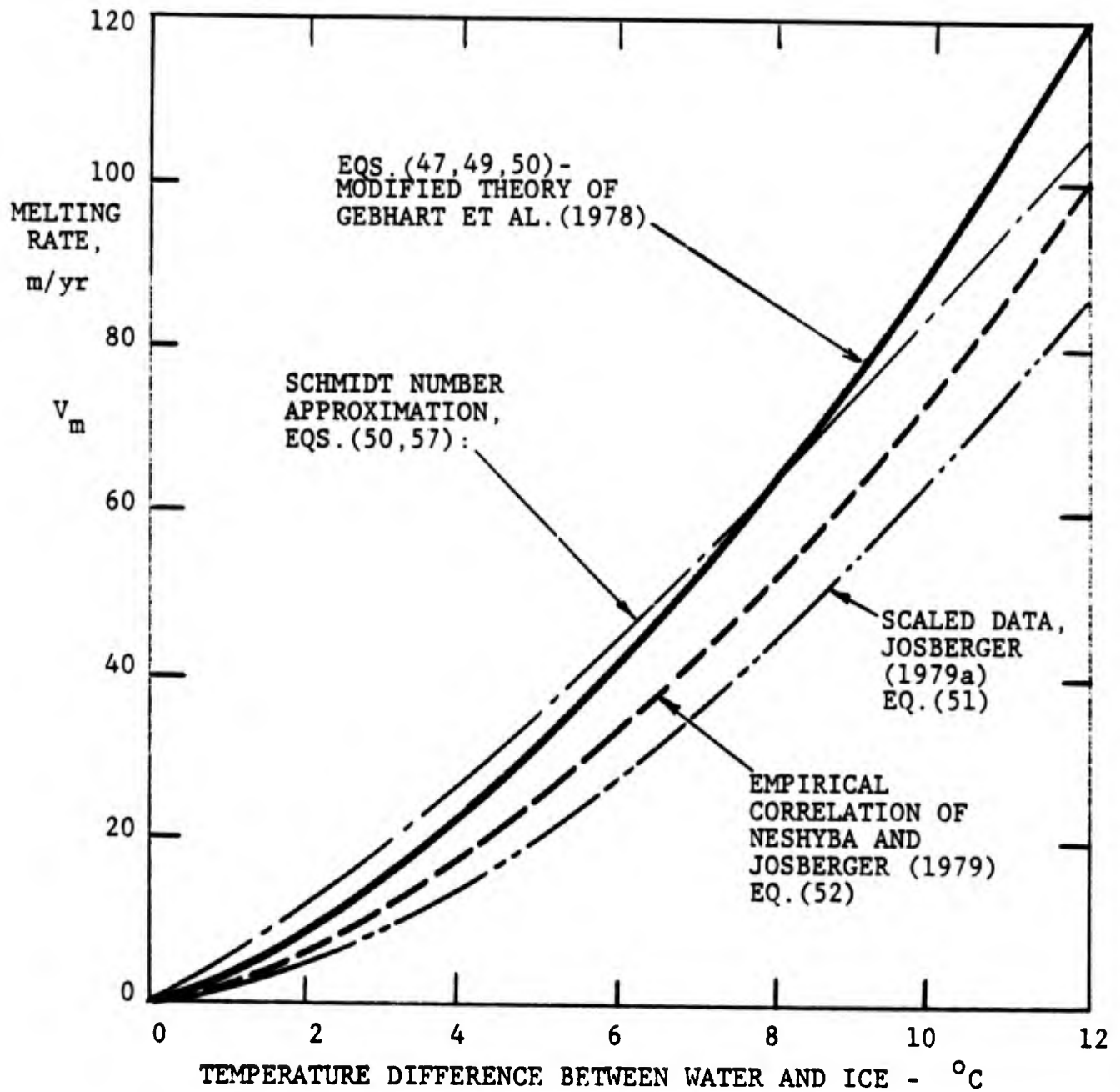


Figure 24. FOUR ESTIMATES OF THE FREE CONVECTION MELTING RATE OF A LARGE, NEARLY VERTICAL ICE SURFACE.

shows this relation plotted for $D = 200$ m as a dashed double-dot line. The rates are comparable to the Gebhart estimate but somewhat smaller.

A third estimate was given by Neshyba and Josberger (1979), who re-evaluated the melting rate data which Morgan and Budd (1977) inferred from analysis of Antarctic iceberg size and latitude distributions. By fitting eight of the Morgan and Budd data points to a least-squares parabola and subtracting the constant intercept as a "calving wastage", Neshyba and Josberger arrived at the following estimate of vertical buoyant melt rates:

$$V_m \text{ (m/yr)} = 2.78(T_w - T_i) + 0.47(T_w - T_i)^2 \quad (52)$$

again with temperatures in $^{\circ}\text{C}$. It is not known what draft this expression applies to, since the data encompassed a wide variety of iceberg sizes. Figure 24 shows Eq. (52) as a dashed line which is quite comparable to the other estimates.

A fourth and final estimate can be obtained by making a simple Schmidt-number approximation for the saline boundary layer thickness near the wall. The thermal boundary layer thickness may be estimated from the classical analysis of Eckert and Jackson (1951):

$$\delta_T \sim (1 + 0.494 \text{ Pr}^{2/3})^{1/10} \text{ Pr}^{-8/15} \quad (53)$$

Since the energy and salinity conservation relations are mathematically analogous (Kays and Crawford 1980), one can

reasonably estimate the salinity boundary layer thickness as

$$\delta_S \sim (1 + 0.494 Sc^{2/3})^{1/10} Sc^{-8/15} \quad (54)$$

where $Sc = Pr \cdot Le$ is the Schmidt number of seawater. Thus the ratio of saline to thermal boundary layer thickness can be estimated by dividing Eq. (54) by Eq. (53). Taking, at $0^\circ C$, from Figure 3, $Pr = 13.3$ and $Sc = 2980$, we obtain

$$\delta_S/\delta_T = \frac{0.0214}{0.277} = 0.077 \quad (55)$$

Note that this estimate is somewhat less than that of Eq. (7), which was for forced convection.

If we now make a linearized approximation for the equation of state of seawater,

$$\Delta\rho/\rho = -\beta \Delta T + \alpha \Delta S \quad (56)$$

where α and β are average values taken from Figure 2, we may substitute into Eq. (48) and carry out the integration. The result is the following estimate of net buoyancy in the flow:

$$(\Delta\rho/\rho)_{av} = -\beta (T_w - T_i) + 0.077 \alpha (S_w - S_i) \quad (57)$$

Substituting Eq. (57) into Eq. (47) and taking $(S_w - S_i) = 35 \text{ }^\circ/\text{oo}$, we may use Eq. (50) to evaluate the melting rates. The results are shown as a dash-dot line in Figure 24.

Since the four estimates in Figure 24 are obtained from four greatly different points of view and yet give comparable

results, we conclude that Figure 24 presents a useful engineering estimate of melt rates to be expected from buoyant effects on the vertical or nearly vertical sides of an iceberg. The writers think that perhaps the two higher curves might be better estimates. The three highest curves predict no length effect on the melting rate, while the lowest curve (Josberger 1979a) is computed for an iceberg draft of 200 meters.

For nonvertical ice surfaces, it is recommended (Kreith 1973) that the quantity "g" in the Grashof number, Eq.(47), be replaced by $g \cos\theta$, where θ is the angle between the tangent to the ice-wall and the vertical.

Lacking a more definitive theory, we suggest that Figure 24 represents a reasonable approximation at this time. The third author of this report has decided to investigate a more exact theory of turbulent buoyant ice melting as an M.S. thesis topic. The thesis will be completed in June 1980.

Chapter 7

MELTING DUE TO FORCED CONVECTION

INTRODUCTION

In Chapter 4, Figure 17, we saw that the prevailing winds in the Labrador Sea are capable of driving an iceberg at relative velocities from 10-30 cm/s in excess of the local current speeds. These relative velocities persist as long as the winds are steady. Similar relative velocities occur for several hours when an iceberg suddenly moves into a region of significantly higher or lower water currents. In fact, relative velocities of order 5 cm/s probably always persist near an iceberg due to the normal differences between bottom and surface currents for a floating body of such large draft. All of these velocity differences contribute to forced convection melting of an iceberg. Melting due to air convection is negligible.

The exact theory of forced convection berg melting is quite complex, as shown in a comprehensive theory by Griffin (1977). Even if pressure gradient effects are neglected, the flow past an iceberg generates a thick velocity boundary layer. The wall temperature varies somewhat due to salinity intrusion at the melt interface. Melt water release creates a "wall-blowing" effect which alters the local heat transfer. Even if the initial ice surface is smooth, the melting process creates surface ripples (Tatinclaux and Kennedy 1977) which tend to enhance the heat transfer. The equations of motion are closely coupled through density, salinity, and the wall transfer rates. Griffin

(1977) gives a complete analysis for laminar flow past a flat plate and indicates an approximate solution for turbulent flow. For turbulent flow, in spite of these complexities, the final results, when compared with data for melting rate of a towed ice block (Stolfi et al. 1977, 1979) are in reasonable agreement with the simple and classical expression for heat transfer in flat plate flow (Kreith 1973):

$$Nu_x = 0.0295 Re_x^{0.8} Pr^{0.4} \quad (58)$$

Overall melting of the ice block, based on body length L , is correlated by the analogous expression

$$Nu_L = 0.037 Re_L^{0.8} Pr^{0.4} \quad (59)$$

It is proposed here to develop similar expressions for forced convection past tabular and non-tabular iceberg shapes.

APPROXIMATE SOLUTION FOR TWO ICEBERG SHAPES

For surfaces approximating a flat plate, such as the bottom of an Antarctic tabular iceberg, Eqs.(58) and (59) could be used for the melting rate, except that they are accurate only for moderate Reynolds numbers, 10^5 - 10^7 . In applying these formulas for $Re_x \geq 10^9$, Griffin (1977) probably underestimates the melting rate by about 50%. For higher Reynolds numbers, probably the most accurate estimate in the literature is the Reynolds analogy proposed by White (1974),

$$St_x = \frac{Nu_x}{Re_x Pr} = \frac{\frac{1}{2}C_f}{1 + 12.8(Pr^{0.68} - 1)(\frac{1}{2}C_f)^{\frac{1}{2}}} \quad (60)$$

which is valid for any Prandtl number greater than 0.5, combined with White's formula for skin friction at high Reynolds numbers on a flat plate:

$$C_f = 0.455/\ln^2(0.06 Re_x) \quad (61)$$

Equation (60) is valid not only for a flat plate but for any smooth surface (e.g. pipe flow) where pressure gradients are negligible. We will use Eq.(60) again in Chapter 8.

For Arctic tabular and non-tabular iceberg shapes (Figures 11 and 13), the pressure gradients are too strong to be neglected, and Eqs.(60,61) will underestimate the true forced convection melting rates. Some sophisticated finite difference and energy integral techniques for computing heat transfer with varying wall temperature and arbitrary pressure gradient are discussed in Section 6-11.4 of the text by White (1974). However, it turns out that these complex digital computer procedures are no more accurate than a very simple quadrature method proposed by G. S. Ambrok and discussed and improved in the text by Kays and Crawford (1980). The final result of Ambrok's method is an expression for local Stanton number as a function of distance x along the surface:

$$St_x = \frac{0.0295 Pr^{-0.6} \Delta T^{0.25} \mu^{0.2}}{\left\{ \int_0^x \rho U \Delta T^{1.25} dx \right\}^{0.2}} \quad (62)$$

where $\Delta T = T_w - T_i$ is approximately constant for our present problem of iceberg melting. If the stream velocity $U(x)$ is

also constant, Eq.(62) reduces to the flat plate expression, Eq.(58).

For our purposes we assume that temperature difference and water density are constant in Eq.(62). The stream velocity $U(x)$ for the model tabular (Fig. 11) and non-tabular (Fig.13) icebergs was simulated by potential flow, building up the proper shape through a series of distributed sources and sinks, as discussed e.g. in Chap. 8 of the text by White (1979). The integral in Eq.(62) was then evaluated by numerical quadrature. Finally, the local heat transfer rate St_x was integrated by quadrature to obtain the average heat transfer to the iceberg. The final result can be given in terms of the average Nusselt number based on waterline length (the straight line distance from bow to stern) L_o :

$$\text{a) Tabular: } \quad Nu_{L_o} = 0.058 Re_{L_o}^{0.8} Pr^{0.4} \quad (63)$$

$$\text{b) Non-tabular: } \quad Nu_{L_o} = 0.055 Re_{L_o}^{0.8} Pr^{0.4}$$

The use of waterline length L_o eliminates the need to evaluate the arc length or keel-length along the bottom of the iceberg.

Equations (63) show that, after all the laborious numerical computations are completed, Ambrok's theory predicts that the average melting rates for the two icebergs differ only about five per cent, although both are about 30% higher than the flat plate estimate, Eq.(59), even if the latter is based on the keel-length. The formulas also predict that the melting rates are less for the large bergs, decreasing about 37% for

each ten-fold increase in iceberg length.

The melting rates from Eqs.(63) are plotted in Figure 25 for various iceberg lengths. Note that the rates are given per °C of water/ice temperature difference. Thus, for even moderate relative water velocities (10-30 cm/s), the rates given in Figure 25 are significantly larger than the buoyant convection rates in Figure 24. For example, at 4°C, the buoyant melting rate in Figure 24 is about 20 m/yr. By comparison, at, say, 20 cm/s in Figure 25, the melting rate of a 300-m berg is about 9 cm/day/°C, which when multiplied by 4°C and converted to an annual rate gives $V_m = 130$ m/yr, or 6.5 times more. Thus, over the whole span of water temperatures from 1°C-12°C, forced convection melting is considerably larger than buoyant melting.

MELTING AT THE ROOT OF AN ICE FLAW

It is well known that a crack or flaw in an iceberg may be attacked by waves or water currents and thereby enlarged or lengthened, eventually causing calving or fracture. Robe, Maier, and Kollmeyer (1977) document the case of a very large flaw being accentuated during the deterioration process.

Presently there is no existing theory of the effect of wave erosion on an ice flaw, but the following simple analysis will illustrate the manner in which a flaw accentuates local heat transfer. Consider warm water flowing toward a notched flaw of half-angle θ , as shown in Figure 26. The flow enters the flaw and then turns back along the sides of the wedge. According to potential theory for a re-entrant wedge (White 1974,

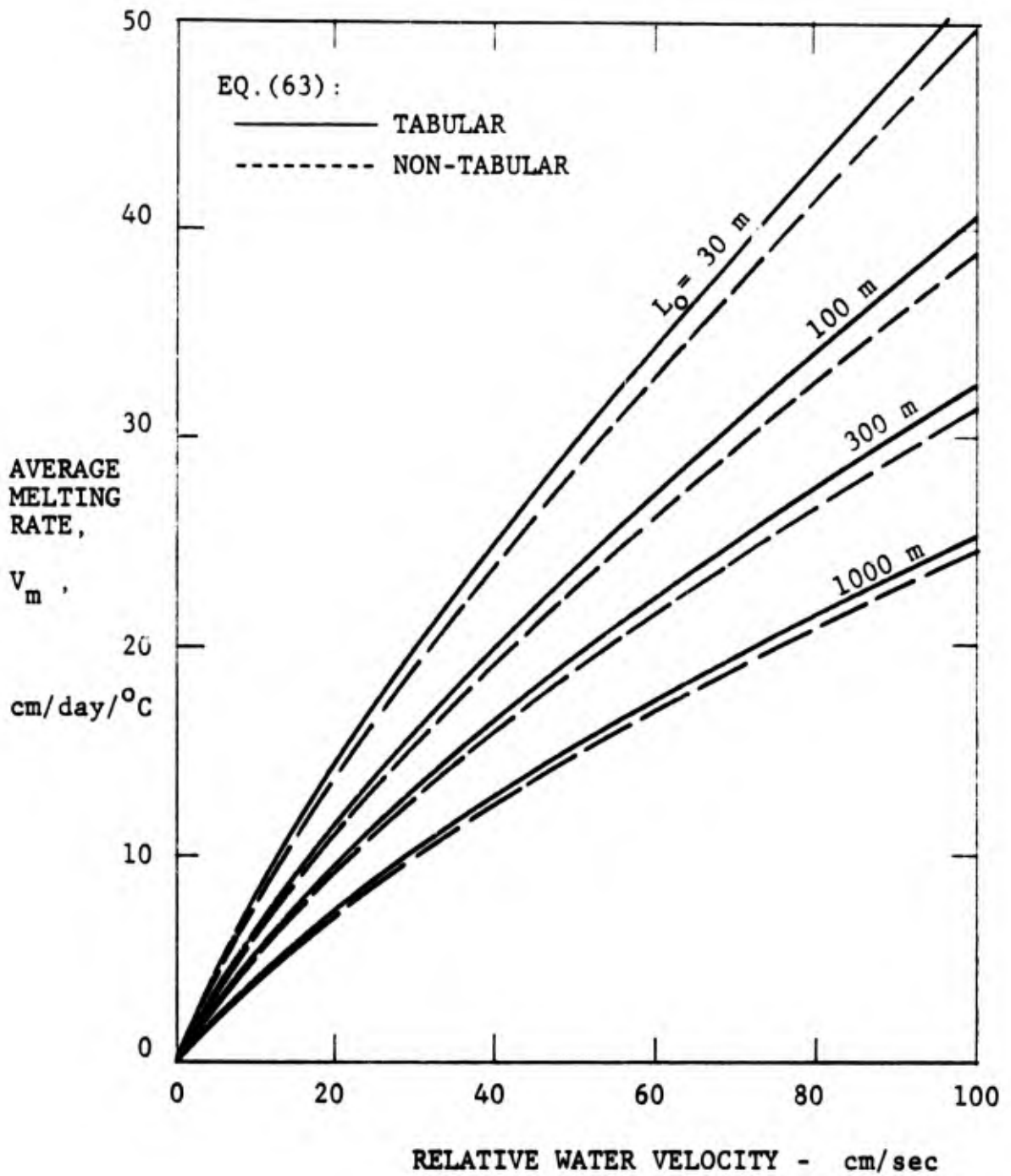


Figure 25. THEORETICAL ICEBERG AVERAGE MELTING RATE DUE TO FORCED CONVECTION, FOR VARIOUS WATERLINE LENGTHS.

page 275), the stream velocity along the wedge surface varies with distance x from the notch tip according to

$$U(x) = K x^m \quad (64)$$

where K is a constant which depends only on the depth of the flaw and the exponent m depends only on the half-angle θ of the notch:

$$m = \theta / (\pi - \theta) \quad (65)$$

with θ in radians. We may estimate the effect of the flaw, then, by substituting Eq.(64) into Ambrok's theory, Eq.(62). The exact melting rate depends upon the size of the iceberg and the notch depth, but the relative melting rate compared to a nearly flat notch ($\theta = 90^\circ$) depends only on the notch angle θ . The computed results are tabulated in Figure 26. A ten-degree half-angle notch, for example, melts 55% faster according to this theory. However, no attempt will be made here to define any statistically meaningful "standard flaw" size to make any further computations of iceberg deterioration due to this mechanism. Perhaps further experimental data on iceberg flaws could contribute to our quantitative knowledge of this melting process.

It should be noted that the present correlations are also valid for exposed surface air melting if the properties of air are inserted into Eqs. (63). However, air melting is negligibly small: only a few mm/day even for warm air at high winds.

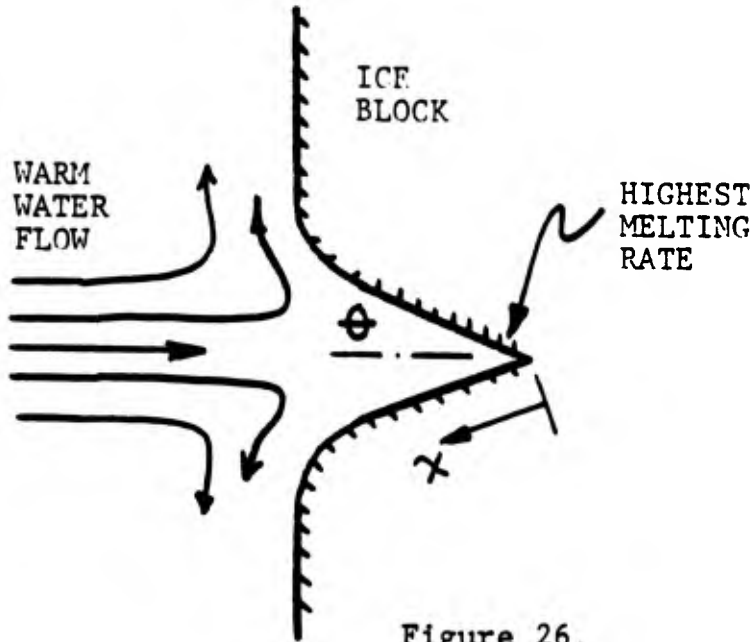


Figure 26.

EFFECT OF NOTCH HALF-ANGLE ON MELTING RATE AT THE ROOT OF AN ICE FLAW

<u>HALF-ANGLE</u>	<u>RELATIVE MELTING RATE</u>
90°	1.000
80°	1.024
70°	1.052
60°	1.084
50°	1.125
40°	1.176
30°	1.246
20°	1.351
10°	1.552
5°	1.783
1°	2.460

Chapter 8

WAVE EROSION OF AN ICEBERG

The final and probably most important iceberg melting mechanism is to be studied here is that of wave erosion at the waterline. It is clear from the numerous published observations of icebergs (e.g., Groen 1969) that waves, even in cold waters, can rapidly erode a notch or ledge into the side of an iceberg, after which calving or fracture can occur. The present chapter will develop quantitative estimates for the erosion rates due to waves, and Chapter 9 will analyze the fracture conditions for ice masses which have been undercut by waves.

The only laboratory wave erosion experiment known to the writers is a brief wave tank study by Josberger (1977), whose small flapper-generated waves ($H = 5$ cm, $T = 0.4$ s) produced rays propagating normal to a vertical ice sheet. Even though the water temperature was only 4°C , the waves carved out a waterline notch 8 cm deep in only 45 minutes. The notch extended about one wave height above the waterline and about $K^{-1} = 1/2$ below the waterline. Since similar equipment was readily available here, the present study has produced two additional brief wave erosion experiments in a wave tank.

When the present study began, it was planned to base the erosion analysis on the very interesting environmental wave turbulence and Reynolds stress statistics reported by Shonting et al. (1971, 1979). Since Shonting and his coworkers have successfully correlated wave turbulent statistics with sea state,

it was proposed that these environmental parameters could be combined with the well-documented digital computer turbulence energy transport models (Section 8.5 of Cebeci and Bradshaw 1977) to make quantitative estimates of wave-induced heat transfer against an ice surface. However well intentioned and plausible this plan seemed, the fact is that, after months of analysis in the early part of this project, no successful engineering computations were realized. It was finally decided to pursue an alternative method. Fortunately, a very simple second approach did develop and seems to be quite successful in predicting quantitative wave erosion rates.

The Wave Friction Factor Diagram

From a simplified point of view, "wave action" consists merely of oscillating velocities in the neighborhood of a solid surface. If this action is significant, it is probably turbulent, i.e. high orbital velocities and amplitudes. Presumably an oscillating turbulent boundary layer will arise near the solid surface, resulting in periodic friction against the surface. If the water is warm and the surface cold, this friction will interact with the thermal boundary layer to cause periodic heat transfer to the surface, whose average will be a steady mean heating of the surface. One should be able to correlate this steady heat transfer with the wave Reynolds number and the water Prandtl number.

In fact, the only "solid surface" whose frictional wave action has been well documented is the sea bottom in shallow (continental shelf) waters. Wave action study of breakwaters,

ships, and other man-made solid surfaces has been confined to correlation of the forces and moments caused by the waves, not the friction and heat transfer.

However, bottom friction due to waves has been extensively studied as a fundamental cause of sedimentation in shallow waters. The best bottom friction correlation known to the writers is the wave friction factor diagram of Jonsson (1966), which is reproduced in Figure 27. The ordinate is the mean bottom shear stress, non-dimensionalized by water density and maximum wave orbital velocity:

$$C_{fw} = \tau_{wm} / (\frac{1}{2} \rho_w u_m^2) \quad (66)$$

The abscissa is the wave orbit Reynolds number, based on bottom orbital velocity and amplitude:

$$Re_a = u_m a_m / \nu_w \quad (67)$$

The curves in Fig. 27 are based on existing data as correlated by Jonsson (1966). The diagram resembles but is not coincident with the famous Moody friction factor diagram for pipe flow (White 1979).

For a smooth bottom, the wave friction reaches a minimum which may be either laminar or turbulent:

$$\begin{aligned} \text{a) laminar, } Re_a < 31000: & \quad C_{fw} \approx 2 Re_a^{-\frac{1}{2}} \\ \text{b) turbulent, } Re_a > 31000: & \quad C_{fw} \approx 0.09 Re_a^{-0.2} \end{aligned} \quad (68)$$

For a rough wall, the friction increases as the ratio a_m/ϵ decreases, where ϵ is the average roughness height. Like pipe friction, the rough wall data are only weakly dependent on Reynolds number.

Except for differences in magnitude, the orbital behavior of periodic waves has much the same character at the surface or at the bottom or, indeed, any point in the water column. It therefore seems reasonable to assume that Figure 27 will correlate the mean friction against any solid surface immersed in waves, if C_{fw} and Re_a are based on the local orbital velocity and amplitude at that surface. Above the bottom, the orbits are ellipses, and there are non-zero vertical velocities also. Let a be the local orbit semi-major axis length and let u_m and w_m be the local horizontal and vertical orbit velocity amplitudes. Then our fundamental assumption is that Figure 27 is valid also for local mean shear at any point, as follows:

$$C_{fw} = \tau_{wm}/(\frac{1}{2}\rho_w V^2), \quad Re_a = aV/\nu_w, \quad V^2 = u_m^2 + w_m^2 \quad (69)$$

with the roughness parameter being a/ϵ . Further, it is assumed for simplicity that the waves have period T and height H and that the orbits may be described by linearized Airy theory (White 1975):

$$\begin{aligned}
 u_m &= \frac{\pi H}{T} \cos(\phi) \frac{\cosh(k(z+d))}{\sinh(kd)} \\
 w_m &= \frac{\pi H}{T} (1 + \sin^2 \phi)^{\frac{1}{2}} \frac{\sinh(k(z+d))}{\sinh(kd)} \\
 a &= \frac{H}{2} \frac{\cosh(k(z+d))}{\sinh(kd)}
 \end{aligned}
 \tag{70}$$

where d is the water depth, $k = 2\pi/\lambda$ is the wavenumber, and ϕ is the angle between the wave rays and the (iceberg) local surface tangent. The wavelength λ is related to period and water depth by the Airy formula:

$$\lambda = \frac{gT^2}{2\pi} \tanh(kd)
 \tag{71}$$

From Eqs. (69) and (70) and Figure 27 we can compute an engineering estimate of the mean wave friction against the iceberg surface as a function of z , where $z=0$ is the waterline and $z=-d$ is the bottom.

The Reynolds Analogy

The second and final assumption about wave erosion is that the wave friction can be directly related to wave heat transfer through a Reynolds analogy. This assumption seems reasonable because wave oscillations against a relatively flat surface (an iceberg) should cause little if any pressure gradient, and the only severe limitation to the use of Reynolds analogy, especially in turbulent flow, is the presence of strong pressure gradients (White 1974).

For a smooth ice surface, we use the Reynolds analogy given by Eq. (60), with $C_f = C_{f_w}$ from Figure 27 and the Stanton number correlated with local orbit velocity:

$$St = \frac{q_w}{\rho V c_p \Delta T}, \quad V = (u_m^2 + w_m^2)^{\frac{1}{2}} \quad (72)$$

Iceberg surfaces are somewhat rough, with typical roughness heights of the order of $\epsilon = 1$ cm. This has only a modest effect on forced convection heat transfer, where the roughness is only a tiny fraction of the iceberg length. But in wave action, the proper parameter is ϵ/a , not ϵ/L , and roughness will increase both the friction and the heat transfer.

Let subscript "o" denote friction and heat transfer for zero roughness. Then there are at least four different Reynolds analogy correlations in the literature which account for roughness. The first is the formula given by Ashton (1972) for a corrugated or wavy surface:

$$St = St_o (1 + 10 \epsilon/\ell) \quad (73)$$

where ℓ is the wavelength of the corrugations. Since ℓ is quite variable and difficult to estimate for icebergs, we will not use this correlation here.

There are two popular analogies correlated with the roughness Reynolds number $Re_\epsilon = V\epsilon/\nu$. The first is the formula of Owen and Thompson (1963), as modified by Seidman (1972):

$$St = \frac{\frac{1}{2}C_f}{1 + 0.52(\frac{1}{2}C_f)^{0.725} Re_\epsilon^{0.45} Pr^{0.8}} \quad (74)$$

This relation has been recommended in a recent comprehensive review of wall roughness effects by Hodge (1979). The second formula is suggested in a text by Edwards et al. (1976):

$$St = \frac{\frac{1}{2}C_f}{1 + (\frac{1}{2}C_f)^{\frac{1}{2}} \{5.19 Pr^{0.44} (\frac{1}{2}C_f)^{0.1} Re_\epsilon^{0.2} - 8.5\}} \quad (75)$$

Although highly recommended, these two formulas both seem to suffer from the same two types of pathology: 1) at zero roughness we do not recover the smooth surface result, Eq. (60); and 2) at very high roughness ratios typical of small-amplitude wave action, they predict that St decreases with roughness, which is adverse to the facts. Therefore we will not use either of Eqs. (74) or (75).

The fourth analogy, which we will adopt here, is the simple correlation proposed by Nunner (1956):

$$St/St_o = (C_f/C_{fo})^{\frac{1}{2}} \quad (76)$$

which expresses the observed fact that, for a given flow condition, roughness increases the heat transfer only about half as much as it increases the local shear stress.

Calculations of Iceberg Erosion by Waves

With Eq. (76) and the friction factor diagram, Figure 27, calculations were made for a wide variety of wave heights and periods to determine the wave-induced melting rates near the waterline of an iceberg. The orbit parameters were computed as a function of z from Eqs. (70). Figure 28 shows the theoretical smooth surface melting rates on a vertical ice wall for various periods if $H = 1$ meter. At short periods (< 5 sec) a narrow notch is cut in the berg, while at longer periods the erosion extends much deeper. In either case, an overhanging ice slab is left by the progress of the wave melting, which reaches only to H above the waterline.

The maximum melting rate occurs at the waterline and can be quite large, e.g. for $T = 3$ sec in Figure 28, V_m at the waterline equals 1.0 m/day/ $^{\circ}$ C. The dimensionless waterline melting rate correlates exactly, within the assumptions of the present theory, with the wave Reynolds number $Re_H = H^2/Tv_w$ and the roughness ratio ϵ/H . The final correlations are

$$\begin{aligned} \text{a) Smooth wall: } & V_m T/H \doteq 0.00015 Re_H^{-0.12} \\ \text{b) Rough wall: } & V_m T/H \doteq 0.000146 (\epsilon/H)^{0.2} \end{aligned} \tag{77}$$

These values are plotted in Figure 29 for typical Reynolds numbers. Note that these melting rates are all per $^{\circ}$ C of water-ice temperature difference.

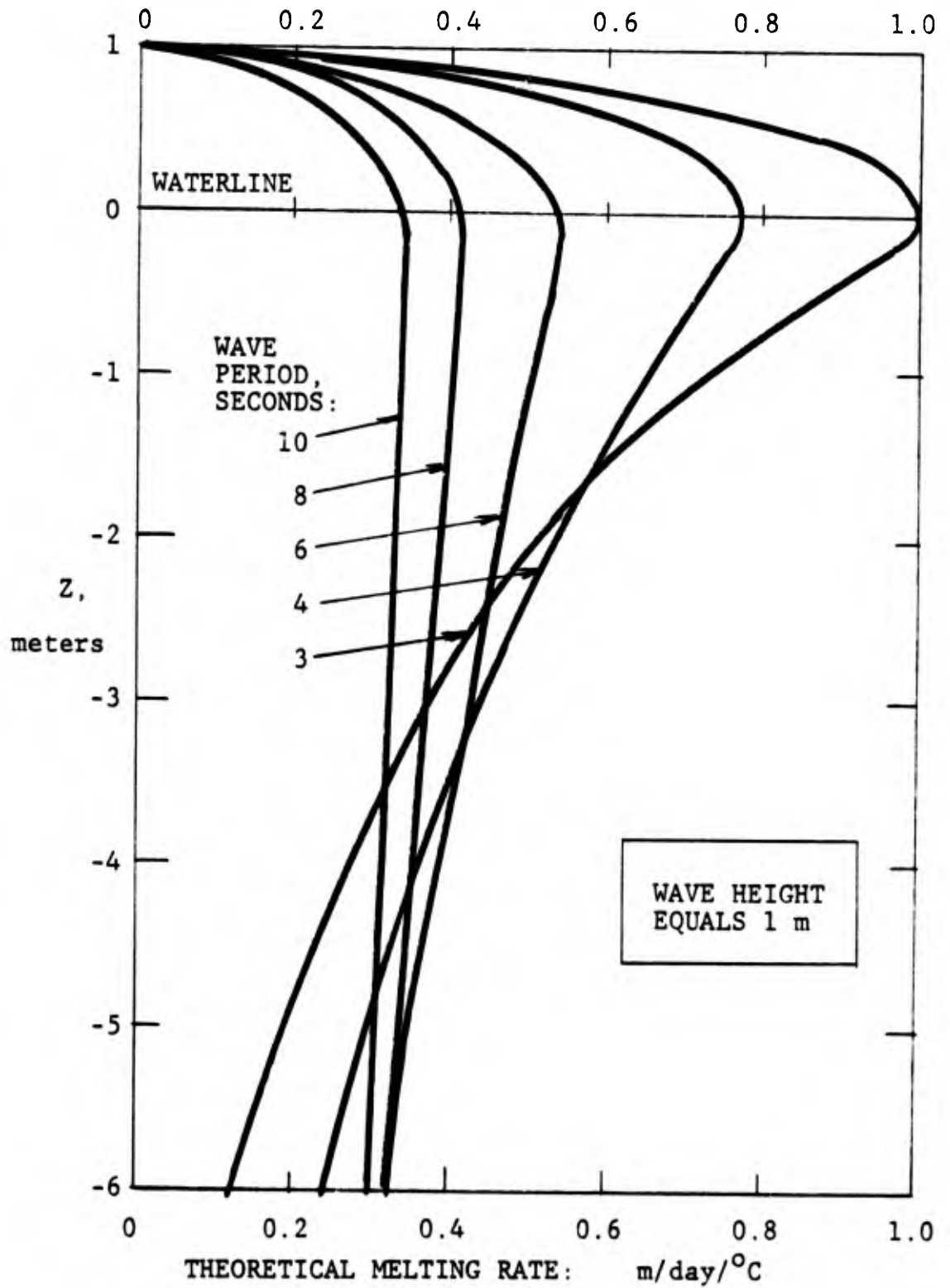


Figure 28. COMPUTED WAVE EROSION RATE PROFILES FOR A SMOOTH SURFACE AT H = 1 m.

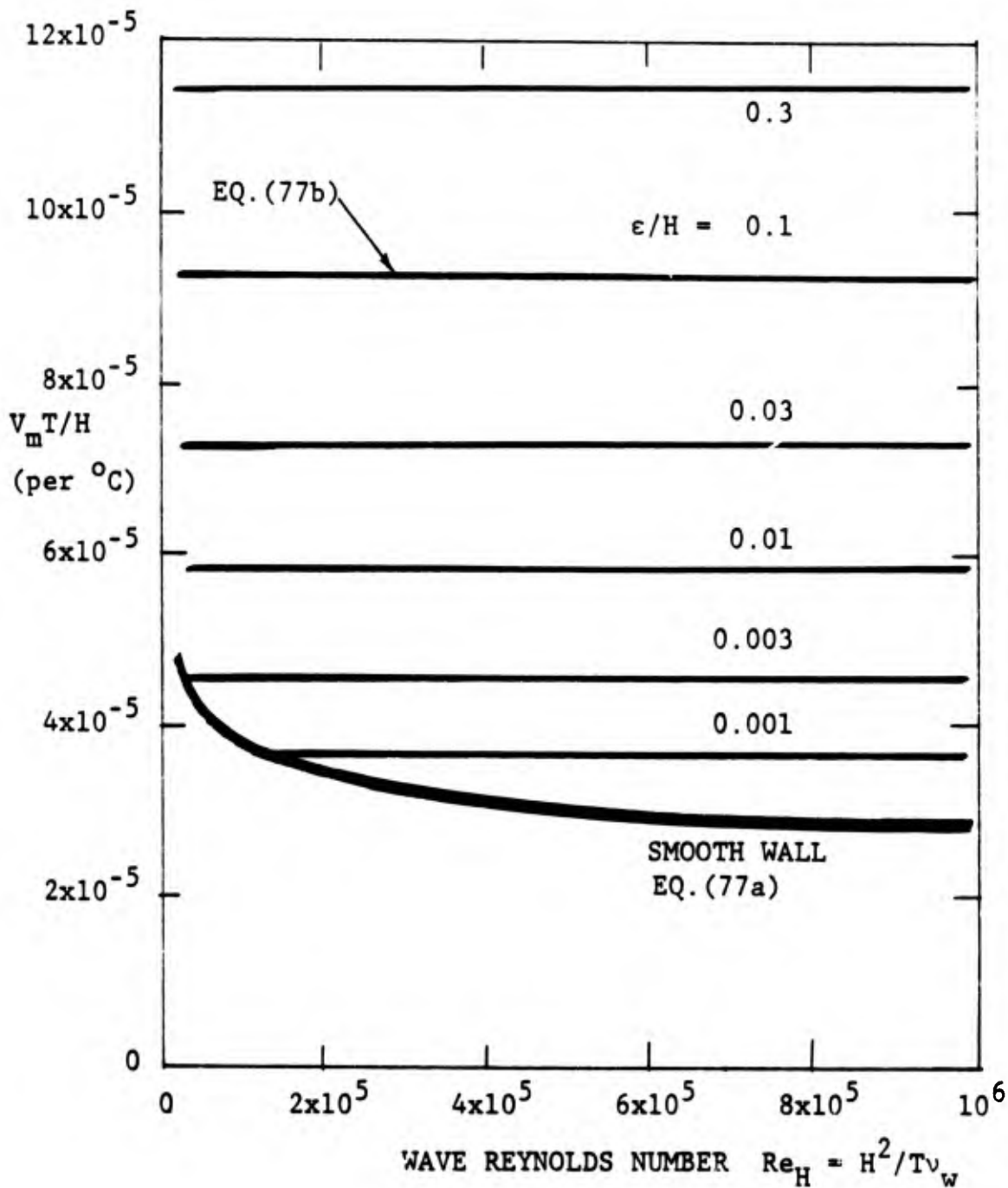


Figure 29. DIMENSIONLESS MAXIMUM WATERLINE WAVE EROSION MELTING RATE.

Regardless of wave height and surface roughness, the melting rate shapes are a function only of wave period as given by Figure 28. Only the magnitudes of melting rate are scaled according to the formulas of Eqs. (77). Thus we may find the total volume of ice removed by wave erosion, per unit perimeter of ice wall, by integrating the area under the curves in Figure 28. The result is what we might term the "strip-volume melting rate", \dot{v} , which is the ice volume removed per day per °C per meter of waterline perimeter. Numerical values of the strip-volume melting rate are plotted in Figure 30 for various wave heights and periods. These volume removal rates may also be correlated in dimensionless fashion, as shown in Figure 31. The correlation formulas are, per °C:

- a) Smooth surface: $\dot{v}/gHT \doteq 3.71 \times 10^{-6} Re_H^{-0.12}$ (78)
- b) Rough surface: $\dot{v}/gHT \doteq 5.22 \times 10^{-6} (\epsilon/H)^{0.2}$

Then, if the average period T and height H of the prevailing waves are known, the total ice volume eroded away by waves in time t_1 is given by the double integration

$$\text{Volume} = \int_0^{t_1} \int_0^P \dot{v} \, ds \, dt \quad (79)$$

where ds is the arc length around the waterline and P is the total iceberg perimeter subjected to the wave action. Again note that these results are per °C of temperature difference.

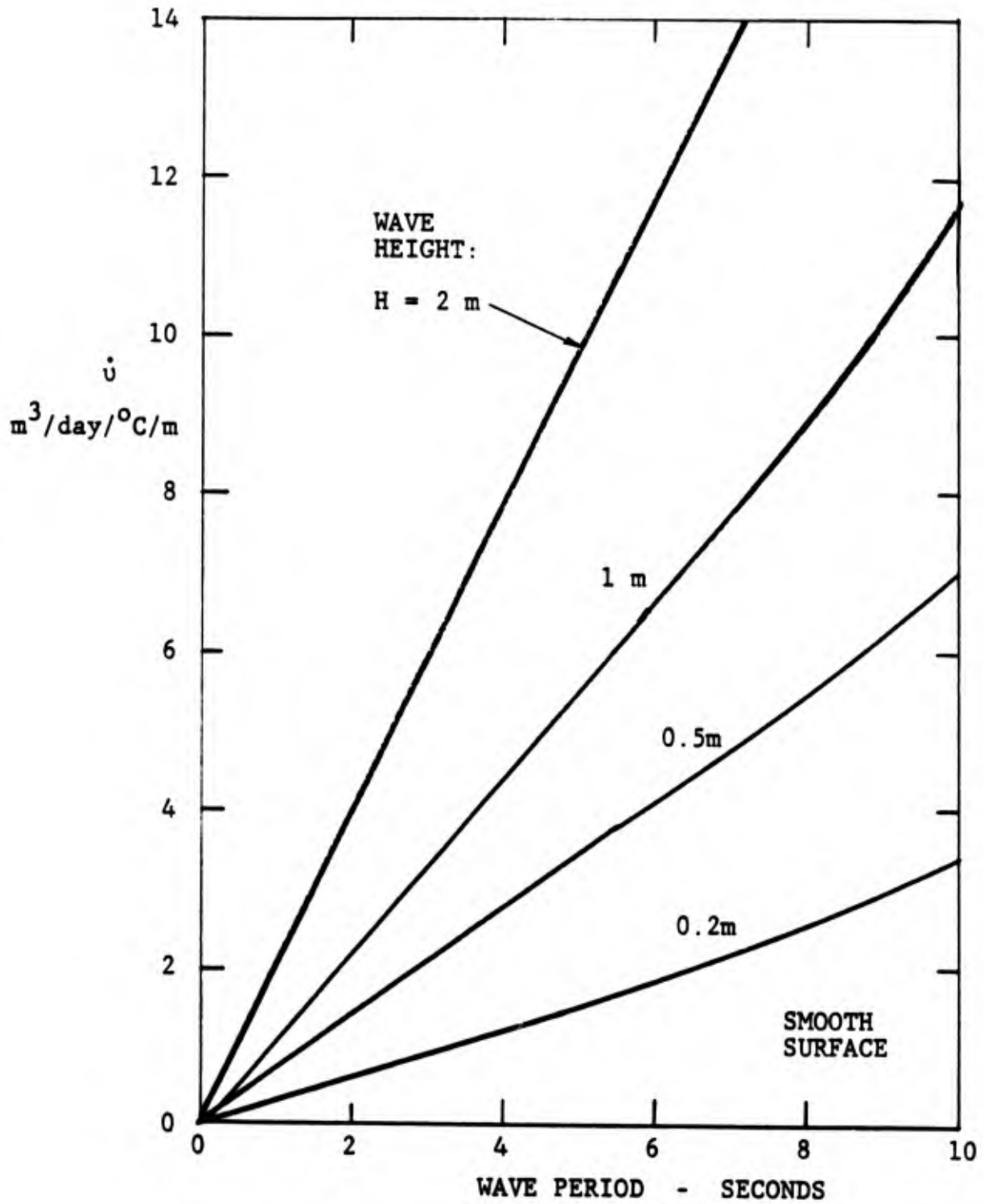


Figure 30. THEORETICAL STRIP-VOLUME WATERLINE MELTING RATE DUE TO WAVE EROSION.

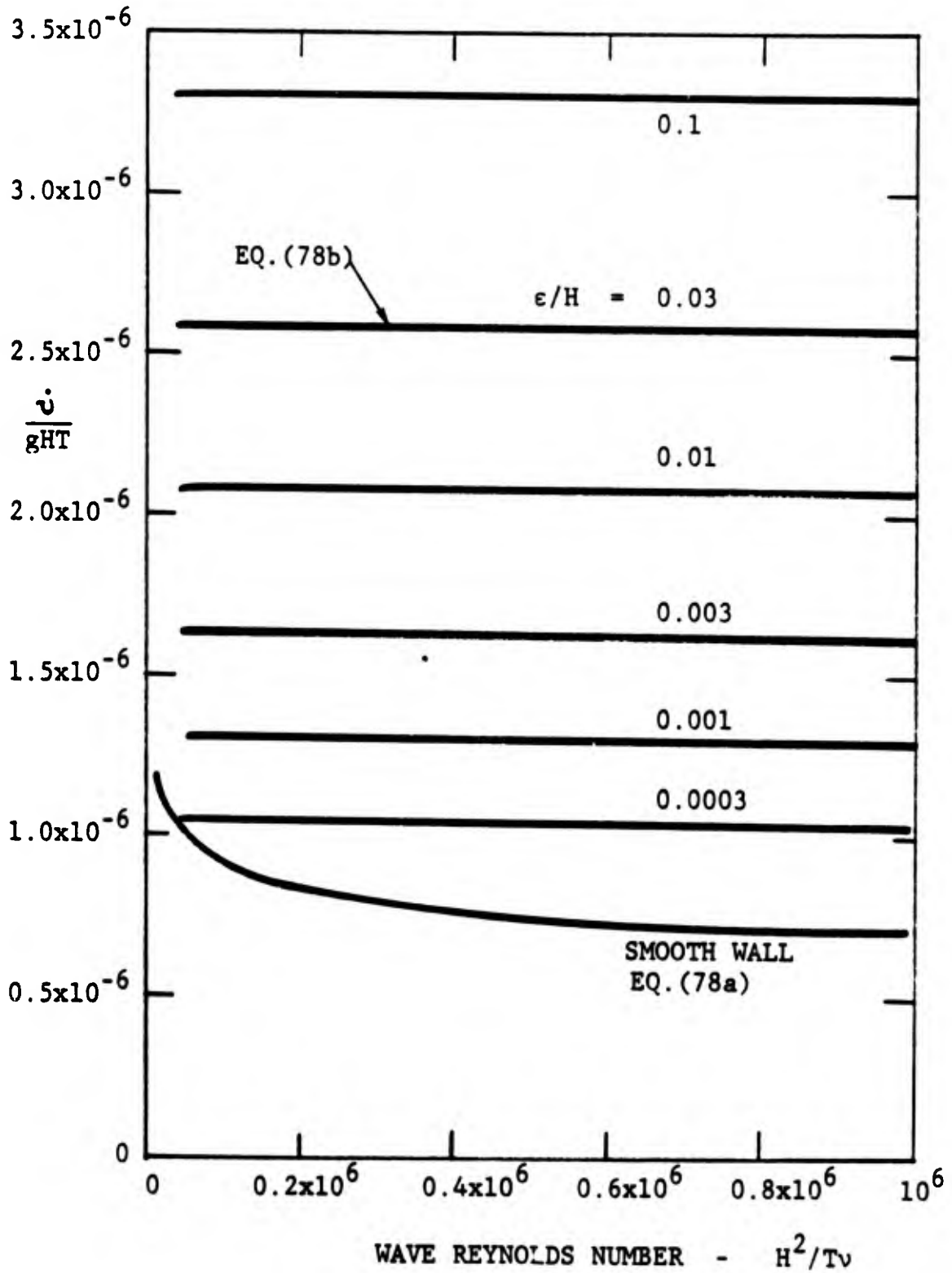


Figure 31. DIMENSIONLESS STRIP-VOLUME MELTING RATE OF AN ICE BLOCK DUE TO WAVES.

Laboratory Wave Erosion Experiments

As mentioned, Josberger (1977) reports a single wave erosion experiment: waves at $H = 5$ cm, $T = 0.4$ sec. which melted a notch 8 cm deep in 45 minutes in a vertical ice wall. The water temperature was 4°C , and we will assume the ice temperature was 0°C . The experimental waterline melting rate is thus 8cm/45 min or 2.56 m/day. For the present theory, we compute $Re_H = 3470$, so that Eq. (77a) predicts $V_m T/H = 5.64 \times 10^{-5}$, or $V_m = 7.05 \times 10^{-6} \text{ m/s/}^{\circ}\text{C}$ equals $0.61 \text{ m/day/}^{\circ}\text{C}$ times $4^{\circ}\text{C} = 2.44 \text{ m/day}$, which is within 5% of the experimental value. This lends some confidence to the present theory. We have used the smooth-wall correlation because Josberger reported that the notch itself remained smooth during the melting, although cusps formed at distances greater than H below the waterline.

The present study conducted two further experiments with the melting of floating ice blocks in the University of Rhode Island circular wave tank. The wave flapper is at the outside boundary of the tank and generates circular waves which propagate inward toward the tank center. Near the center the waves have average height $H = 6$ cm with period $T = 0.4$ sec. The floating blocks were placed at the tank center, so that their entire perimeter was subjected to wave action.

The first test ice block was 26 cm wide, 26 cm long, and 19 cm high and floated in the configuration shown in Figure 32. The water temperature was 13.5°C , with the ice surface again assumed at 0°C . The theoretical erosion rate profile was computed for the given period and is sketched also in

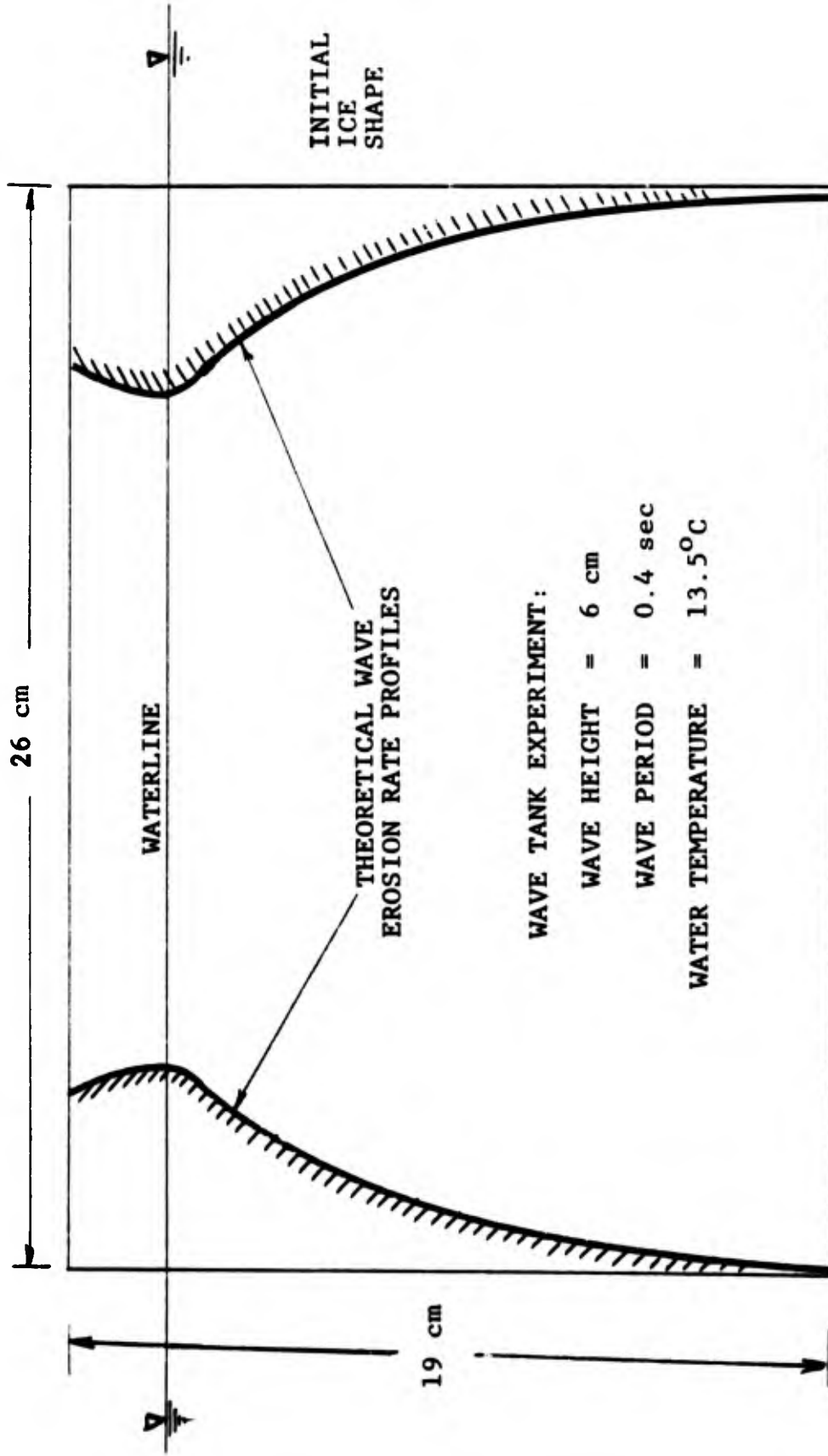


Figure 32. THEORY AND EXPERIMENT FOR EROSION OF AN 11.6 KG. ICE BLOCK IN A CIRCULAR WAVE TANK.

Figure 32. According to this theory, the block should take on this pinched-in shape as erosion progresses.

Figure 33 is a photograph of the actual test block after ten minutes of wave erosion at 13.5°C. Note the similarity of the eroded shape with the theoretical shape in Figure 32. Note also that a slight amount of dry-docking occurred in the rear of the block, where a fusion fault formed when the block was initially frozen. The waves slightly overtopped the block.

When the strip-volume melting rate is computed from Figure 31 and integrated around the entire perimeter of the block, the predicted time for total melting of the block is 31 minutes. The actual total melting time t_f was 27 minutes, or 13% less. Since the block was initially square, if we neglect corner rounding, the mass history of the melting block is given theoretically by

$$m/m_0 = (1 - t/t_f)^2, \quad t_f = 31 \text{ min.} \quad (80)$$

This relation is plotted in Figure 34 and compared with the experiment. The agreement is quite reasonable: the theory is for a smooth wall while the actual block (Figure 33) developed cusps over its entire surface during the melting process.

The second test block was rather elongated: 25 cm wide, 71 cm long, and 13 cm high. Not being square, its walls were subjected to a somewhat non-uniform radial wave field, but the theory again assumed that $H = 6$ cm and $T = 0.4$ sec. The strip-volume melting rate is essentially the same as for the first block, except that this time the water temperature was 19°C. The predicted total melting time was 21.4 minutes,



Figure 33. PHOTOGRAPH OF THE TEST BLOCK FROM FIGURE 32
AFTER TEN MINUTES OF WAVE EROSION.

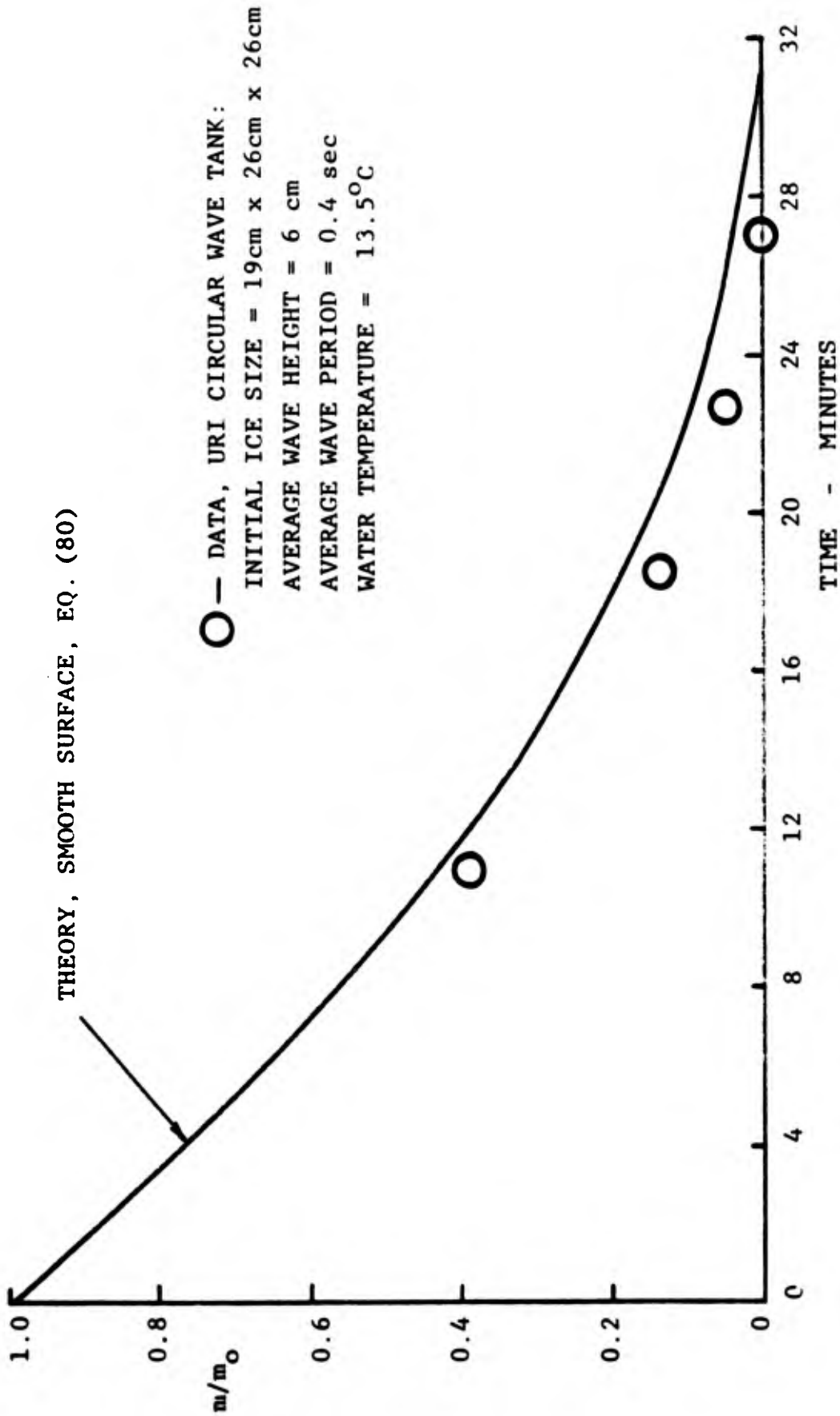


Figure 34. MELTING OF AN 11.6 Kg ICE BLOCK IN A WAVE TANK.

whereas the measured time was 20.6 minutes, or 4% less. The rectangular shape gives the following mass versus time relation:

$$m/m_0 = (1 - t/t_f) (1 - 0.36t/t_f) \quad (81)$$

with $t_f = 21.4$ minutes. This smooth-wall theoretical result is plotted in Figure 35 and compared with the experiment. The agreement is fair, especially considering the shape distortions and roughness cusps which occurred on the actual test block.

Based on these three laboratory wave erosion experiments, we conclude that the present theory has the potential to be a quite reasonable engineering estimate of the waterline melting of icebergs in a wave environment.

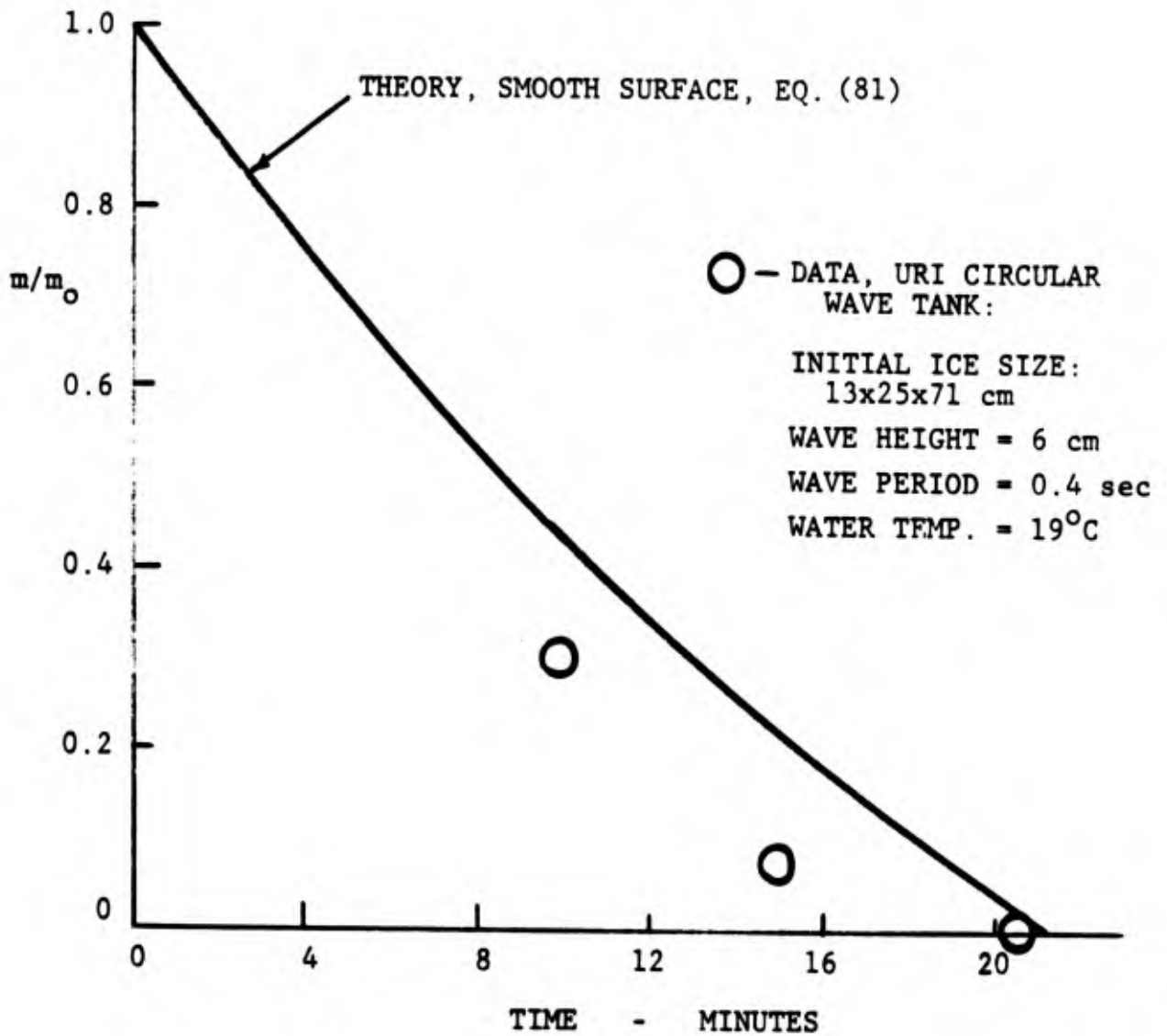


Figure 35. MELTING OF A 21.2 Kg ICE BLOCK IN A WAVE TANK.

Chapter 9

CALVING OF OVERHANGING ICE SLABS

Introduction

The wave erosion theory of Chapter 8 led to a prediction of rounded notches being cut by waves into the waterline of an iceberg. Some representative notch shapes were shown in Figure 28. As these notches proceed deeper into the berg, they leave an overhanging ice slab protruding above the waterline. At some critical overhang distance or "rupture length", l_r , the root stresses due to the weight of the slab will cause fracture and calving of the slab. The present chapter attempts an accurate analysis of fracture stresses in such an overhanging slab.

Figure 36 shows the geometry of the overhanging slab to be analyzed. For an iceberg, the support is large and the overhang small, $l \ll B$, so that the ratio $\beta = B/A$ is of order 0.8 to 0.99. The simple rectangular-shaped slab of thickness t and length l was selected, and no analyses were made of rounded or pinnacled slabs. The axisymmetric geometry was selected as being more representative of an iceberg than a two-dimensional shape. Computations were made using both elementary strength of materials and thick plate theory (Figure 36a) and a digital computer finite element model (Figure 36b).

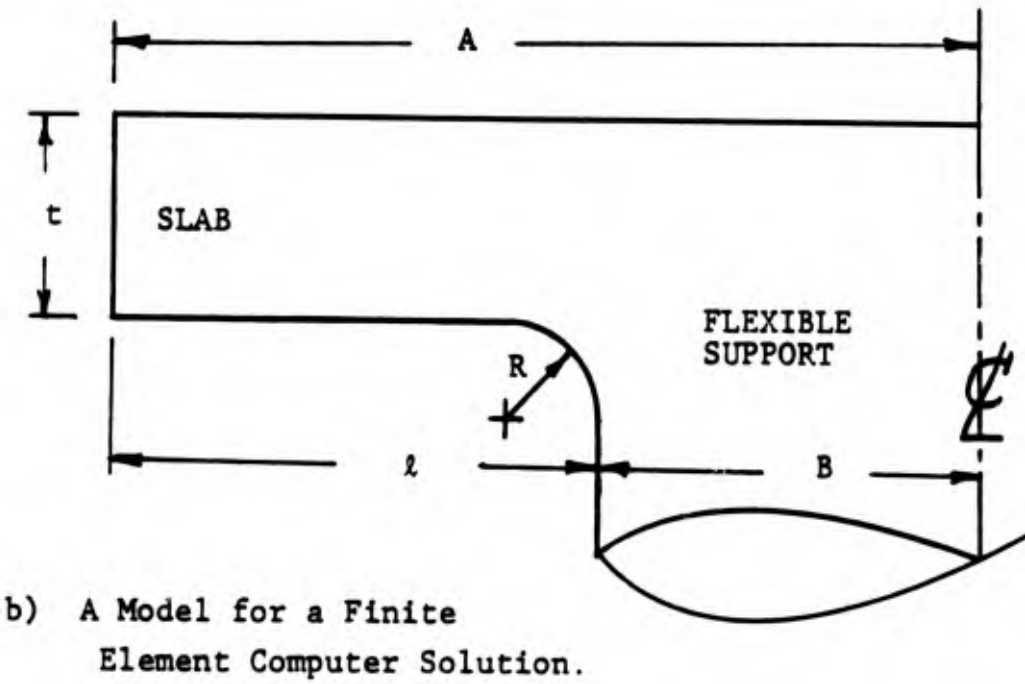
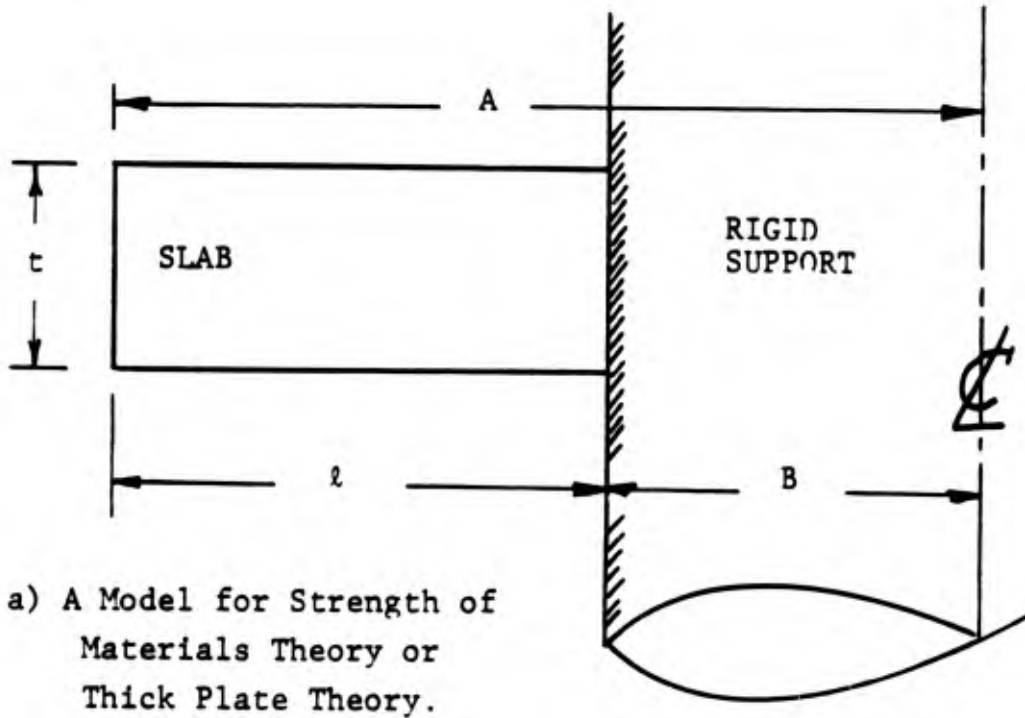


Figure 36. GEOMETRY OF AN AXISYMMETRIC OVERHANGING ICE SLAB.

Thin Plate Theory

The maximum stress at the root of a thin cantilever plate loaded by its own (uniform) weight is given in the text by Roark and Young (1975). In terms of the parameters defined in Figure 36, the final result for rupture length of the overhang is

$$l_r = (1 - \beta)(\sigma_{\max} t / \gamma)^{\frac{1}{2}} (C_1 / 3C_2)^{\frac{1}{2}} \quad (82)$$

where σ_{\max} is the fracture stress, γ is the ice specific weight, and C_1 and C_2 vary only with the length ratio β and Poisson's ratio ζ for the material:

$$C_1 = 1 + \zeta + (1 - \zeta) \beta^2 \quad (83)$$

$$C_2 = \zeta \beta^2 + \frac{1}{2}(1 - \zeta) \beta^4 + \frac{1}{2}(1 + 3\zeta) - (1 + \zeta) \ln(\beta)$$

For ice, we adopt the physical property values recommended by Hobbs (1974):

$$\begin{aligned} \gamma &= 8810 \text{ N/m}^3 \\ \sigma_{\max} &= 22 \text{ bar} \\ \zeta &= 0.34 \end{aligned} \quad (84)$$

However, Eq. (82) is not accurate for a real iceberg geometry because it does not account for large thickness and the root fillet radius R . This theory should not be used for design calculations, but it does establish the quantity $(\sigma_{\max} t / \gamma)$ as a fundamental parameter in iceberg calving.

Thick Plate Theory

An improvement is made by using thick plate theory, again assuming a cantilever slab attached to a rigid central shaft (Figure 36a). A complete analysis is given in Chapter 26 of the text by Panc (1975). The final result for rupture length is very similar to Eq.(82) plus a thickness correction:

$$l_r = (1 - \beta)(C_1/3C_2)^{\frac{1}{2}} (\sigma_{\max} t/\gamma + C_3 t^2)^{\frac{1}{2}} \quad (85)$$

where
$$C_3 = \frac{1+\zeta}{10(1-\zeta)} + \frac{1}{10\beta^2} \quad (86)$$

The additional term $C_3 t^2$ can be quite large for an iceberg geometry. This expression is more accurate but again is not recommended for design because it neglects the root fillet and the flexibility of the support.

Finite Element Solution

To make as accurate an analysis as possible, within the limits of elasticity theory (Timoshenko and Goodier 1970) for ice as a brittle material, it was decided to formulate a finite element solution for the geometry shown in Figure 36b. A complete finite element structural analysis program, called SAP-IV, is available at the University of Rhode Island and can be applied directly to this problem (Bathe et al. 1973). This program accepts either triangular or quadrilateral elements of any size and simulates the elasticity problem for a variety of boundary conditions. Quadrilateral elements were selected and a typical mesh definition is shown in

Figure 37. Finite element computations were made for a variety of fillet radii R , slab thickness t , and ratios $B/A = \beta$. The only loading applied was the weight of the elements themselves. The stresses were computed and the fracture condition, which occurred near the center of the fillet, was calculated from the maximum shear stress criterion.

Since the finite element method for structural analysis is now well documented, the details of the computation scheme will not be given. The general theory of finite element elasticity analysis is treated in Martin and Carey (1973) or Oliviera (1968). Further details relevant to the type of computation used in the present application may be found in Tong and Pian (1967) and in Clough and Rashid (1965).

The finite element solutions for rupture length are plotted versus ice slab thickness in Figure 38 for $\beta = 0.90$ and in Figure 39 for $\beta = 0.99$. In both cases, for a constant fillet radius R , there is a minimum rupture length which occurs at a small thickness t_{crit} . For $\beta > 0.75$, both the critical thickness and the minimum rupture length are practically independent of β and are given by

$$\begin{aligned} t_{crit} &= 1.26 R^{1/2} \\ \lambda_{min} &= 2.12 R^{1/2} \end{aligned} \tag{87}$$

where all lengths are in meters. Equations (87) are valid only for a fracture stress of 22 bars.

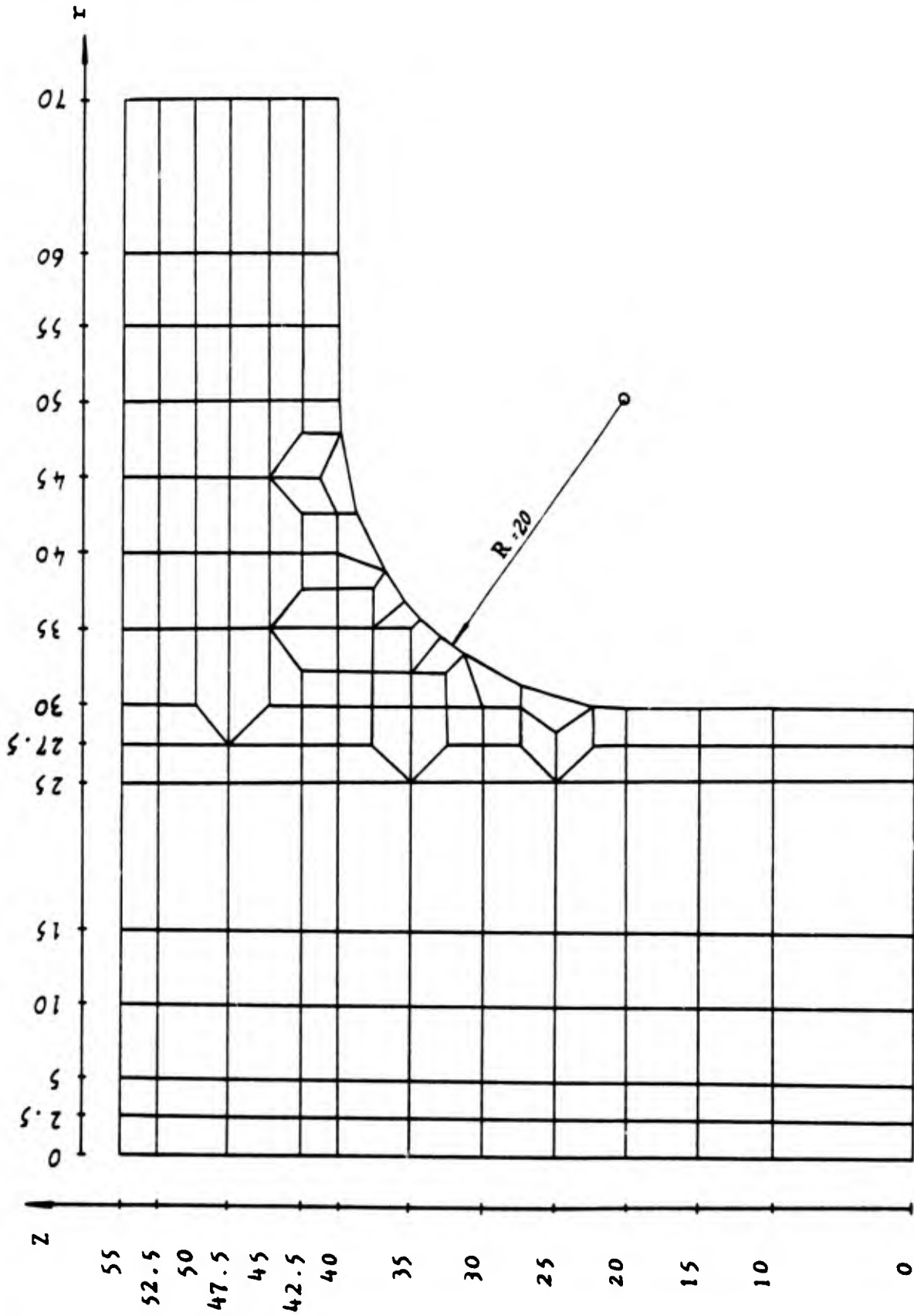


Figure 37. A TYPICAL FINITE ELEMENT MESH FOR THE SLAB OVERHANG PROBLEM.

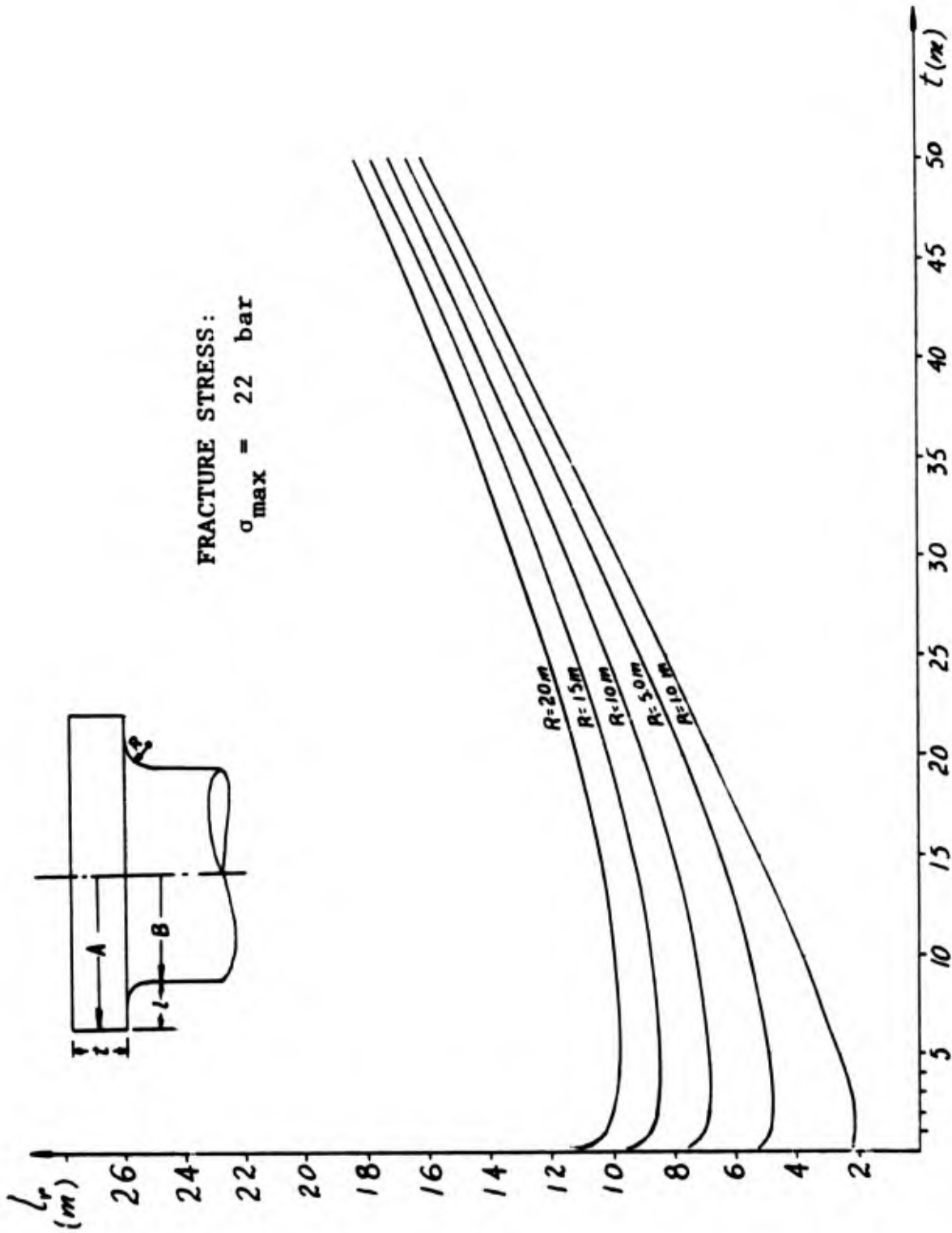


Figure 38. FINITE ELEMENT COMPUTATION OF RUPTURE LENGTH VERSUS ICE SLAB THICKNESS FOR $\beta = B/A = 0.90$.

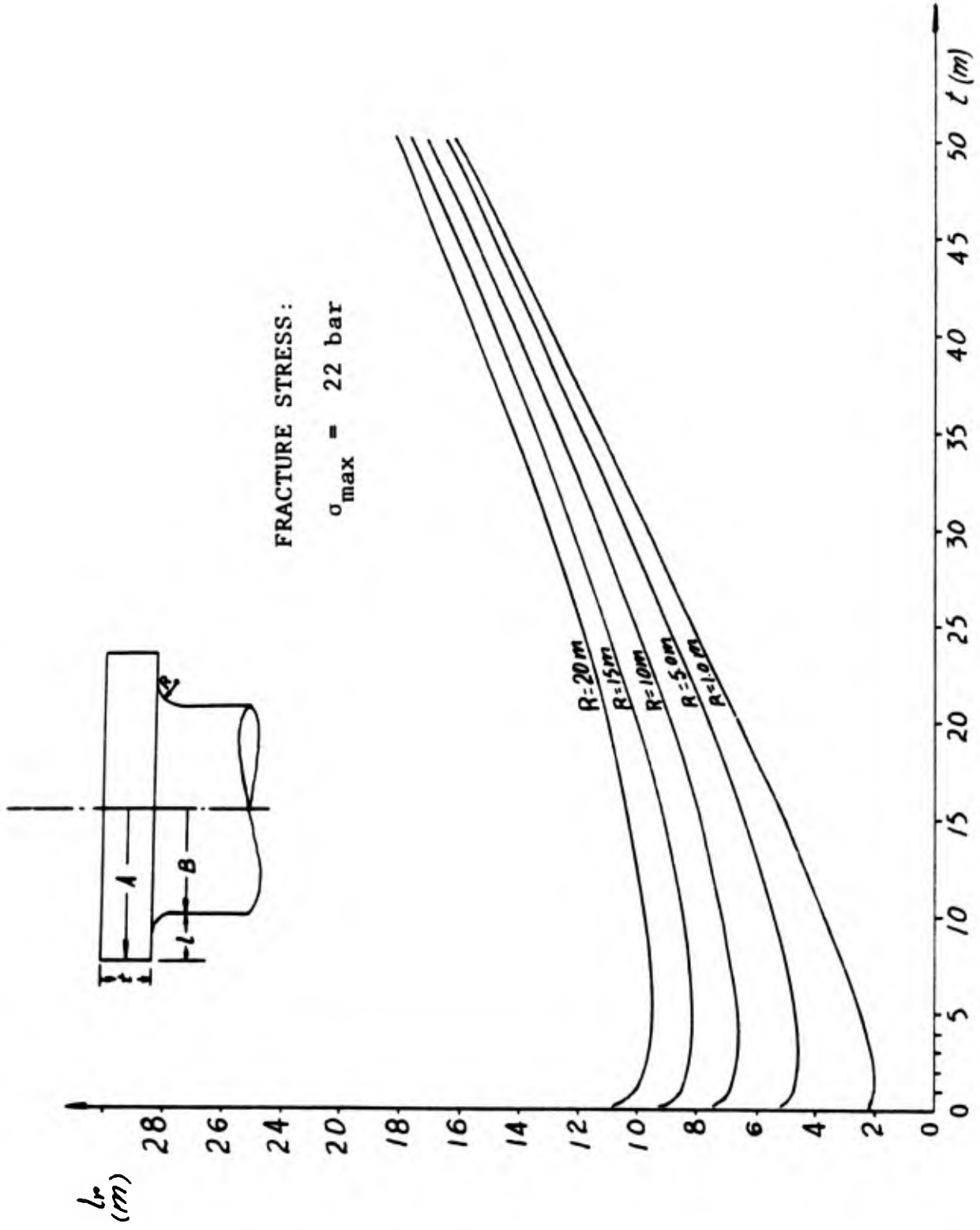


Figure 39. FINITE ELEMENT COMPUTATION OF RUPTURE LENGTH VERSUS ICE SLAB THICKNESS FOR $\beta = B/A = 0.99$.

The finite element solutions are cross-plotted in Figs. 40-42 for a fracture stress $\sigma_{\max} = 22, 15, \text{ and } 6$ bar, respectively, spanning the range of reported ice strengths in the literature. The abscissa R/t lies in the given range, zero to 2.0, for typical icebergs with wave-eroded notches. If the overhang ratio β is greater than 0.8, its effect on the curves is negligible.

Although there is no exact analytic expression known for the results computed in Figures 38 through 42, their variation is very similar to that predicted by thick plate theory, Eq. (85). Accordingly, correlations were attempted and it was found that the finite element stress computations could be related to thick plate theory by the following simple correlation:

$$\sigma_{\max}(\text{computed}) = 2.14 (R/t\beta)^{-1.07} \sigma_{\max}(\text{thick plate}) \quad (88)$$

Substitution into Eq. (85) gives the following correlation expression for the finite element rupture length results:

$$L_r = (1-\beta) (C_1/3C_2)^{\frac{1}{2}} \left\{ \left(\frac{\sigma_{\max} t}{2.14\gamma} \right) (R/t\beta)^{1.07} + C_3 t^2 \right\}^{\frac{1}{2}} \quad (89)$$

Equation (89) is in very good agreement with the results plotted in Figures 38 through 42, but it is algebraically complex. Since the results are only slightly dependent upon β , we may take average values for the constants in Eq. (89) and thus obtain the following simpler correlation:

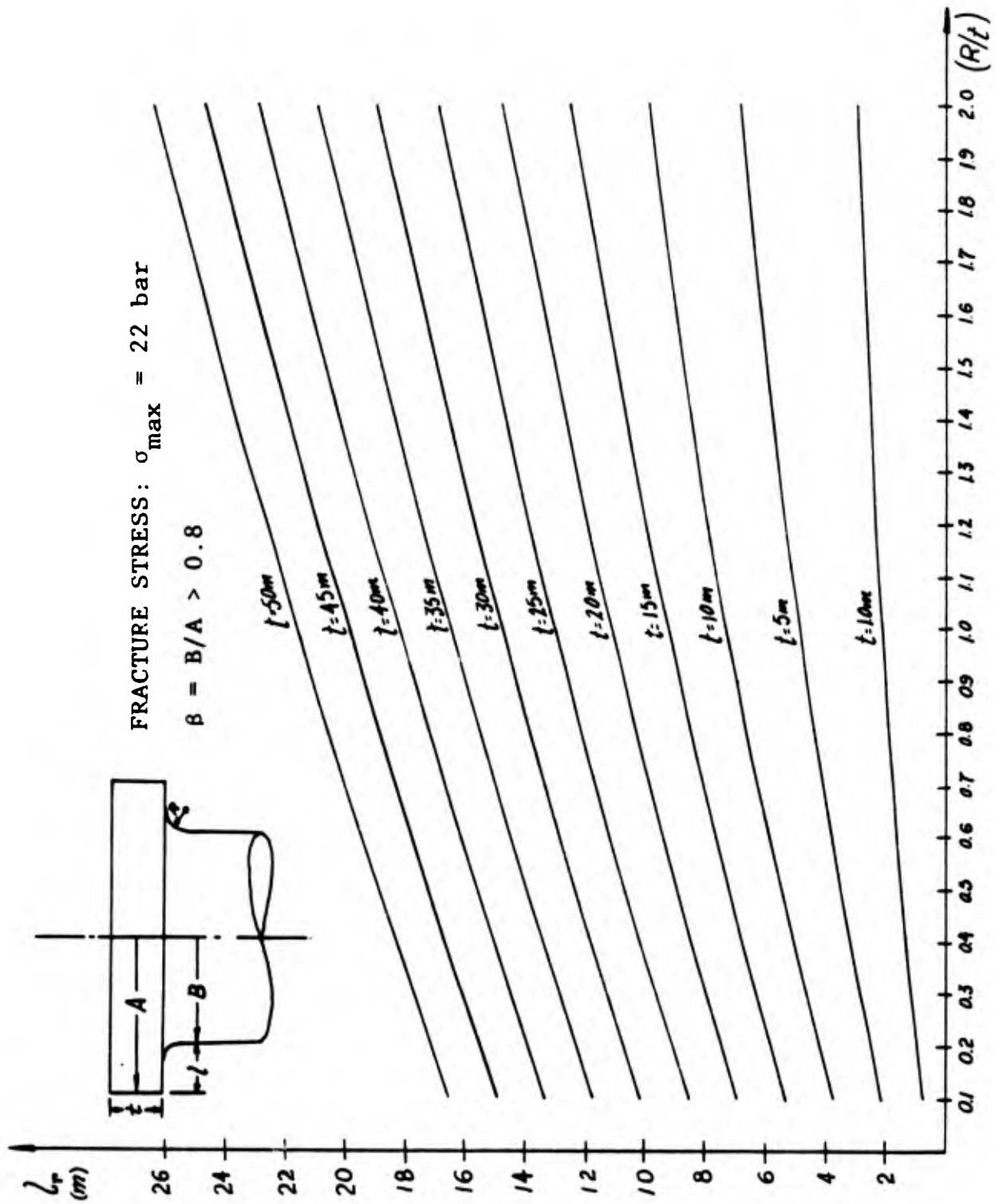


Figure 40. FINITE ELEMENT COMPUTATIONS OF RUPTURE LENGTH VERSUS FILLET RADIUS RATIO FOR $\sigma_{max} = 22 \text{ bar}$.

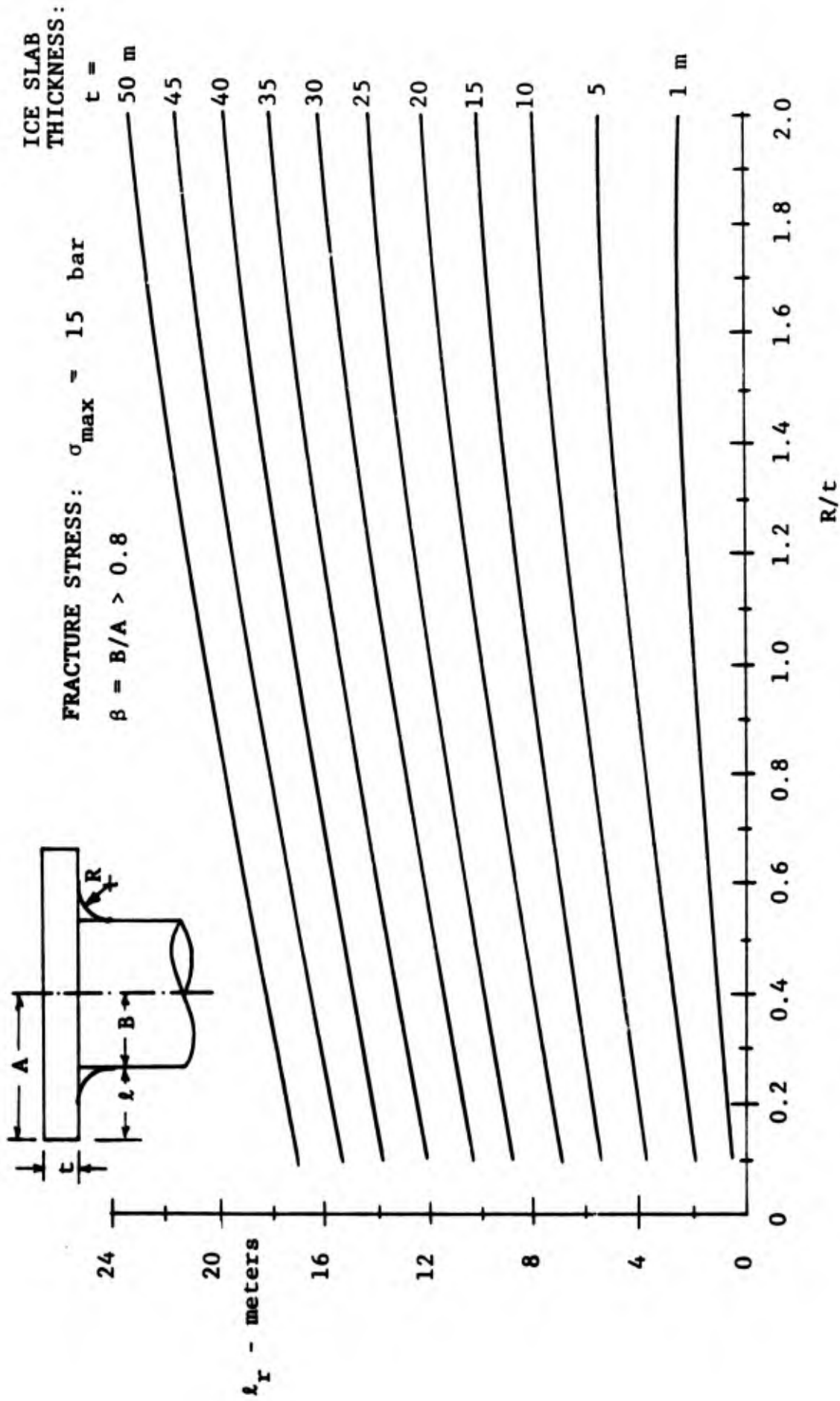


Figure 41. FINITE ELEMENT COMPUTATIONS OF RUPTURE LENGTH VERSUS FILLET RADIUS RATIO FOR A FRACTURE STRESS OF 15 bar.

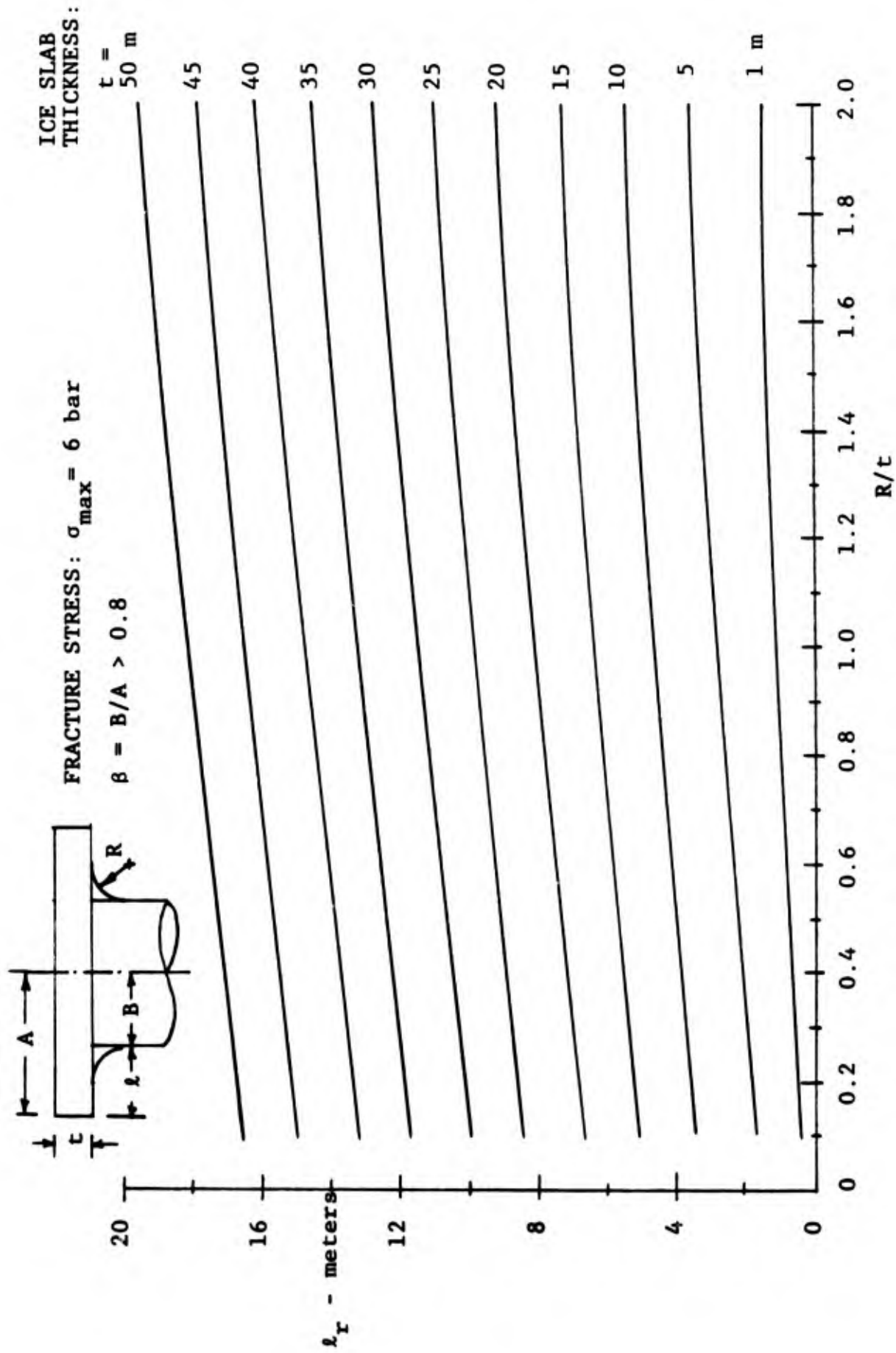


Figure 42. FINITE ELEMENT COMPUTATIONS OF RUPTURE LENGTH VERSUS FILLET RADIUS RATIO FOR A FRACTURE STRESS OF 6 bar.

$$l_r = 0.33 \{0.15(\sigma_{\max} t/\gamma)(R/t)^{1.07} + t^2\}^{\frac{1}{2}} \quad (90)$$

This expression is accurate to about $\pm 5\%$ when compared to the exact finite difference results. In fact, since the exponent of the radius term is nearly unity, there is very little error if we take it as unity and simplify still further:

$$l_r = 0.33 \{0.15(\sigma_{\max} R/\gamma) + t^2\}^{\frac{1}{2}} \quad (91)$$

Equation (91) is the engineering estimate which is recommended in this report for use in predicting calving conditions. The results plotted here, Figures 38 through 42, assume that the ice density $\gamma = 8810 \text{ N/m}^3$. All of the numerical constants in Eq.(91) are dimensionless. When compared to finite element computations, the accuracy is about $\pm 7\%$.

Application to Calving by Wave Erosion

The above calving theory is somewhat idealized by the rectangular shape of the ice slab and its rounded fillet (Figure 36) and by the use of elasticity theory to predict the fracture condition. Nevertheless, we recommend Eq.(91) as a reasonable estimate of the iceberg calving condition. Even if this equation is extremely accurate, though, it is difficult to estimate the fillet radius of an ice slab undercut by waves. The present report cannot really resolve

the question of fillet radius definition, which will require more laboratory experimentation, preferably with a random wave field, plus further field observations of iceberg waterlines. However, the experiment of Josberger (1977) and in the present report (Figure 33) and the present theory (Figure 28) all indicate that the wave-induced fillet radius is of order $\frac{1}{4}$ the wave height. Further, wave action is relatively fast, of order meters per day, so that, regardless of the previous history of the waterline, it should react rapidly to the prevailing wave environment.

For an engineering estimate, then, we postulate that the fillet radius beneath an eroded ice slab will be equal to the local wave height H prevailing at any given time. Then, from Eq.(91), the rupture or calving slab length l_r can be estimated, for $\sigma_{\max} = 22$ bar and $\gamma = 8810 \text{ N/m}^3$, by

$$l_r = 0.33(37.5 H + t^2)^{\frac{1}{2}} \quad (92)$$

where all lengths are in meters. Alternately, one could read the rupture length from Figures 40 through 42, with $R = H$.

For a non-stationary wave field, the waterline erosion rate V_m from Figure 29 or Eqs.(77) would have to be integrated over time until $l = l_r$. For a steady wave field, Eqs.(77) could be combined with Eq.(92) for an assumed average wave height H and period T , giving the estimate time to calve $\Delta t = l_r/V_m$. For a smooth wall with $v_w = 0.000018 \text{ m}^2/\text{s}$,

Equations (77a) and (92) combine to yield, for $T_w - T_i = 1^\circ\text{C}$,

$$\Delta t_{\text{calving}}(\text{days}) \approx 0.226(37.5H + t^2)^{\frac{1}{2}} T^{0.8} H^{-0.6} \quad (93)$$

with H and t in meters and T in seconds.

An iceberg surface is usually slightly rough, with an estimated average roughness of about $\epsilon = 1$ cm. Substituting this roughness into Eq. (77b) and combining with Eq. (92), we obtain the following calving time estimate, for $T_w - T_i = 1^\circ\text{C}$,

$$\Delta t_{\text{calving}}(\text{days}) \approx 0.0657(37.5H + t^2)^{\frac{1}{2}} T H^{-0.8} \quad (94)$$

again with H and t in meters and T in seconds. Equations (93) and (94) are the recommended estimates and are plotted in Figure 43 for a slab thickness $t = 20$ m and a water/ice temperature difference of 1°C . We see that the calving time decreases significantly with increasing wave height and decreasing wave period. There is, unfortunately, a very strong roughness effect which will make it difficult to estimate calving times accurately in the field. Perhaps field observations will indicate a different roughness effect from that predicted in the present study.

Figure 43 indicates, as expected, that short wave periods and large wave heights create the greatest wave erosion. The estimates are limited on the low-period end, as shown in Figure 43, by the deep-water wave breaking criterion (White 1975):

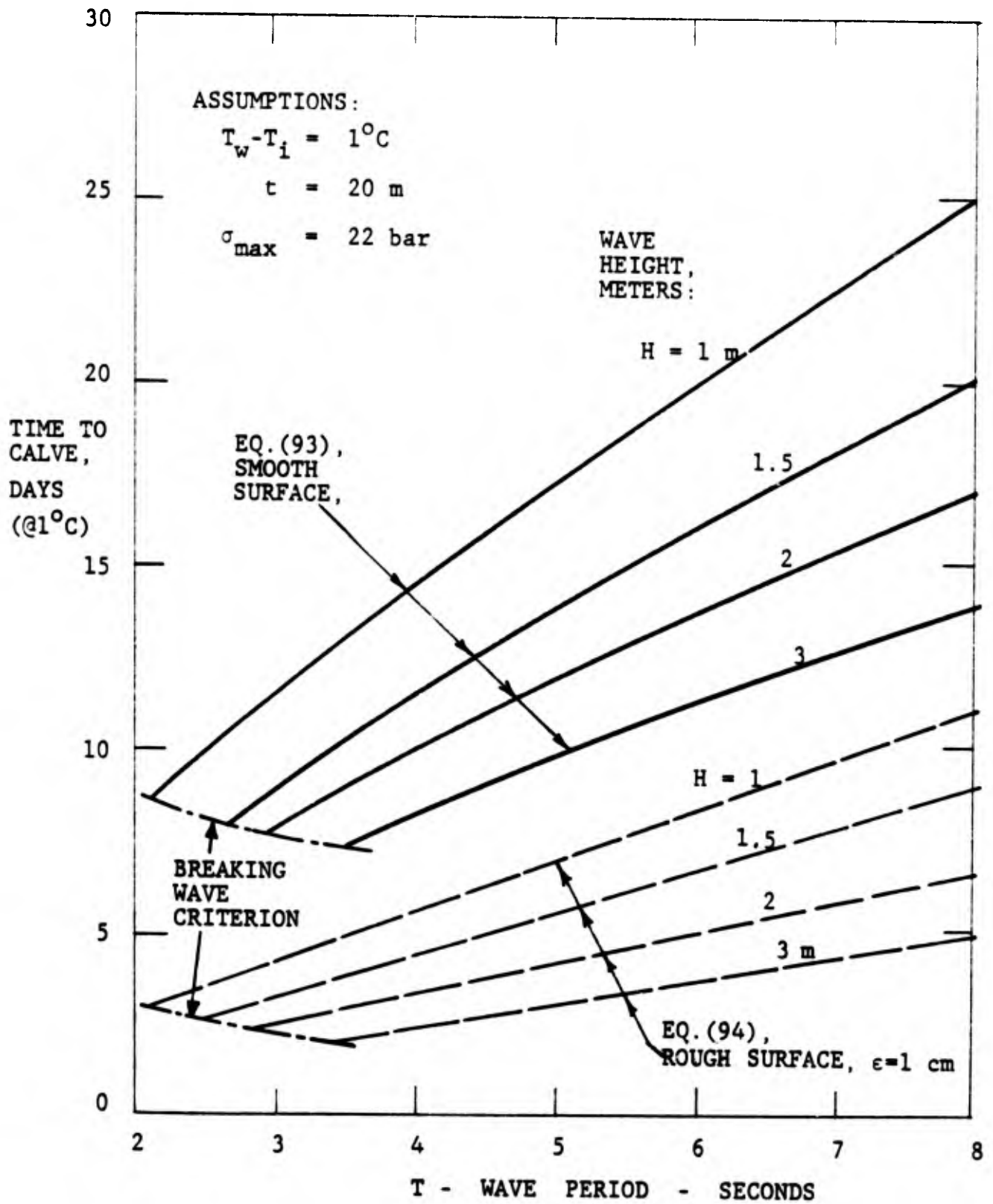


Figure 43. CALVING TIME DUE TO STEADY WAVE EROSION FOR A ROUGH SURFACE --- (Eq.94) AND A SMOOTH SURFACE — (Eq.93), SLAB THICKNESS $t = 20 \text{ m}$. DIVIDE THESE TIMES BY $(T_w - T_i)$ IN $^\circ\text{C}$.

$$(H/\lambda)_{\max} \doteq 1/7 \quad , \quad \lambda = gT^2/2\pi \quad (95)$$

Below the dash-dot lines in Figure 43 presumably no waves can exist. No theory was developed in the present study for the enhancement (if any) of wave erosion due to breaking wave effects.

It should be noted that Eqs. (93) and (94) and Figure 43 are given for a water/ice temperature difference of 1°C . The calving times are inversely proportional to $(T_w - T_i)$ and should be adjusted accordingly if the temperature difference is not unity. For example, at $T = 4$ sec and $H = 1.5$ m, with $t = 20$ m, Figure 43 indicates that a smooth ice slab will calve in 11.5 days if $(T_w - T_i) = 1^{\circ}\text{C}$. If the water is actually 10°C warmer than the ice, then it will calve in only 1.15 days.

Finally, it should be noted that wave action in the real environment does not occur in the lee of the waves impinging on the iceberg. Thus it would seem that estimation of the amount of ice mass lost in a calving event would be very shape-dependent and would require field observations.

Chapter 10

CONCLUSIONS

The present study has attempted to make engineering estimates of iceberg deterioration by a variety of possible mechanisms. It is proposed that the formulas derived here represent an improvement over existing deterioration estimates. All of the formulas are simple enough to be programmed and used on a small shipboard computer to predict, say, the loss of mass of an iceberg over a one-day period based on local environmental conditions.

The basic results of the study are as follows:

1. The stability of an iceberg can be estimated with reasonable precision from the above-water shape. The recommended formula for computing stability, based on observation of the exposed shape, is Eq.(29).
2. An iceberg may encounter relative water velocities due either to winds or to sudden changes in water currents. The response time due to a sudden current change is given by Eq.(36), and the response to a sudden wind by Eq.(38). The relative velocity caused by steady wind is given by Eq.(41) and contributes significantly to melting of the iceberg submerged surfaces.
3. As shown in Figure 15, the Basset "history" term is negligible in computing the dynamics of an iceberg.
4. Two iceberg submerged shapes were constructed and tested for submerged-body drag in a wind tunnel. At the highest

Reynolds number tested (1.1×10^6), the tabular model (Figure 11) had a drag coefficient of 0.22. The non-tabular model (Figure 13) had a drag coefficient of 0.77.

5. Maximum surface melting due to solar insolation in the Labrador Sea is approximately 7 cm/day on a clear day in June. Average melting, based on measured insolation, varies from 0.5 cm/day in winter to 4 cm/day in summer. A complete annual estimate is given in Figure 22.
6. Surface melting due to air convection is very small. Average air temperatures rarely reach more than 8°C . Even a steady wind of 20 knots will cause surface melting of only 8 mm/day/ $^{\circ}\text{C}$.
7. Buoyant vertical convection of meltwater on the submerged surface is moderately important with melting rates being approximately 2 cm/day/ $^{\circ}\text{C}$ of water/ice temperature difference. Theoretical estimates of buoyant melting are given in Figure 24.
8. Forced convection on the submerged surface is a substantial contribution to iceberg deterioration, because persistent local winds drive icebergs at a relative water/ice velocity of 10-30 cm/s, as shown in Figure 17. Resultant melting rates are 5-20 cm/day/ $^{\circ}\text{C}$ and decrease moderately with iceberg size, as shown in Figure 25.
9. A surface flaw such as a notch enhances the melting rate and may lead to calving or twinning. Some theoretical estimates are shown in Figure 26. The present study was not able to develop a realistic statistical analysis of

the effect of flaws on iceberg deterioration.

10. Wave erosion seems to be the primary cause of iceberg deterioration, due both to high melting rates and subsequent calving of undercut ice slabs. Waterline melting rates are correlated in Figure 29 and can be as high as $150 \text{ cm/day/}^{\circ}\text{C}$ of water/ice temperature difference. The volume of ice melted away by wave erosion is correlated in Figure 31. These formulas are in good agreement with three laboratory experiments of ice melting in a wave tank.
11. The fracture stress in an overhanging ice slab undercut by wave erosion, is computed by elementary plate theory and also by a digital computer finite difference method. The length of overhang which causes calving is plotted in Figures 4-42 and a general formula is given in Eq.(91). When combined with the wave erosion formulas, Eqs.(77), a formula can be derived, Eq.(93) or (94), for the time it takes an iceberg to calve in a given wave environment. The theoretical calving times are plotted in Figure 43.

This study has resulted in a variety of reasonable engineering estimates of deterioration. However, it is recommended that further research be conducted on the dominant mechanisms, especially wave erosion, calving stresses, and the effect of flaws or cracks in the ice.

REFERENCES

- Allaire, P.E. (1972), "Stability of Simply Shaped Icebergs", Technology, October-December.
- Allen, J.H., et al. (1971), Cruise Report (C.S.S. Dawson), unpublished report, Faculty of Engineering and Applied Science, Memorial University of Newfoundland.
- Ashton, G.C. (1972), "Turbulent Heat Transfer to Wavy Boundaries", Proceedings 1972 Heat Transfer and Fluid Mechanics Institute, Stanford, Calif., pp. 200-213.
- Basset, A.B. (1888), A Treatise on Hydrodynamics, Dover Publications, New York.
- Bathe, K.J., Wilson, E.L., and Peterson, F.E. (1973), "SAP-IV: A Structural Analysis Program for Static and Dynamic Response of Linear Systems", Report No. EERC-73-11, National Science Foundation, June.
- Bendell, M.S. and Gebhart, B. (1976), "Heat Transfer and Ice-melting in Ambient Water Near Its Density Extrema," Int. J. Heat Mass Transfer, Vol. 19, p. 1081.
- Benedict, C.P. (1979), "Dimensional Modelling of Icebergs", Cold Regions Science and Technology, Vol. 1, No's 3 & 4, pp 299-306.
- Breslau, L.R., James, J.E., and Trammell, M.D. (1970), "The Underwater Shape of a Grounded Ice Island off Purdhoie Bay," Alaska, Offshore Technology Conference, Houston, Texas, Preprints.
- Bruneau, A.A. and Dempster, R.J. (1972), "Engineering and Economic Implications of Icebergs in the North Atlantic", Oceanology International, March.
- Budhia, H. and Kreith, F. (1972), "Melting or Freezing in a Wedge", Int. J. Heat Mass Tr., Vol. 15, pp 1459-1477.
- Budyko, M.I. (1972), "The future climate", Trans. Amer. Geophys. Union, Vol. 52, pp. 868-874.
- Caldwell, D.R. (1974), "The Effect of Pressure on Thermal and Fickian Diffusion of Sodium Chloride", Deep-Sea Research, Vol. 21, pp. 369-375.
- Cebeci, T. and Bradshaw, P. (1977), Momentum Transfer in Boundary Layers, McGraw-Hill Book Co., New York.
- Cebeci, T. and Khattab, A. (1975), "Prediction of Turbulent Free-Convective Heat Transfer from a Vertical Flat Plate", J. Heat Transfer, August, pp. 469-471.

- Cheesewright, R. (1968), "Turbulent natural convection from a vertical plane surface", J. Heat Transfer, Vol. 90, pp 1-8
- Chen, C.T. and Millero, F.J. (1976), "The specific volume of seawater at high pressure", Deep-Sea Research, Vol. 23, p. 595.
- Clift, R., Grace, J.R., and Weber, M.E. (1978), Bubbles, Drops, and Particles, Academic Press, New York.
- Clough, R.W. and Rashid, Y. (1965), "Finite Element Analysis of Axisymmetric Solids", ASCE Proceedings, J. Engineering Mechanics Division, Vol. 91, EM1, p. 71.
- Colbeck, S.C. (1977) "Short-term forecasting of water run-off from snow and ice", J. Glaciology, Vol. 19, No. 81, pp 571-588.
- Doherty, B.T. and Kester, D.R. (1974), "Freezing point of seawater", J. Mar. Res., Vol. 32, pp 285-300.
- Duffie, J.A. and Beckman, W.A. (1974), Solar Energy Thermal Processes. Wiley-Interscience, New York.
- Eckert, E.R.G. and Jackson, T.W. (1951), "Analysis of turbulent free convection boundary layer on a flat plate", NACA Report No. 1015.
- Edwards, D.K., Denny, V.E., and Mills, A.F. (1976), Transfer Processes, Hemisphere Publishing Corp, Washington.
- Fujii, T. et al. (1970), "Experiments on Natural Convection Heat Transfer from the Outer Surface of a Vertical Cylinder to Liquids", Intl. J. Heat & Mass Transfer, Vol. 13, pp. 753-787.
- Fujino, K., Lewis, E.L., and Perkin, R.G. (1974), "The freezing point of seawater at pressures up to 100 bars", J. Geophys. Res., Vol. 79, No. 12, pp. 1792-1797.
- Gade, H.G. (1979), "Melting of ice in seawater: a primitive model with application to the Antarctic ice shelf and icebergs," J. Phys. Ocean., Vol. 9, January, pp. 189-198.
- Gebhart, B. (1979), "Buoyancy induced fluid motions characteristic of applications in technology", J. Fluids Engrg., Vol. 101, March, pp. 5-28.
- Gebhart, B. and Mollendorf, J.C. (1978), "Buoyancy-induced flows in water under conditions in which density extremes may arise," J. Fluid Mech., Vol. 80, part 4 pp. 673-707.
- Gebhart, B. and Mollendorf, J.C. (1977), "A new density relation for pure and saline water," Deep-Sea Research, Vol. 24, pp. 831-848.

George, W.K. Jr. and Capp, S.P. (1979), "A Theory for Natural Convection Turbulent Boundary Layers next to Heated Vertical Surfaces", Intl. J. Heat & Mass Transfer, Vol. 22, pp. 813-826.

Gilpin, R.R. et al. (1977), "Radiative heating in ice", J. Heat Transfer, Vol. 99, May, pp. 227-232.

Griffin, O.M. (1977), "Heat, mass, and momentum transfer effects on the ablation of icebergs in seawater", Symposium on Iceberg Utilization, Iowa State University, Ames, pp. 229-244.

Foren, P. (1969), The Waters of the Sea, Van Nostrand Reinhold Co., London.

Hardy, J.E. and Schwartz, S.H. (1979), "Laser Anemometer Measurements in Turbulent Natural Convection over a Vertical Flat Surface", ASME Paper 79-HT-106.

Hibler, W.D. III (1979), "A dynamic thermodynamic sea ice model", J. Phys. Ocean, Vol. 9, July, pp. 815-846.

Hobbs, P.V. (1974), Ice Physics, Clarndon Press, Oxford.

Hodge, B.K. (1979), "An assessment of rough surface boundary layer calculation methods", ASME Symposium on Turbulent Boundary Layers, June 18-20, pp. 197-208.

Holdsworth, G. and Glynn, J. (1978), "Iceberg Calving from Floating Glaciers by a Vibrating Mechanism", Nature, Vol. 274, Aug. 3rd, pp. 464-466.

Holdsworth, G. (1977), "Some Mechanisms for the Calving of Icebergs", Symposium on Iceberg Utilization, Iowa State University, Ames, pp. 160-175.

Huang, N.E. (1979), "On surface drift currents in the ocean," J. Fluid Mech., Vol. 91, part 1, pp. 191-208.

Huppert, H.E. and Turner, J.S. (1978), Iceberg Utilization, Proceedings of The First International Conference, Pergamon Press, New York.

Job, J.C. (1978), "Numerical modelling of iceberg towing for water supplies - a case study", J. Glaciology, Vol. 20, No. 84, pp. 533-542.

Jong, B. de (1973), Net radiation received by a horizontal surface at the earth, Delft Univ. Press, distributed by Academic Book Services, Groningen, The Netherlands.

- Jonsson, I.G. (1966), "Wave boundary layers and friction factors", Proc. 10th Conf. on Coastal Engineering, Tokyo, pp. 127-148.
- Josberger, E.B. (1977), "A laboratory and field Study of Iceberg Deterioration", Symposium on Iceberg Utilization, Iowa State Univ., Ames, pp. 245-264.
- Josberger, E.G. (1979a), "Laminar and turbulent boundary layers adjacent to melting vertical ice walls in salt water", Ph.D. Thesis, Univ. of Washington, Seattle.
- Josberger, E.G. (1979b), "The effect of bubbles released from a melting ice wall on the melt-driven convection in salt water", Iceberg Dynamics Symposium, St. John's Newfoundland, June 4-5.
- Kato, H. Nishiwaki, N., and Hirata, M. (1968), "On turbulent heat transfer by free convection from a vertical plate", Intl. J. Heat & Mass Transfer, Vol. 11, pp. 1117-1125.
- Kaufman, D.W. (ed.) (1960), Sodium Chloride, Van Nostrand Reinhold, New York.
- Kays, W.M. and Crawford, M.E. (1980), Convection Heat and Mass Transfer, 2nd Edition, McGraw-Hill Book Co., New York.
- Kollmeyer, R.C. (1965), "Iceberg Deterioration", Interim Report, U.S. Coast Guard, Washington, D.C., pp. 41-64, Report No. 11.
- Kollmeyer, R.C. (1979), "West Greenland outlet glaciers: an inventory of major iceberg producers", Cold Regions Science and Technology, Vol. (No's 3 & 4, pp. 175-181.
- Krieth, F. (1973), Principles of Heat Transfer, 3rd Ed., Intext Educ. Pub., New York.
- Larson, J.R. and Schoenhals, R.J. (1964), "Turbulent free convection in near-critical water", U.S. Atomic Energy Comm. Report COO-1117-16, August.
- Lazaridis, A. (1970), "A Numerical Solution of the Multi-Dimensional Solidification of Melting Problem", Int. J. Heat & Mass Transfer, Vol. 13, pp. 1459-1477.
- Lebedev, V.L. (1965), "Measurement of the Draft of Icebergs on the Mirny Road", February-March, 1958, Society Antarctic Expedition, Vol. 2.
- LeDrew, B.R. and Gustajtis, K.A. (ed.) (1978), "An oil spill scenario for the Labrador Sea", C-CORE Tech. Report No. 78-2, Memorial Univ. of Newfoundland, St. Johns, March, 796 pages.

- Madsen, O.S. (1977), "A realistic model of the wind-induced Ekman Boundary Layer", J. Phys. Ocean., Vol. 7, No. 2.
- Martin, H.C. and Carey, G.F. (1973), Introduction to Finite Element Analysis, McGraw-Gill Book Co., New York.
- Martin, S. and Kauffman, P. (1977), "An experimental and theoretical study of the turbulent and laminar convection generated under a large ice sheet floating on warm salty water", J. Phys. Ocean., Vol. 7, No. 2, pp. 272-283.
- Mason, H.B. and Seban, R.A. (1974), "Numerical Predictions for Turbulent Free Convection from Vertical Surfaces", Intl. J. Heat & Mass Transfer, Vol. 17, pp. 1329-1336.
- Morgan, V.I. and Budd, W.F. (1977), "The distribution, movement and melt rates of Antarctic icebergs", Symposium on Iceberg Utilization, Iowa State University, Ames, pp. 220-228.
- Mountain, D. (1979), "On prediction iceberg drift", Cold Regions Science and Technology, Vol. 1, No's 3 & 4, pp. 273-282.
- Murray, J.E. (1969), The Drift, Deterioration and Distribution of Icebergs in the North Atlantic Ocean, Ice Seminar, CIM Special Volume 11.
- National Oceanic and Atmospheric Administration, Mariner's Weather Log, Climatological Data, U.S. Ocean Station Vessel "Bravo", North Atlantic, bimonthly.
- Neshyba, S. and Josberger, E.G. (1979), "On the estimation of Antarctic iceberg melt rate", Iceberg Dynamics Symposium, St. John's Newfoundland, June 4-5.
- Noto, K. and Matsumoto, R. (1975), "Turbulent Heat Transfer by Natural Convection along an Isothermal Vertical Flat Surface", J. Heat Transfer, November, pp. 621-624.
- Nunner, W. (1956), "Heat transfer and pressure drop in rough tubes", VDI-Forschungsheft, No. 455, Series B. pp. 5-39.
- Ockendon, J.R. and Hodgkines, W.R. (1975), Moving Boundary Problems in Heat Flow and Diffusion, Clarendon Press, Oxford.
- Odar, F. (1969), "Unsteady motion of a sphere along a circular path in a viscous fluid", J. Appl. Mech., Vol. 36, pp. 1-3.
- Oliviera, E.A. (1968), "Theoretical Foundations of the Finite Element Method", Int. J. Solids and Structures, Vol. 4, pp. 929-952.

- Owen, P.R. and Thomson, W.R. (1963), "Heat transfer across rough surfaces," J. Fluid Mech., Vol. 15, pp. 321-334.
- Pao, R.H. (1961), Fluid Mechanics, John Wiley & Sons, New York.
- Panc, V. (1975), Theories of Elastic Plates, Academia, Czechoslovakia.
- Paterson, W.S.B. (1975), The Physics of Glaciers, Pergamon Press, New York.
- Reed, M. (1980), "A fishery-oil spill interaction model: formulation and application", Ph.D. dissertation, Univ. of Rhode Island, Dept. of Ocean Engineering.
- Riggs, N. et al. (1979) "Iceberg drift observations in Lancaster Sound", Cold Regions Science and Technology, Vol. 1, No's 3 & 4, pp. 283-291.
- Roark, R.J. and Young, W.C. (1975), Formulas for Stress and Strain, McGraw-Hill Book Co., New York.
- Robe, R.Q., Maier, D.C. and Russell, W.E. (1979), "Long-term drift of icebergs in Baffin Bay and the Labrador Sea" Cold Regions Science and Technology, Vol. 1, No's 3 & 4, pp. 183-193.
- Robe, R.Q. and Maier, D.C. (1979), "Long-term tracking of Arctic icebergs", Report CGR/DC-8/79, Coast Guard R&D Center, Groton, CT, 41 pages.
- Robe, R.Q., (1978), "Upwelling by Icebergs", Nature, Vol. 271, Feb. 16th, p. 634
- Robe, R. Q., Maier, D.C. & Kollmeyer, R.C. (1977), "Iceberg Deterioration", Nature, Vol. 267, June 9, pp. 405-406.
- Robe, R.Q., (1976), "Physical Properties of Icebergs - Part I - Height to Draft Ratios of Icebergs", U.S. Coast Guard Office of Research and Development, Report No. CG-D-102-76.
- Robe, R.Q. and Farmer, L.D. (1976), "Physical Properties of Icebergs - Part II - Mass Estimation of Arctic Icebergs", U.S. Coast Guard Office of Research and Development, Report No. CG-D-102-76.
- Rossiter, R. and Gustajtis, K.A. (1978), "Iceberg Sounding by Impulse Radar", Nature, Vol. 271, Jan. 5th, pp. 48-50.
- Saitoh, T. (1976), "Natural convection heat transfer from a horizontal ice cyclinder", Appl. Sci. Res., Vol. 32, p. 429.

- Saunders, O.A. (1939), "Natural convection in liquids", Proc. Royal Soc. London, Series A, Vol. 172, pp. 55-71.
- Schechter, R.S. and Isbin, H.S. (1958), "Natural-convection heat transfer in regions of maximum fluid density", AICHE J., Vol. 4, No. 1, pp. 81-89.
- Schenk, J. and Schenkels, R.A. M. (1968), "Thermal free convection from an ice sphere in water", Appl. Sci. Res., Vol. 19, pp. 465-476.
- Siedman, M.H. (1978), "Rough wall heat transfer in a compressible turbulent boundary", AIAA Paper No. 78-163, Jan 16-18.
- Shil'nikov, V.I. (1960), "Experimental Calculation of Iceberg Volume in Antarctic", Problemy Arktik i Antarktiki, No. 6.
- Shonting, D.H. et al. (1979), "The Windwave and Turbulence Observation Program (WAVTOP)", Final Report, U.S. Coast Guard Contract MIPR-Z-7-71825-A, Naval Underwater Systems Center, Newport, Rhode Island.
- Shonting, C. (1971), "Observations of Reynolds Stress in Wind Waves", Pure 7 Appl. Geophys., Vol. 81, No. 4, p. 202.
- Smith, E.H. (1931), "The Marion Expedition to Davis Strait and Baffin Island", U.S. Government Printing office.
- Smith, R.A. (1977), "Iceberg Cleaving and Fracture Mechanics - A Preliminary Survey", Symposium on Iceberg Utilization, Iowa State University, Ames, pp. 176-190.
- Spichkin, V.A. (1967), "Variation in the Height Ratio of the Underwater and Above-Water Parts of Icebergs in Relation to Their Shape", Soviet Antarctic Expedition, Vol. 6.
- Stewartson, K. and Waechter, R.T. (1976), "On Stefan's Problem for Spheres", Proc. Royal Society, Vol. A348, pp. 415-426.
- Stolfi, R. et al. (1979), "Experiments involving melting of a large ice block towed in sea water", Iceberg Dynamics Symposium, St. John's Newfoundland June 4-5.
- Stolfi, R. et al. (1977), "Ice moving in seawater", Symposium on Iceberg Utilization, Iowa State Univ., Ames, pp. 199-219.
- Sukhov, B.P. (1977), "Measurement of iceberg draft", Symposium on Iceberg Utilization, Iowa State Univ., Ames, pp. 265-275.

Tatinclaux, J.C. and Kennedy, J.F. (1977), "Ripple formation at ice-flow interfaces: potential effects on iceberg transport", Symposium on Iceberg Utilization, Iowa State Univ., Ames. pp. 176-282.

Timoshenko, S. and Goodier, J. (1970), Theory of Elasticity, 3rd Edition, McGraw-Hill Book Co., New York.

Tong, P. and Pian, T.H.H. (1967), "The Convergence of the Finite Element Method in Solving Linear Elastic Problems", Intl. J. of Solids and Structures, Vol. 3, pp. 865-879.

Touloukian, Y.S., Hawkins, G.A. and Jakob, M. (1948), "Heat transfer by free convection from heated vertical surfaces", ASME Transactions, Vol. 70, p. 13.

Tuan, Y. (1959), "Heat transfer in natural convection flow of water", M.S. Thesis, University of Washington, Seattle.

U.S. Naval Oceanographic Office (1967), Oceanographic Atlas of the North Atlantic Ocean: Sect. I, Physical Properties.

U.S. Navy, "Summary of Synoptic Meteorological Observations: Ocean Station Bravo", Vol. i, North Atlantic Coastal Marine Areas.

Vanier, C.R. and Tien, C. (1970), "Free convection melting of ice spheres", AICHE, J., Vol. 16, p. 76.

Vanier, C.R. and Tien, C. (1968), "Effect of maximum density and melting on natural convection heat transfer from a vertical plate", Chemical Engineering Progress Symposium Series, Vol. 64, No. 82, pp. 240-254.

Waibler, P.J. (1958), "Natural convection heat transfer with water at high Grashof numbers", Ph.D. Thesis, Univ. of Ill.

Warner, C.Y. and Arpaci, V.S. (1968), "An Experimental Investigation of Turbulent Natural Convection in Air at Low Pressure along a Vertical heated Flat Plate", Intl. J. Heat & Mass Transfer, Vol. 11, pp. 397-406.

Weeks, W.F. and Mellor, M. (1977), "Some Elements of Iceberg Technology", Symposium on Iceberg Utilization, Iowa State University, Ames, pp. 45-98.

Weeks, W.F. and Campbell, W.J. (1973), "Icebergs as a fresh water source: an appraisal", J. Glaciology, Vol. 12, p. 207.

White, F.M. (1974), Viscous Fluid Flow, McGraw-Hill Book Co., New York.

White, F.M. (1975), "Hydrodynamics of Coastal Areas", Chapter 2
McGraw-Hill Book Co., New York.

White, F.M. (1979), Fluid Mechanics, McGraw-Hill Book Co., New
York, 701 pages.